Investigation into the Catalytic Dehydrocoupling of Bridged Disilanes

A thesis presented to the University of Auckland in partial fulfilment of the requirements for the degree of a Master of Science in Chemistry

Jack Francois

AUID: 395308975

June 2022

Supervisor: Erin Leitao

Abstract:

As humanity continues into the 21st century, society continues to progress towards more electronic-centric lifestyles. The use of expensive and rare transition state metals within semiconductors continues to an issue as the rare metals become scarcer. The search to identify highly efficient semiconductor substituents discovered the potential of crystalline silicon. The structural rigidity of the crystalline silicon has limited electronic application and redirected attention towards the development of elastomeric compounds, capable of bending, rolling folding and stretching while maintaining high-performance electronic conductivity. Advancements in silicon chemistry have identified polysilanes, organosilicon polymers possessing of a Si-Si backbone. The σ-conjugation along the polysilane Si-Si backbone provides a semiconducting material with unique electronic properties, meanwhile possessing the flexibility and desirable physical properties of organic compounds. However, the susceptibility of the Si-Si bond to UV irradiation and high moisture conditions facilitates polysilane chain breakdown. Attempts to reinforce the Si-Si backbone through covalent molecular bridges have been developed, where the incorporation of a molecular bridge between two silicon atoms reinforces the disilane bond and increases the overall robustness of the bridged polysilane. Careful selection of the bridging molecule may allow for enhancement of the electronic properties of the bridged disilane. Naphthalene-bridge disilanes have been shown to exhibit unique electronic properties due to the σ-π mixing between the bridge and silicon centres. However, limitations regarding disilane dehydrocoupling have prevented successful synthesis of bridged disilane oligosilanes.

This work focuses on the continued development of bridged polysilanes aimed towards the synthesis of bis(phenyl)silyl precursors as disilane building blocks with terminal hydride ends for successive dehydropolymerisation. The first section is directed towards the identification of experimental procedures capable of synthesising benzyl silane bridges from chloro(aryl)silanes and benzyl bromide substrates. These reactions are conducted for the expansion of the potential bridging molecular substrates to non-aromatic molecules**.** The second section details an intramolecular dehydrocoupling investigations on the 1,8-bis(phenylsilyl)naphthalene precursor with a series of four transition-metal dehydrocoupling catalysts. The four catalysts selected were either rhodium ($[Rh(cod)Cl]_2$, $Rh(PPh_3)_3Cl$) or zirconocene-based complexes (Cp_2ZrBu_2, Cp_2ZrMe_2). The catalytic investigation aimed to identify potential catalysts for the preparation of bridged disilanes and bridged polysilane chains, with a focus on the $[Rh(cod)Cl]_2$ catalyst. The $[Rh(cod)Cl]_2$ catalyst was confirmed as a highly efficient dehydrocoupling catalyst for intramolecular dehydrocoupling disilane synthesis, significant more efficiency than $Rh(PPh_3)_3Cl$ under mild conditions. Increased catalytic loading and increased temperature failed to prove tertiary dehydrocoupling with the $[Rh(cod)Cl]_2$ catalyst. *In situ* zirconocene catalysts were identified as potential catalysts for disilane building blocks in contrast to previous evidence. Investigation into zirconocene-based complexes revealed while the $[Cp_2Zr]$ is a capable hydrosilane dehydrocoupling catalyst, direction lithiation of the hydrosilane provides improved yields

and conversion rates at the cost of purity. NMR spectroscopy revealed varying stereoselectivity between the zirconocene and rhodium catalysts, with mechanistic insight provided to explain the observed stereoselectivity between the two different dehydrocoupling catalyst classes. The final section details a second intramolecular dehydrocoupling investigation where the previous dehydrocoupling catalysts are applied to two ferrocene-bridged disilyl precursors 1,1-bis(phenylsilyl)ferrocene) and 1,1-bis(diphenyl silyl)ferrocene). Experimental analysis revealed none of the investigated catalysts were capable of reaction success, but that compound degradation was significant for zirconocene catalysts, proposed to be consequential of the use of lithiation additives.

Acknowledgements

I would like to express the most special thanks to my MSc supervisor Dr. Erin Leitao. Your guidance and motivation aided my studies throughout the difficulties of COVID restrictions and lockdowns. Your insightful suggestions and detailed focus were always helpful. Thank you for the fortuitous chance I received which allowed myself to be a student under your supervision.

I would like to thank PhD candidates Emeka Itumoh, Kunwoo Park and Luke Park for their assistance in getting started in the lab and consistent aid throughout the years. A special thanks to Mr. Radesh Singh for the day-to-day running of the lab and the purchase of chemical reagents. Thank to Mr Paavan Kumar for day-to-day maintenance of laboratory instrument. Thanks to Michael Schmitz for NMR spectroscopy and to Mansa Noir for the mass spectrometry

I would like to thank all the past members of the Leitao Lab for the great time we had together. A special thanks to Henry, William, Andrew, Devin, Malachy, Fabio. Although limited by COVID and lockdowns, everyone helped my research experience to be fun and memorable. Thank you to Sahil, Emma, Mason, Saawan for close association with the Leitao lab group.

A special thanks to my friends Raghunandan Raman and Anuruddha Caldera for helping my transition to Auckland fun and creating great memories in TT/Anzac. Thanks to Steve, Allison, Harry, Martin and Maddie for be your support and willingness to become my second family.

To Liza, thank you for all your continued love and encouragement. A very special thank you to my family for the unquestioned emotional support throughout my entire studies. The biggest thank you for Maynard for being the perfect dog as he always knows he is.

Table of Contents

List of Figures:

Figure 3.14 $^{29}Si\{^{1}H\}$ NMR spectrum of the Cp_2ZrCl_2/2MeLi dehydrocoupling reaction with **4** after 72 h.

Figure 3.15 Structure of the active Rh(I) catalysts for the $Rh(PPh_3)_3Cl$ (Left) and $[Rh(cod)Cl]_2$ (Right) catalysts.

Figure 3.16 Structure of the stereoselective-determining Rh(I) catalyst complex for each respective Rh(I) catalyst.

Figure 3.17 $^{29}Si\{^{1}H\}$ NMR spectra for the dehydrocoupling catalyst reactions with **7b** (Green = purified **7b**, Red = $[Rh(cod)Cl]_2$, Blue = Cp_2ZrCl_2/2nBuLi).

Figure 3.18 $^{29}Si\{^{1}H\}$ NMR spectrum of the dehydrocoupling reaction between 1,1-bis(phenylsilyl)ferrocene (**7a)** and the $[Rh(cod)Cl]_2$ catalyst.

Figure 3.19 $^{29}Si\{^{1}H\}$ NMR spectrum of the dehydrocoupling reaction between 1,1-bis(phenylsilyl)ferrocene (**7a)** and the Cp_2ZrCl_2/2nBuLi catalyst.

List of Schemes:

Scheme 3.5. Proposed synthesis of the **2c** disilyl precursor from the **1c** substrate through the Visco (Top) and Schrock (Bottom) Grignard reaction conditions.

Scheme 3.6 Proposed synthesis of the **2b** disilyl precursor from the **1a** substrate through the Visco (Top) and Schrock (Bottom) Grignard reaction conditions.

Scheme 3.7 Proposed synthesis of the **2a** disilyl precursor from the **1a** substrate through the Visco (Top) and Schrock (Bottom) Grignard reaction conditions.

Scheme 3.8 Catalyst investigation results from previous research on the synthesis of the naphthalene-bridged disilane **5** from dehydrocoupling reaction with the **4** substrate.

Scheme 3.9 Proposed $[Rh(cod)Cl]_2$ catalysed dehydropolymerisation of 1,8-bis(phenylsilyl)naphthalene (**4**) for the synthesis of a bridged polysilane

Scheme 3.10 Synthetic strategy for the synthesis of 1,8-bis(phenylsilyl)naphthalene (**4**).

Scheme 3.11 Synthesis of the meso (5ab) and chiral (5ab) through dehydrocoupling of 4 with the $[Rh(cod)Cl]_2$ catalyst.

Scheme 3.12 Proposed dehydrocoupling mechanism for the $[Cp_2Zr(H)Cl]$ active catalyst with the (**4**) substrate through σ-bond metathesis reactions.

Scheme 3.13 Catalytic dehydrocoupling of **4** using Cp_2ZrCl_2/2nBuLi

Scheme 3.14 β-hydride abstraction elimination pathway for the formation of the zirconocene $[Cp_2Zr^{II}]$ complex.

Scheme 3.15 Reaction scheme for the lithiation of **4** and coordination to the zirconocene complex.

Scheme 3.16 Conversion of the **4**-zirconocene complex monochloro-,monosilyl-zirconocene catalyst to the catalytically active monohydrido-,monosilyl- zirconocene complex

Scheme 3.17 Catalytic mechanism by which the in situ zirconocene catalyst produces the **5a/5b** disilane through the active hydride-, silylzirconocene catalyst.

Scheme 3.18 Catalytic dehydrocoupling of **4** using Cp_2ZrMe_2

Scheme 3.19 Formation of the active catalyst for the Rh(I) catalysts; $[Rh(cod)Cl]_2$ (Top) and $Rh(PPh_3)_3Cl$ (Bottom).

Scheme 3.20 Proposed mechanism for dehydrocoupling of **4** to **5** using $[Rh(cod)Cl]_2$ via oxidative addition/reductive elimination

Scheme 3.21 Proposed mechanism for dehydrocoupling of **4** to **5** using $Rh(PPh_3)_3Cl$ via oxidative addition/reductive elimination.

Scheme 3.22 Proposed σ-bond metathesis mechanism step for the formation of the 5a/5b disilane.

Scheme 3.23 Catalytic intramolecular dehydrocoupling reaction results of previous research for the bis(phenylsilyl)ferrocene) (**7a**) disilyl precursor with the $Rh(PPh_3)_3Cl$ and Cp_2ZrCl_2/2nBuLi catalysts.

Scheme 3.24 Depiction of two pathways for siloxane synthesis; through facile insertion of H_2O to a disilane (**8**) (Top) or through rhodium-catalysed siloxane formation (Bottom).

Scheme 3.25 $[Rh(cod)Cl]_2$ catalysed dehydropolymerisation of the ferrocene-bridge **7a** substrate.

Scheme 3.26 Synthetic approach for the synthesis of the **7a** and **7b** disilyl precursors.

Scheme 3.27 Reaction Scheme indicating the lithiation of the ring instead of the zirconocene

Scheme 4.1 Proposed synthesis of a di(benzyl silane) precursor through Grignard methods with a chloro(methyl)silane reagent.

Scheme 4.2 Proposed dehydropolymerisation scheme whereby two catalysts; 1 & 2, are utilised for poly(5b) synthesis. Catalyst 1. = Intramolecular dehydrocoupling catalyst and Catalyst 2. = Intermolecular dehydrocoupling catalyst.

Scheme 4.3 Proposed dehydropolymerisation scheme for the naphthalene-bridged disilane with methyl species bound to each silicon.

List of Tables:

List of Abbreviations:

Cal'd	Calculated
cod	1,5-Cyclooctadiene
Cp	Cyclopentadienyl
Cp_2ZrCl_2	Zirconocene Dichloride
dmpe	1,2-bis(dimethylphosphino)ethane
dppe	1,2-bis(diphenylphosphino)ethane
ESI	Electrospray Ionisation
ESI-MS	Electrospray Ionisation Mass Spectrometry
MeLi	Methyllithium
*n*BuLi	n-Butyllithium
NMR	Nuclear Magnetic Resonance
PDHS	Poly(di-hexyl-silane)
PPh_3	Triphenylphosphine
$[Rh(cod)Cl]_2$	Chloro(1,5-cyclooctadiene)rhodium(I) dimer

Chapter 1. Introduction

1.1 Silicon presence within modern electronics

Silicon is a ubiquitous element, abundantly present in nature and throughout all areas of society. As the second most abundant element within the Earth's crust, most individuals encounter silicon everyday through its incorporation within modern electronic devices. Silicon is the 5th most abundant element in modern smart phones, accounting for 6 % of the phone's weight.[1] This exists as crystalline silicon, found within in the microchip and device transistors as a semiconducting materials, as well as within solar cells.[2] Electronic construction contributes 5 % of total silicon production each year, typically in the form of silicon wafers.[1] The use of silicon in electronics is so well-acknowledged, America's epicentre of high technology is commonly referred to as 'Silicon Valley'. The application of silicon within modern electronics relies on the "switchable" nature of crystalline silicon as an electronic-conducting material. Industrial methods rely on exposing pure silicon to form a protective silica layer, which is selectively degraded to allow a controlled flow of current within the microchip. Dopants are frequently added to the material to increase conductivity (Table 1.1).[3] The low cost and availability of silicon at large scales allows for commercial dominance other alternative semiconducting materials such as GaN[4] and Ge.[5]

Table 1.1 *Relative Resistivity and Conductivity values for selected metals and materials.*[6]

Material	Resistivity (Ω cm^{-1})	Conductivity (Ω^{-1} cm^{-1})
Rubber	1-100 × 10^{13}	1-100 × 10^{-15}
Glass	1-10000 × 10^{9}	1-10000 × 10^{-13}
Graphite	3-60 × 10^{-5}	1.67-33.3 × 10^{3}
Germanium	1-500 × 10^{-3}	2.0 -1 × 10^{3}
Silicon	0.10 – 60	1.67 × 10^{-2} – 10.0
Silver	1.63 × 10^{-8}	6.17 × 10^{7}
Copper	1.72 × 10^{-8}	5.95 × 10^{7}

Commercial research strategies to optimise the use of silicon in silicon wafers has primarily followed doping approaches. These involve the addition of pentavalent[7] or trivalent metals[8] as doping agents for both N- and P-type doping respectively. These strategies utilise the metalloid nature of Si to control electron or electron hole flow within crystalline silicon. However, non-crystalline silicon semiconductors have been developed with the goal of creating a less rigid, more flexible silicon semiconductor. Polysilane compounds have been identified as capable semiconductors with potential application within modern electronics.[9] Polysilanes are organosilicon polymers consisting of a catenated Si-Si backbone. The delocalisation of σ electrons along the Si-Si backbone imparts a semi-

conducting character.[10] The conductivity of polysilanes has driven the development of polysilanes as flexible silicon-based semiconductors for the replacement of crystalline silicon within modern electronics.

1.2 Stability of the Si-Si bond in Polysilanes

This σ-conjugation along the Si-Si backbone is source for the unique properties of polysilanes. This conjugation allows polysilanes to exhibit similar electronic properties to π-conjugated materials. The σ-conjugation arises through the non-dispersive charge transport of electron holes throughout the Si-Si backbone.[11] However, the weak nature of the Si-Si allows for facile cleavage of the disilane.[12] Cleavage of the Si-Si bond may proceed through homolytic degradation or exposure to UV irradiation ($\lambda < 254$ nm) or strong nucleophilic reagents (Na, K). The susceptibility of the Si-Si bond to homolytic degradation has been described through MO theory, where the low value for triplet σ_{SiSi}-σ^*_{SiSi} transitions weaken the Si-Si stability.[13] Facile cleavage of the Si-Si bond through homolytic degradation methods limits the stability of the polysilane and requires protection to maintain polysilane chain length. Additionally, the weak nature of the Si-Si allows for the insertion of nucleophiles between the two silicon atoms. The electropositive nature of silicon combined with a relatively large size makes silicon increasingly susceptible to nucleophilic attack.[14] Polysilanes in the presence of water will react to form siloxane bonds (Figure 1.1). Siloxane bonds are more thermodynamically stable than disilanes as evident through their relative bond energies (452 kJ mol^{-1} vs. 197 kJ mol^{-1} for Si-O vs. Si-Si).[6] While siloxane bonds enhance the thermodynamic stability of the silane polymer, the degradation of the Si-Si backbone results in the loss of σ-conjugation and inherent semiconducting character of the polymer. This places a requirement for polysilane applications, whereby storage and application require moisture-free environments.

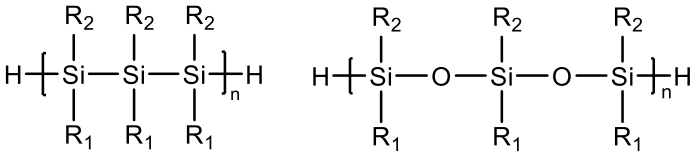

Figure 1.1 *Structural formula for polysilanes and polysiloxanes. R_1, R_2 = Alkyl or aryl, n = number of repeat units.*

1.3 Properties and Applications of Polysilanes

1.3.1 Semiconducting properties and applications

It was initially proposed the semi-conducting property was a consequence of a loss of electron from the Si-Si bonding orbitals. However, subsequent investigations confirmed identified electron holes as the charge carrier for σ-conjugation.[15] Theoretical investigations of the electronic states of polysilanes identified charge carrier generation occurs through light absorption with experimental results indicating electron hole generation. Band-to-band transitions were not supported as potential source for charge

carrier generation as only singlet excitons were observed through photon absorption.[16] Light absorption produces an electron hole is then delocalised across the entire polysilane backbone**.** As the number of dimer units within the chain increases, the wavelength of the absorption maxima decreases, signifying an increase to the energy of the σ-σ* transition. The σ-conjugation in polysilanes is heavily dependent on the conformation of the Si-Si backbone of the polysilane, observable through UV/vis spectroscopy. [17,18] This has consequently resulted in the conductivity of the polysilane being dependent on the conformational structure of the polysilane.[19,20] The structural conformation of oligosilanes, specifically the dihedral angles are noticeably different to organic chains. This is due to the steric repulsion present between the side groups of positions 1,3 and 1,4 in the polysilane chain.[21] Oligosilanes possess their own proposed naming system for the dihedral angles (Figure 1.2).[22] These incorporate the same dihedral angles as organic (*anti*, *ortho* & *gauche*), with the addition of transoid (ω ≈ 165°;), deviant (ω ≈ 150°;), ortho (ω ≈ 90°;) and cisoid (ω ≈ 40°;). Dihydropolysilanes are the only polysilane compounds to exhibit conformation behaviour like their organic polymer analogues.

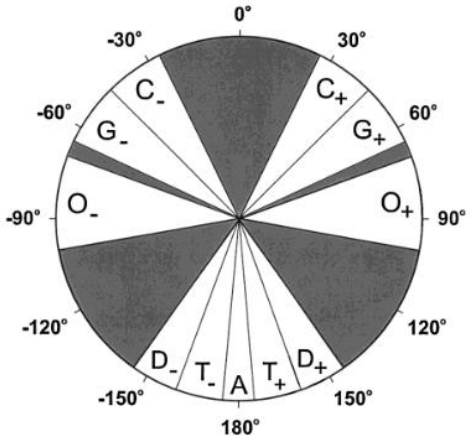

Figure 1.2 *Diagram of the dihedral angles within polysilanes with the suggested symbols from Michl & West.*[22]

In contrast to organic semiconductors, polysilanes possess a great degree of conformational freedom while maintaining electronic conductivity. The π-bonding within organic semiconductors restricts free rotation severely. However, the angles in polysilanes are all approx. tetrahedral, due to no d-orbital participation within the system.[23] As electron hole transport occurs through the σ-bonding orbitals of Si-Si, polysilanes experience a lack of rotational restriction[24] while allowing σ-delocalisation.

A study by Tsuji et al[25] utilising di-bridged silane dimers was able to investigate the dependency between conformational change and the σ-σ* transition via UV spectroscopy. The di-bridged dimers were designed to limit the geometry of the specific silyl centres. It was confirmed the absence of an *anti*-conformation Si-Si bond displayed no sharp peak within the UV spectra, with a sharp peak around 240 nm only observed in the presence of the *anti*-conformation. This conclusion was supported by configuration interaction-space calculations.

However, the configurations of the polysilane substituents play a significant role in the maintenance of σ-conjugation throughout the polysilane. The presence of cisoid turns added to the terminal of the polysilane failed to increase the length of σ-conjugation throughout the backbone,[25] indicating the transoid conformational requirement for extension of σ-conjugation through the Si-Si backbone. It was observed the HOMO-LUMO band of all transoid polymers decreased rapidly with continued extension of polysilane chain length. This decrease was significantly reduced for cisoid-containing polysilanes. The conformational impact on conductivity is observed between linear polysilanes possess higher conductivity values over cyclic silanes, as they more readily adopt transoid conformations that maximises σ-electron delocalisation**.**

As the configuration of the substituents bound has a significant impact on σ-delocalisation throughout the polysilane Si-Si backbone, this must be considered during the synthesis of polysilanes as potential semiconductors. With transoid conformations reported to maximise the length of σ-conjugation and improve conductivity, the focus for catalytic dehydrocoupling is ensuring stereoselective synthesis of the chiral disilane diastereomers.

Additionally, the nature of the substituents bound to the polysilane may contribute towards σ-conjugation. West et al was the first to show aryl substituents can stabilise electron hole formation through by indirect oxidisation of the Si-Si bonds.[26] This is supported by the observation where the incorporation of aryl substituents into the polysilane improves the conductivity of the polysilane in comparison to alkyl species.[27]

1.3.2 UV Absorption and Thermochromism

The σ-conjugation present with polysilane is responsible for other physical properties of polysilanes, including the strong UV absorption observed for polysilanes when dissolved in solution.[17] UV absorptions correlate to the σ_{SiSi}-σ^*_{SiSi} energy transitions present within the Si-Si bonds, the same transition responsible for the σ-electron delocalisation along the Si-Si backbone.[28] Dialkyl substituted polysilanes possess absorption maxima in the 300 – 325 nm range, with a red-shifts of 25-35 nm with each substitution of an alkyl group for an aryl species.[29] As the degree of polymerisation increases for a polysilane, the absorption wavelength maxima (λ) will increase with until n = 40 to 50 units, where the value plateaus.[30]

The strong UV absorption observed with polysilanes in solution has allowed for observation of the thermochromic properties of polysilanes.[31] Polysilane thermochromism is evident by the absorption maxima red-shift peaks observed under low temperatures. This red-shift, correlating to the rearrangement of the Si-Si backbone, indicates under low temperatures the silicon backbones arrange into *trans* conformations.[30] The adoption of trans conformation throughout the backbone increases the degree of σ-conjugations, producing the observed for the red shift. Polysilanes under high temperatures exhibit the opposite behaviour with blue-shifts. Bukalov et al.[32] conducted a series of thermochromic

studies on solutions of PDHS (poly(di-hexyl-silane) to at three temperatures.[32] At room temperature (20 °C), PDHS absorbs at 320 nm in the UV region. Decreasing the temperature produced a second red-shifted signal peak at 357 nm. This intensity increased under continued decreased in temperature, at the cost of intensity of the 320 nm peak. It was proposed the peaks correlated to the ordered (357 nm) and disordered (320 nm) states of the polysilane

However, while polysilanes are strong absorbers of UV radiation, excessive exposure of UV irradiation facilitates Si-Si bond cleavage with radical rearrangements resulting in chain degradation. This disrupts the σ-conjugation throughout the Si-Si backbone. Photodegradation of polysilanes using UV light (λ < 254 nm) converts polysilanes into smaller monomeric silylene subunits and a terminal-based silyl radical polymer (Scheme 1.1). The photodegradation mechanism is observable through the addition of triethylsilane as a trapping agent.

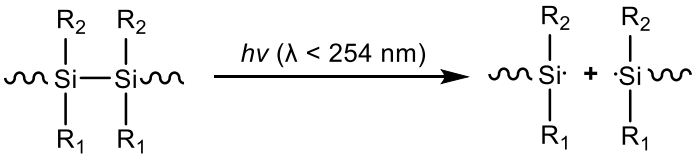

Scheme 1.1 *Photolytic degradation of polysilanes.*

Photodegradation produce a mixture of reaction products; siloxanes, cyclic polysilanes and low M_W linear oligosilanes. Siloxane formation occurs favourably in the presence of water and moisture through rearrangement reactions. Under inert and moisture-free conditions, linear and cyclic polysilanes are both favoured with cyclic polymer formation favoured under very dilute conditions.[33] Thermodynamic calculations of the mechanism determined one photon possesses insufficient energy to produce two radicals. Repeated UV photon exposure was required for degradation to proceed.

1.3.3 Photoconductivity and Optoelectronic Applications

The ability of polysilanes to strongly absorb UV radiation allows for their application within photoconductive materials. While excessive exposure to UV irradiation degrades the Si-Si backbone of polysilanes, controlled irradiation allows for the photoconductivity properties of polysilanes to be observed. The photoconductivity of polysilanes were studied in detail with the poly(methylpropyl)silane by Fujino et al.[15] Utilising a sandwich-type cell with a quartz substrate, a layer of the polysilane was sandwiched by a Gold/ITO electrode, with deposition of a gold layer ensuring transparency for the top side of the device. It was determined the photocurrent to be linearly dependent on the irradiated light intensity, with the electron holes to be the source of conductivity. Generation of the electron holes was proposed to occur photochemically with the absorption of light. Subsequent investigations have focused on identification the causes for charge transport along the polysilane backbone.[34] Confirmation that charge transport proceeds through the Si-Si backbone was provided by Abkowitz et al.[35] using Time of Flight techniques. Subsequent studies confirmed charge transport is

associated the σ-conjugation.[11,16] This association with σ-conjugation lead to proposals of a conformational dependence for hole delocalisation, supported by high charge mobility rates were observed for polymers in the *trans* conformation. This is conformation dependency has been confirmed by a recent theoretical study.[36]

Studies investigating the conformational dependency of polysilane conductance has relied on the measurement of polysilanes conductivity through the use of scanning tunnel microscope (STM) break junction techniques.[37] Use of this techniques relies of the modification of the silane terminal ends with thiol functionalities. Li et al[38] revealed using the above technique the confirmed the difference in conductivities between cis and trans isomers, and cyclic vs. linear polysilanes. This study and other similar studies showed cyclic polysilanes possess lower conductance values in comparison to their linear polysilane analogues. This has been proposed to be due to diminished σ-conjugation along the Si-Si backbone, limited by the absence of the *anti*-conformation inherent within linear chains. Emanuelsson et al[39] further revealed a difference in conductivity between *trans* isomers with respect to the substituents position. Polysilanes in a *trans* conformation with substituents both in the equatorial positions exhibit greater conductance than conformers where the substituents are both *trans* and in the axial positions.

Initial studies into the role of substituents on polysilane photoconductivity indicated photoconductivity proceeds regardless of the nature of the substituents of the polysilane chain.[35] However, it was observed aryl-polysilanes possess greater conductance values than their alkyl analogues. This observation was confirmed in doping studies, revealing the use of dopants can control the electronic conductivity of the polysilane.

Fukushima et al. confirmed selective substituents (i.e. aryl species) were able to optimise conductivity, withs doped polysilanes containing aryl species possessed greater conductivities over their doped alkyl analogues.[40] It was additionally observed doping of polysilanes through vapor-deposition techniques yielded higher conductivities than through solution phase techniques. This was contributed to the presence of moisture within the solvent, facilitating Si-Si degradation. The addition of N-type dopants further increases the migration rate of electron holes and conductivity of the polysilane. The use of C_{60} buckminsterfullerene as a dopant has allowed for polysilane application within organic solar cells.[41,42] The use of dopants is supported by the low oxidation potentials of polysilanes, a consequence of the σ-conjugation.[43]

The photoconductivity of polysilanes are utilised within the fabrication of thin film layers.[18,43] However, they are most frequently been applied within photolithography systems[24] and as photoresists.[12] Poly(methylphenylsilane) and poly(methylpropylsilane) have both been applied as photoresists within photolithography processes.[15] This is proceeds through bleaching of the polysilane under UV irradiation. This process involves placing a polysilane layer above the silicon wafer where post UV

exposure, the degraded polysilanes was washed away using a positive photoresist developer to produce a specifically designed pattern of polysilane on the silicon wafer. Subsequent chemical etching processes imprint the pattern into the silicon wafer.[44]

1.3.4 Silicon Carbide Properties and Applications

While the interesting properties of polysilanes have direct recent attention towards potential application in modern electronics, polysilanes have been commercially utilised since the 1980's with the discovery of ceramic silicon carbide (SiC) synthesis through polysilanes. This application relies on the weak nature of the Si-Si and facile cleavage for the synthesis of high tensile strength ceramic silicon carbide. Silicon carbides have been commercial mass produced since 1893.[45] SiC's stability under extreme temperatures and high voltages lead to their use as semi-conductors within light-emitting diodes (LEDs) [46]and detector[47] devices. However, modern manufacture focuses on silicon carbide's ceramic properties for applications. Previous synthetic procedures for ceramic SiC required very extreme temperatures (T > 2500 °C).[12] The use of polysilanes in silicon carbide synthesis has become the industrial standard for commercial ceramic silicon carbide synthesis.[48] This entails the thermal degradation of the polysilanes under inert conditions at 1300℃ to produce β-silicon carbide, obtained in high yields (Scheme 1.2). The reaction proceeds through pyrolysis of the poly(dimethyl)silane polymer. During pyrolysis, one of the methyl substituents bound to each silicon is inserted within the Si-Si bonds, forming the polycarbosilane compound. Through a second step, the polycarbosilane is converted to the fibrous β-silicon carbide. The production of a more tensile product at a low reaction temperature (1300 °C vs 2500 °C) led to this procedure to become the dominate commercial synthetic strategies.[49] Subsequent investigations have broadened the potential scope of polysilane substrates largely focused on expansion of varied alkyl groups.

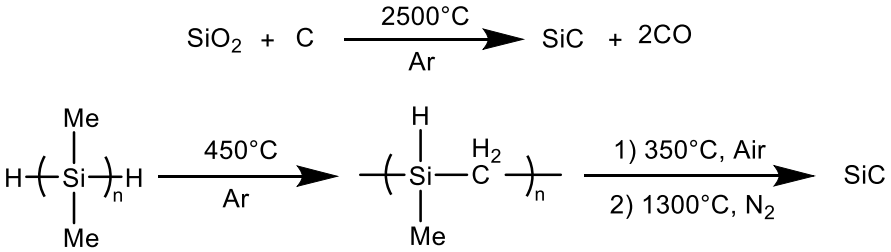

Scheme 1.2 *Synthesis of silicon carbide through silicon dioxide w/ graphite and polysilane (n = number of repeating units)*

1.4 Synthesis of Polysilanes

Strategies towards polysilane synthesis have been designed to incorporate a range of silane substrates. The unavailability of unsaturated Si monomers suitable for addition polymerisation have driven attempts to develop a range of silane polymerisation mechanisms for a variety of silane substrates.

Discussed below are a notable selection of varied polymerisation strategies developed for polysilane synthesis of varied silane substrates.

1.4.1 Reductive Coupling

Polysilane synthesis was first achieved through the condensation of dichlorodisubstitutedsilanes through the addition of sodium metal under heat (Scheme 1.3). The driving force for Si-Si coupling is the elimination of a salt (typically NaCl). This Wurtz-style reaction was reported for poly(diphenyl)silane in the 1920's[50] producing highly crystalline white solids, insoluble in common organic solvents.[50] While research over the last 75 years has aimed to displace it, Wurtz-style coupling methods remain the dominant synthetic strategy for polydialkylsilanes and polydiphenylsilanes.[51,52]

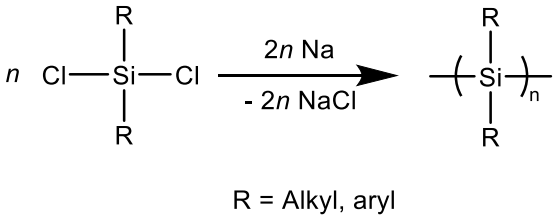

Scheme 1.3 *Wurtz-style coupling of di(disubstituted)chlorosilane (n = number of repeating units).*

Wurtz-coupling approaches possess specific limitations regarding polymer synthesis. The formation of NaCl salts at a large scale requires purification for characterisation of the product polysilane. Use of the strong and harmful reagents required for successful silane formation requires additional treatment of the salt waste post-separation for proper and safe disposal. Lack of control over polymer chain length produces polysilane chains with large molecular weight distributions.[50]

1.4.2 Ring Opening Polymerisation

Polysilane Ring Opening Polymerisation (ROP) reactions require cyclic silane substrates which are exposed to an anionic initiator to "open" the cyclic monomer to produce a linear polysilane chain (Scheme 1.4, Step I). Initiators react to produce a reactive terminal silyl anion. These may include organolithium compounds (RLi) or tertiary anionic silanes ($R_3Si^-K^+$) Chain propagation (Scheme 1.4, Step II) proceeds until termination, controlled through the presence of alcohol as a terminating agent[14,53].

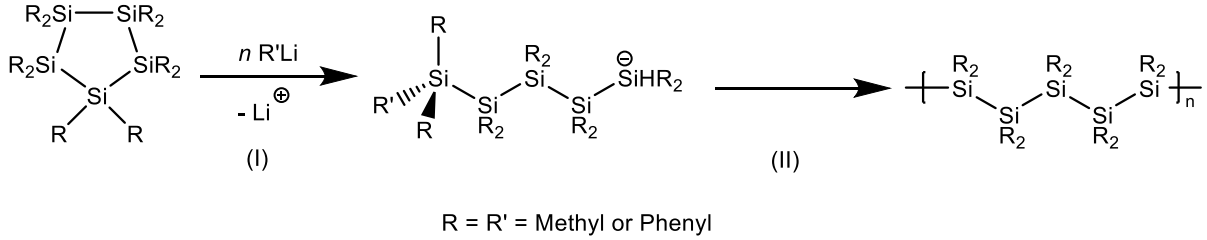

Scheme 1.4 *Proposed mechanism for ring-opening polymerisation of cyclic silanes using an organolithium initiator (n = number of repeating units).*

1.4.3 Electroreductive synthesis

Electroreductive methods for polysilane synthesis were first proposed by Kashiumura et al., in 1999.[54] This approach used dichlorosilane substrates with a Mg electrode and $LiClO_4$ as the electrolyte.). Mechanistic investigations failed to clearly identify the precise mechanism. The proposed polysilane synthesis mechanism occurs through a step-growth polymerisation method. Initiation occurs through reduction of the substrate to a silyl anion, which undergoes dimerization with another dichlorosilane equivalent. Subsequent chain growth proceeds through reactions with (more and more) silyl anion equivalents (Scheme 1.5). It was observed sonication of the reaction mixture increased the polymer yield.

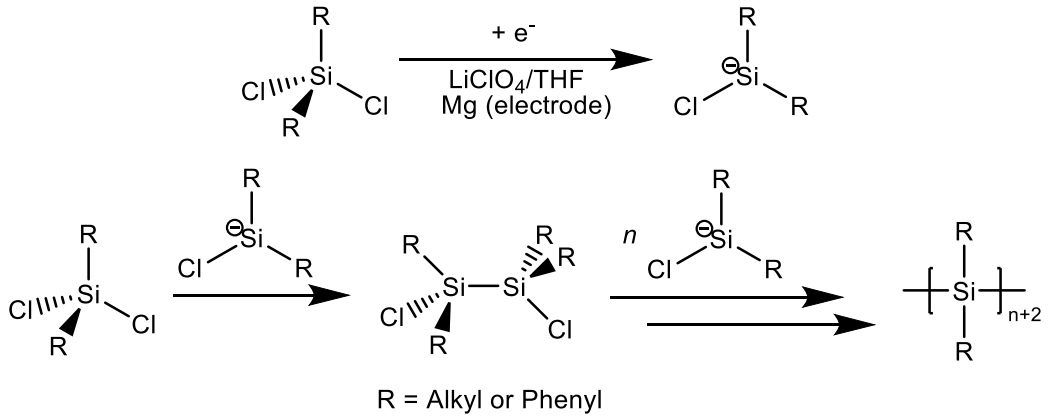

Scheme 1.5 *Proposed mechanism for the electroreductive synthesis of dichlorosilanes (n = number of repeating units).*

1.4.4 Dehydrocoupling

Dehydrocoupling reactions have rapidly gathered momentum within synthetic chemistry due to their potential to efficient replace the use of Wurtz-style reactions. Dehydrocoupling reactions provide synthesis routes to cleanly synthesise the desired product from E-H substrates without addition of environmentally harmful by-products.[55] The dehydrocoupling ability of transition metal catalysts for hydrosilane dehydrocoupling was discovered in 1965 with Wilkinson's catalyst ($Rh(PPh_3)_3Cl$). Dehydrocoupling reactions require two hydrosilane substrates (Si-H) in the presence of a suitable catalyst to produce a disilane product with hydrogen gas released as a by-product (Scheme 1.6).

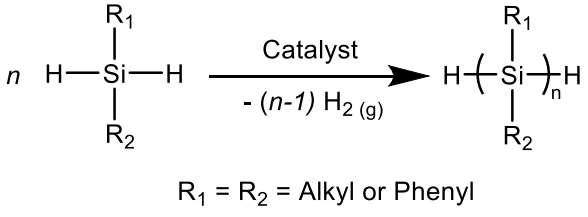

Scheme 1.6 *Catalytic dehydrocoupling reaction for secondary silanes (n = number of repeating units).*

Dehydropolymerisation occurs readily for primary and secondary hydrosilane substrates with most catalysts. Tertiary hydrosilane dehydrocoupling is more difficult due to increased steric factors and lower reactivity of the tertiary Si-H bonds.[56] Select catalysts have been reported to be capable of tertiary silane coupling. Karstedt's catalyst is capable of tertiary silane dehydrocoupling at room temperature and Wilkinson's' catalyst able to catalyse the reaction only under elevated temperatures. Potential dehydrocoupling catalysts for polysilane synthesis are divided into two main classes: late transition metals and early transition metal metallocenes. The two classes differ in reactivity, efficiency, and respective mechanistic pathways. However, a wide series of transition metal catalysts have been identified as capable of efficient silane dehydropolymerisation (Table 1.2).

Table 1.2 *Selected Data from various reported dehydrocoupling reactions for polysilane synthesis*

	Catalyst	Monomer	M_n	PDI
1	Cp_2ZrCl_2/*n*BuLi	$PhSiH_3$[57]	2075	1.18
2	Cp_2TiCl_2/*n*BuLi	$PhSiH_3$[58]	1000	1.5
3	Cp_2ZrMe_2	$PhSiH_3$[59]	1800	1.33
4	Cp_2ZrCl_2/*n*BuLi	cyclohexasilane[60]	2300	1.51
5	$Rh(PPh_3)_3Cl$	dihydro(tetraphenyl)silole[61]	5400	1.1
6	$Ni(dmpe)_2$	9*H*-9-silafluorene[62]	2260	1.08
7	$[(ApSi)_2Pd]$	$MeH_2Si\text{-}SiH_2Me$[63]	2200	1.4
8	$Pt(PEt_3)_3$	$MeH_2Si\text{-}SiH_2Me$[63]	2800	3.0
9	$Cp_2HfCl_2/B(C_6F_5)_3$	$PhSiH_3$[64]	7400	1.7
10	$Pt(cod)_2$	Me_2SiH_2[65]	3200	2.5
11	CpCp*Zr[$Si(SiMe_3)_3$]Me	$PhSiH_3$[66]	1700	1.8

Dehydrocoupling reactions possess distinct advantages over the limitations of the Wurtz-coupling reaction. Dehydrocoupling reactions can synthesise polysilanes under mild reaction conditions. with more selective control over polymer chain length and linear/cyclic nature.[67] The use of hydrosilanes presents a reduced safety concern in comparison to dichlorosilanes. The elimination of hydrogen gas from the reaction mixture aids subsequent purification the reaction mixture. Additionally, select catalysts are capable of dehydrocoupling reactions under neat conditions.[68]

The thermodynamics behind dehydrocoupling reactions indicated reactions proceed to completion with efficient removal of $H_{2(g)}$. Polysilane formation is strongly inversely dependent on the concentration of hydrogen gas in solution. Kinetically, the dehydrocoupling reactions and the reverse hydrogenolysis reaction are sensitive to hydrogen concentration. This requirement to ensure efficient $H_{2(g)}$ removal has

driven dehydrocoupling reactions to be frequently conducted under inert glove box or *in vacuo* conditions.

1.5 Hydrosilane Dehydropolymerisation Catalysts

1.5.1 Late transition metal dehydrocoupling catalysts

The discovery of Wilkinson's catalysts' ability to catalyse silane dehydropolymerisation focused initial catalyst design research towards late transition metal catalysts. Since then, subsequent investigations have expanded the potential scope of metal catalysts. These include Rh[69–71], Pt[65,72,73] , Ni[62,73–75], Ir[76] & Pd[63] catalysts. These catalysts rely on a series of oxidative addition and reductive elimination cycles for dehydrocoupling and polysilane synthesis. Oxidative addition of the hydrosilane to the metal centres is frequently necessary for activation of the catalyst. This proceeds through devolution of the hydrosilane as two ligands; hydride and silyl ligand (Scheme 1.7). While oxidative addition of the hydrosilane occurs for most late transition metal catalysts, σ-bond metathesis mechanisms have been proposed for select catalysts, such as for dinuclear Rh complexes bridged by silyl ligands.[77]

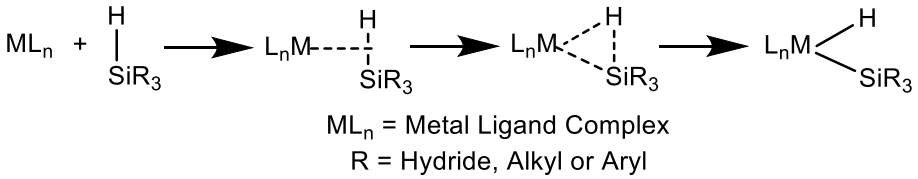

Scheme 1.7 *Coordination of hydrosilanes to a transition metal complex through oxidative addition.*

Investigations into transition metal catalysts for dehydrocoupling polysilane synthesis agree late metals typically exhibit greater dehydrocoupling rates over their early transition metal counterparts. This is most true for rhodium and platinum catalysts. Both metals have reported the synthesis of tertiary-coupled polysilanes using Karstedt's catalyst (Pt) at room temperature[72] and Wilkinson's catalyst (Rh) under extreme temperatures (>100C).[69] However, the expensive nature of Rh and Pt catalysts has directed research towards less scarce transition metal complexes. Additionally, this high activity can come at the cost of selectivity with large molecular weight distribution values observed.[72] Platinum complexes frequently reactions facilitate redistribution of the alkyl/aryl substituents in addition to low selectivity towards dehydrocoupling. A mixture of cyclic and short-chain linear oligosilanes are typically obtained from dehydrocoupling reactions. However, select Pt catalysts have shown promise with greater dehydrocoupling selectivity. These include $Pt(cod)_2$, capable of polysilane synthesis for aliphatic secondary silanes with yields > 90 %. Additionally, they have been shown to catalyse dehydropolymerisation of a silafluorene substrate[65] (Scheme 1.8).

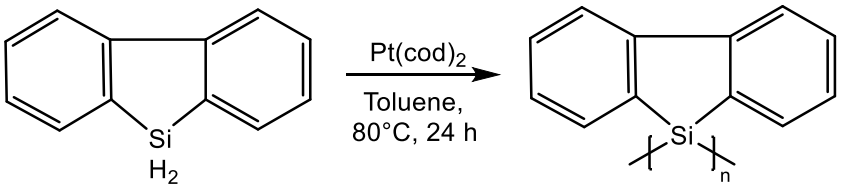

Scheme 1.8 *Report dehydrocoupling of a dihydrosilafluorene substrate.*[65]

Attempts to diversify dehydrocoupling catalysts away from expensive and rare Pt catalysts have driven focus towards nickel-based catalysts. Nickel catalysts received limited interest as a dehydrocoupling catalyst as many nickel catalysts required activation of a nickel-hydride (Ni-H) functionality by an activating agent ($LiAlH_4$).[78] However, a range of nickel-based catalysts have been identified possessing phosphine-type ligands (Figure 1.3). This class of catalysts have exhibited efficient polymerisation of primary and secondary silanes for linear or cyclic polysilanes. The $[(dippe)Ni(\mu\text{-}H)]_2$ catalyst is reported as a capable dehydropolymerisation catalyst for primary and secondary silanes, synthesising $(PhSiH)_n$ and $(PhSiMe)_n$ linear oligosilanes (n = 10 – 16).[59] Use of a $[Ni(dmpe)_2]$ catalyst has exhibited dehydrocoupling ability for a 9H-9-silafluorene substrate.[62]

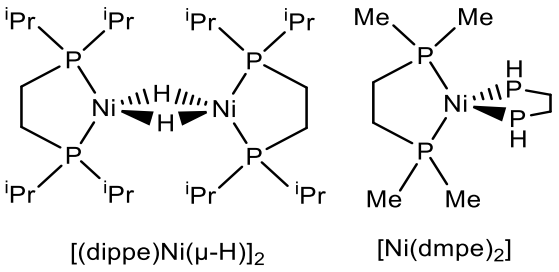

Figure 1.3 *Structures of the Nickel-based dehydrocoupling catalysts reported for polysilane synthesis.*

Iridium catalysts have also been investigated. Due to the known silane redistribution reaction catlaysed by iridium, it was postulated pincer ligand Ir complex (POCOP-Ir) compounds (POCOP = 2,6-$(^tBu_2PO)_2C_6H_3^-$) for catalytic dehydrocoupling and synthesis of polysilanes. An iridium-pincer complex (Figure 1.4) was reported to undergo dehydropolymerisation of phenysilane to form cyclic polysilanes with high selectivity. The major product was the cyclic decasilane polysilane, cyclo-$(PhSiH)_{10}$.[76]

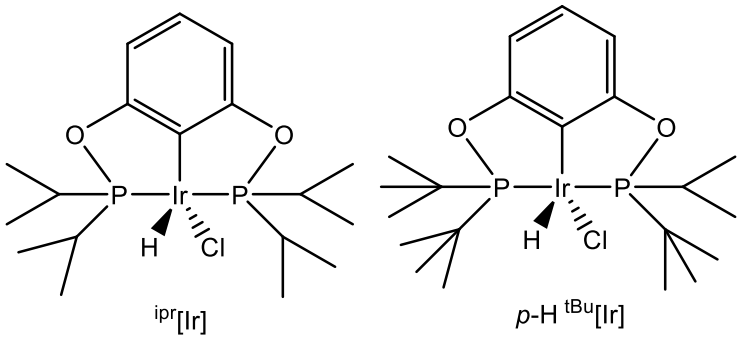

Figure 1.4 *Structures of the Iridium-Pincer based dehydrocoupling catalysts reported for polysilane synthesis.*[76]

As the potential scope of transition-metal catalyst were studied, lanthanide complexes were rapidly identified as high potential candidates.[79] It was proposed f-block metal-silyl complexes may be suitable dehydrocoupling catalysts as the metal-silicon bonds electronics for f-block metals are similar to the metal-silicon bonds for d-block metals. This is supported by the frequent application of lanthanide complexes as silane dehydrocoupling catalysts. However, the dominant use of lanthanide dehydrocoupling applications focus on silane dehydrocoupling with amines to form Si-N compounds.[80–83] Mechanistic investigations into lanthanide complexes confirmed dehydrocoupling proceeds through a sigma-bond metathesis processes.[84] This was supported by steric restraints observed for the catalyst. The catalyst $Cp^*_2LnCH(SiMe_3)_2$ (Ln= Sm, Nd) was unable to react with Ph_2MeSiH and Ph_3SiH substrates at room temperature over a week. However, addition of the primary silane $MesSiH_3$ (Mes = Mesityl) yielded successful dehydrocoupling, producing a dinuclear lanthanide complex bridged by hydrides ($Cp^*_2LnH]_2$) and the product disilane ($MeH_2Si\text{-}SiH_2Mes$). It was proposed the steric properties of the silane substituents, upon coordination of the silane to the Ln centre, may provide steric shielding to prevent further σ-bond metathesis reactions. This is proposed to be the case for secondary and tertiary silanes.

Numerous studies have been devoted to the expansion of non-Rh transition metal dehydrocoupling catalysts. However, rhodium catalysts remain the most investigated and well-understood with respect to their reaction conditions and mechanisms. Wilkinson's catalyst remains the standard rhodium-based dehydrocoupling catalyst for polysilane synthesis. Activation of Wilkinson's catalyst relies on oxidative addition of the hydrosilane. For oxidative addition to proceed rapidly low valent metals are required with a vacant coordination. Formation of the rhodium-silyl (Rh-Si) complexes typically contains Rh in the +3 oxidation state.

Activation of rhodium-based catalysts typically involves the dissociation of an ancillary ligand to create a vacant coordination site for hydrosilane oxidative addition. This behaviour is observed for Wilkinson's catalyst. This requirement may be voided in the case of rhodium-dimers and bimetallic catalysts, where the vacant coordination site is masked in the bimetallic state. Comparison of the

between Wilkinson's catalyst ($Rh(PPh_3)_3Cl$) against its dimeric form ($[Rh(PPh_3)_2\mu\text{-}Cl_2]$) (Figure 1.5) showed the dimeric state possessed similar turnover frequency rates (TOF) but faster consumption of the hydrosilane for the dimeric catalyst.[85] It was concluded addition of the catalyst as a dimer facilitates rapid coordination of the hydrosilane. However, after initial consumption of the hydrosilane, subsequent catalytic cycles for both ($Rh(PPh_3)_3Cl$) and ($[Rh(PPh_3)_2\mu\text{-}Cl_2]$) are identical and thus exhibit similar catalyst rates.[85]

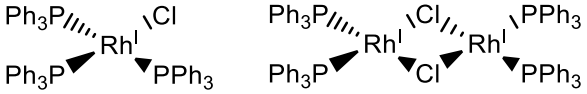

Figure 1.5 *Molecular structure of Wilkinson's catalyst ($Rh(PPh_3)_3Cl$) and the dimeric complex of Wilkinson's catalyst ($[Rh(PPh_3)_2\mu\text{-}Cl_2]$).*

Activation of Wilkinson's catalyst involves the formation of a chloro(hydrido)silyl rhodium(III) complex, produced from oxidative addition of the hydrosilane. The formation of the 5-coordinate trigonal bipyramidal complex is key for catalyst activation. Formation of the catalytically active rhodium-hydride (Rh-H) complex occurs through reductive elimination of a chlorosilane (Scheme 1.9)

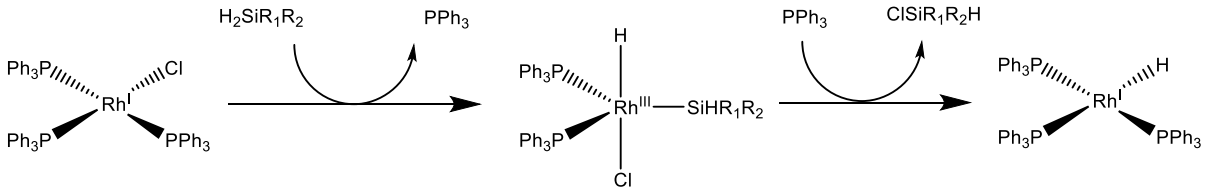

Scheme 1.9 *Activation of $Rh(PPh_3)_3Cl$ via dissociation of PPh_3 and reductive elimination of a chlorosilane*

X-ray diffraction and ^{31}P NMR results indicate the phosphine ligands adopt the axial positions during the 5-coordinate complex structures.[86] It is postulated the formation of the catalyst complex with the phosphine ligands in the *trans* configuration is required for successful dehydrocoupling reactions and Si-Si synthesis.[86]

This is supported through experiments conducted by Hughes[85] whereby two of the monodentate phosphine ligands of Wilkinson's catalyst were substituted with a bidentate 1,2-bis(diphenylphosphino)ethane (dppe) chelating ligand. Dehydrocoupling reactions between ($Rh(PPh_3)_3Cl$) and **(**$[Rh(dppe)_2\mu\text{-}Cl_2]$**)** showed the addition of the dppe ligand significantly lowered the catalytic activity to near zero Si-Si formation. It was postulated the bidentate ligand restrains the Rh-complex to cis-configurations, by which formation of the 5-coordinate complexes were inhibited and prevents continuation of the Si-Si catalytic cycle.

The general consensus for the mechanism of Wilkinson's catalyst dehydrocoupling utilises a series of oxidative addition and reductive elimination cycles with a Rh-H active catalyst.[70,86] In this mechanism,

catalytic dehydropolymerisation begins through oxidative addition of the hydrosilane to the Rh-H complex (Scheme 1.10, step I). This is followed by a reductive elimination of hydrogen gas and restoration of the metal oxidation state to +1 (Scheme 1.10, step II). Through coordination and oxidative addition of a second equivalent of hydrosilane, a di(metallo-silyl) complex is synthesised (Scheme 1.10, step III). Reductive elimination of both silyl ligands restores the metal centre to a +1 oxidation state, restores the catalyst to the initial active catalytic state (Rh-H) and releases the desired disilane product (Scheme 1.10, step IV). Subsequent polymer growth proceeds through re-entry of the disilane/oligosilane to the cycle at stages (I) or (III).

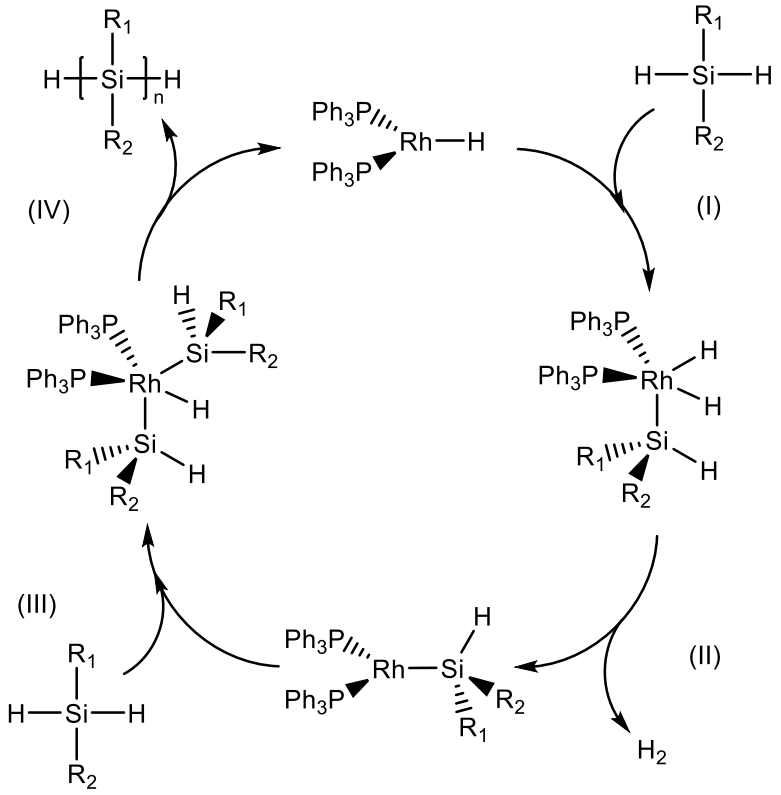

Scheme 1.10 *Oxidative addition (reductive elimination) mechanism for dehydrocoupling of secondary silanes by late transition metals.*

The other mechanisms proposed for Wilkinson's catalysts involve the radical approaches or metal-silylene catalytic intermediates. The role of the halide ligand observed for Rh catalysts is unclear. The use of catalysts without the Rh-X functionality, ($[Rh(cod)(PPh_3)_2]^+PF_6^-$) exhibited low dehydrocoupling rates.[85] However, comparison to the chelated **(**$[Rh(dppe)_2\mu\text{-}Cl_2]$**)** catalyst showed the former displayed slightly greater activity. It was concluded the role of the Rh-X functionality is to facilitate the creation of a vacant coordination site. This occurs through the kinetic trans effect, where the phosphine ligand trans relative to the halide ligand is thermodynamically weakened.[87] Through increasing the lability of a phosphine ligand, the rate of ligand dissociation in increased and activation of the catalyst proceeds at a greater rate.

1.5.2 Metallocene Dehydrocoupling Catalysts

During early studies for the discovery of transition metal dehydrocoupling catalysts, Group 4 metallocenes were rapidly identified for their catalytic potential. Group IV metallocenes catalysts in contrast to late transition metals catalyst dehydrocoupling reaction through completely different means. While notably less reactive in comparison to Rh and Pt-based catalysts**.** Metallocenes have displayed themselves as capable of producing the highest molecular weight polysilanes for primary silanes.[88] The dehydropolymerisation ability of metallocenes were first reported in the 1980's.[68] This was observed through the dehydrocoupling of primary silanes (i.e., phenylsilane) with the addition of Cp_2TiMe_2 at room temperature. Subsequent early metal catalysts have followed the Cp_2MX_2 template, (where M = Zr, Ti or Hf, R = Cp or Cp* and X = halide, alkyl, or silyl). The "X" ligand possesses a great degree of variability which may be utilised to optimise reaction conditions to optimise polymer properties. Metallocene catalysts follow predictable trends with regards catalytic activity, a consequence of the Cp_2MX_2 template. Zirconocene catalysts are the most efficient, followed by titanocene and hafnocene (Figure 1.6).[89] The dehydrocoupling activity for the Hf- and Ti- catalysts may be improved through increasing the reaction temperature to produce polysilane polymers of desirable chain length and yield. Additionally, zirconocene catalysts favour higher linear: cyclic polysilane ratios than Ti- and Hf-metallocenes with greater molecular weight values for oligosilanes.[90,91]

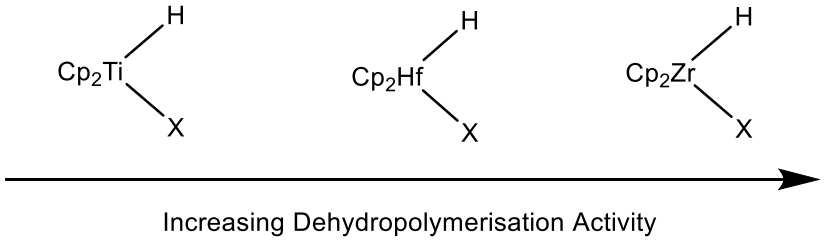

Figure 1.6 *Trend in Group IV metallocene dehydrocoupling catalytic activity with varied metal centres.*[92]

Careful selection of the metal centre for dehydrocoupling catalyst is required where the stereoselectivity of the polysilanes are significant. Numerous studies have detailed the mixed stereoselective exhibit for zirconocene catalysts, where meso and chiral isomers are formed in non-equivalent quantities. In contrast, titanocene catalysts have exhibited great reliability in the selective formation of trans isomers for polysilanes. The use of a bimetallic titanocene catalyst was capable of catalysing dehydrocoupling towards the formation of an all-trans cyclic hexa(phenyl)silene ($[PhSiH]_6$) product.[93,94]

Mechanistic investigations for metallocenes reveal the universal presence of σ-bond metathesis reactions within dehydropolymerisation synthesis. While mechanisms vary significantly between specific metallocene catalysts, dehydropolymerisation for all group 4 metallocene catalysts proceed through a series of σ-bond metathesis reactions involving successive, concerted, 4-centre transition states.[88] Addition of a hydrosilane results in the formation of metal-silyl and metal-hydride complexes

through σ-bond metathesis reactions, where the dehydrocoupling and disilane formation are observed concurrently. Polysilane chain elongation proceeds through step-growth means.[66] Employment of poor π-donor ligands to the metallocene is shown to increases catalytic activity, due to the electron-poor nature of the Group IV centre. The most used poor π-donor ligands are alkyl, hydride, and tertiary silane ligands (Figure 1.7).

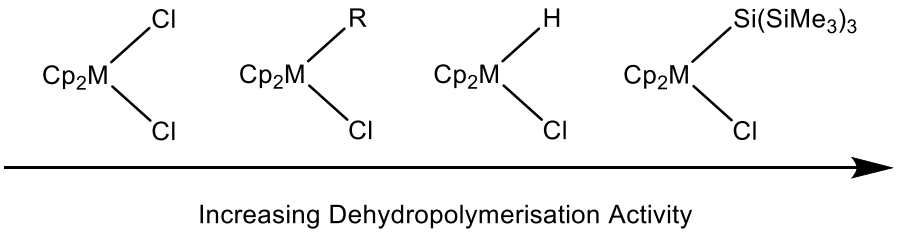

Figure 1.7 *Trend in Group IV metallocene dehydrocoupling catalytic activity with varied ligands.*[92,95]

The reliance on sigma-bond metathesis reactions for dehydrocoupling means that the steric factors of the silane substrate play a greater role on the catalytic activity. The sterically limiting transition state places a greater degree of strain on bulky substrates. This is shown through the high activity of most metallocene catalysts for primary silane dehydrocoupling and the more extreme reaction conditions required to facilitate polysilane synthesis. No metallocene catalysts have yet to be reported capable of efficient tertiary silane dehydrocoupling.[69]

The active catalysts for metallocene catalysts may vary, with two predominant supported mechanisms. The majority of metallocene catalysts proceed through dehydropolymerisation using an unsaturated metal-hydride (M-H) active catalyst. Formation of the active state metallo-hydride species relies on displacement of the chloride ligand through alkyl lithium reagents (Scheme 1.11, step I). This produces a metallo-alkyl species, which is converted to a metallo-silyl complex through interaction of the complex with a hydrosilane (Scheme 1.11, step II). This metallo-silyl complex can react with a hydrosilane equivalent to produce a monohydride metallocene species producing a disilane as a by-product (Scheme 1.11, step III).

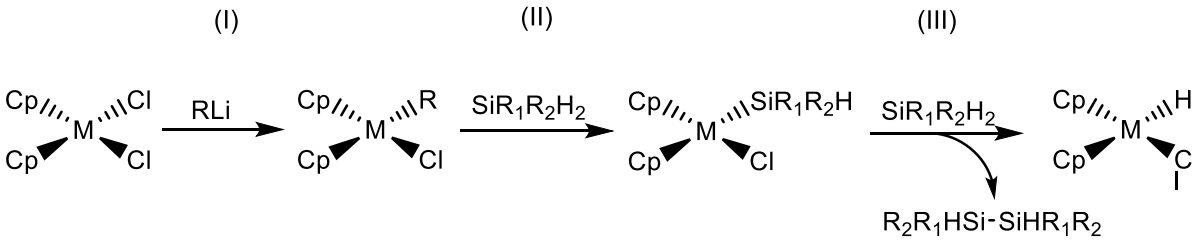

Scheme 1.11 *Activation of the metallocene catalyst using alkyl lithium for polysilane dehydrocoupling synthesis. R_1, R_2 = Alkyl, aryl, hydride.*

The displacement of the alkyl ligand forms the metallocene is a reaction rate limiting step, with induction periods observed dependent on the alkyl ligand present. The addition of MeLi produces a metallo-methyl complex, where the relatively strong strength of the Zr-C bond in comparison to Zr-Si means that the substitution rate is slow and is observed experimentally by an induction period of a few hours before bubbling is observed. However, the addition of *n*BuLi to the metallocene produces a metallo-butyl complex, which may undergo a β-hydride elimination to release the ligand as free butane. This β-hydride elimination facilitates removal of the alkyl ligand and allows for rapid catalyst activation where no induction periods are associated with the addition of *n*BuLi.

Following formation of the active catalyst, the catalytic cycle for the metallo-hydride active catalyst begins with the coordination of a hydrosilane to the active catalyst (Scheme 1.12, step I). Coordination of the silyl ligand involves a σ-bond metathesis reaction. This occurs in a concerted fashion through a four-centre transition state. This step produces a metallo-silyl complex and release of gaseous H_2 (Scheme 1.12, step II). Coordination of a secondary hydrosilane with the metallo-silyl complex forms via another σ-bond metathesis reaction (Scheme 1.12, step III). This reaction restores the metallo-hydride catalytic species and elimnates both silyl ligands as a the desired disilane product (Scheme 1.12, step IV) which upon coordination with a second hydrosilane releases the silane product and the catalytic cycle continues.

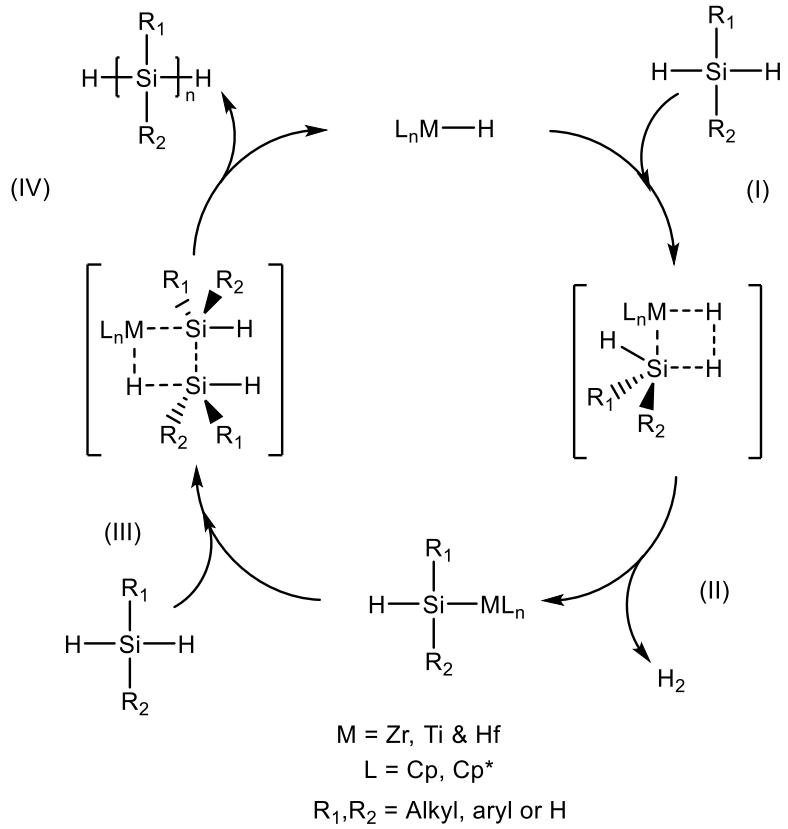

Scheme 1.12 *General silane dehydrocoupling mechanism for σ bond metathesis.*

Metallocene catalysts using this mechanism such as dimethyl zirconocene (Cp_2ZrMe_2), prove highly efficient towards the dehydropolymerisation for primary silanes under mild reactions conditions.[93,96] In contrast, secondary silane dehydropolymerisation does not proceed rapidly through the M-H active catalyst reactions. This is a consequence of the steric limitations brought about by σ-bond metathesis reactions. The additional bulk of the substrate decreases dehydrocoupling efficiency. However, a class of metallocene catalysts have been identified as capable secondary silane dehydropolymerisation catalysts, using *in situ* catalyst generation approaches.

As first proposed by Corey et al,[97] dehydropolymerisation involves the formation of a [Cp_2M] active catalyst. Corey et al reported for Cp_2ZrCl_2/2*n*BuLi catalytic reaction conditions, oligosilanes of three repeating units could be synthesised for secondary silane substrates. Generation of the Cp_2ZrBu_2 catalyst occurs rapidly through the addition of 2 equivalents of *n*BuLi to zirconocene dichloride. Through a β-hydride elimination of one of the butyl ligands, one of the butyl ligands is released as free butane. The other butyl ligand from which a β hydride is abstracted is converted to an allyl ligand. The allyl ligand serves to stabilises the complex, acting to mask the [Cp_2Zr] species in solution.[98] This complex exists in an equilibrium as (Zr^{II}-Allyl and Zr^{IV}-Dialkyl) complexes (Scheme 1.13)

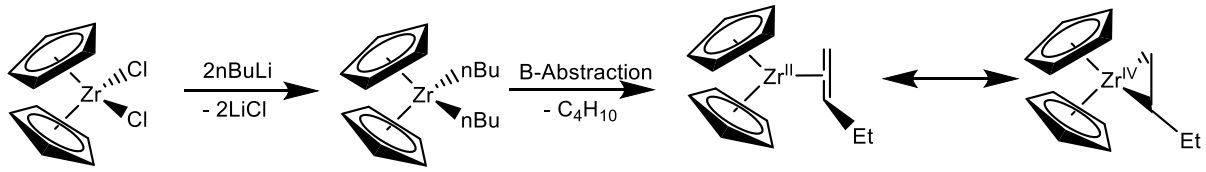

Scheme 1.13 *Activation of the metallocene catalysts via 2 eq. of nBuLi to a transient [Cp_2Zr^{II}]*

The formation of this [Cp_2Zr^{II}] species is correlated to the ability of the catalyst dehydropolymerisation secondary silanes. After formation of the transient [Cp_2M] complex, the specific steps by which dehydrocoupling and polysilane synthesis proceed are unknown.[64] Probing of the mechanism through ESI methods have experienced great difficulty in identifying the highly unstable and reactive catalytic intermediates. This has led to several proposed mechanisms by which the active catalyst enters the catalyst cycle for dehydropolymerisation. The other mechanism will be discussed in section 1.5.3. The presence of the olefin species does allows for potential hydrolysation of the alkene.[99] However, Si-Bu species are not observed during dehydrocoupling species, indicating it is likely the hydrides on the silanes are abstracted to the allyl ligand to release the ligand as free butane.

The most accepted mechanism for the [Cp_2M^{II}] active involves conversion of the catalyst to a monosilyl-, monobutyl metallocene complex. The olefin species is converted to the butyl ligand from hydride abstraction by the newly coordinated silyl ligand. Through interaction of the complex with a second equivalent of hydrosilane, the butyl ligand is released from the complex forming a forming a disilyl-metallocene complex. From this complex, the metallocene is converted to a monohydride,

monosilyl-metallocene, the proposed active catalyst for the [Cp_2M] based reactions. Dehydrocoupling proceeds through the confirmed catalytic cycle detailed below (Scheme 1.14).

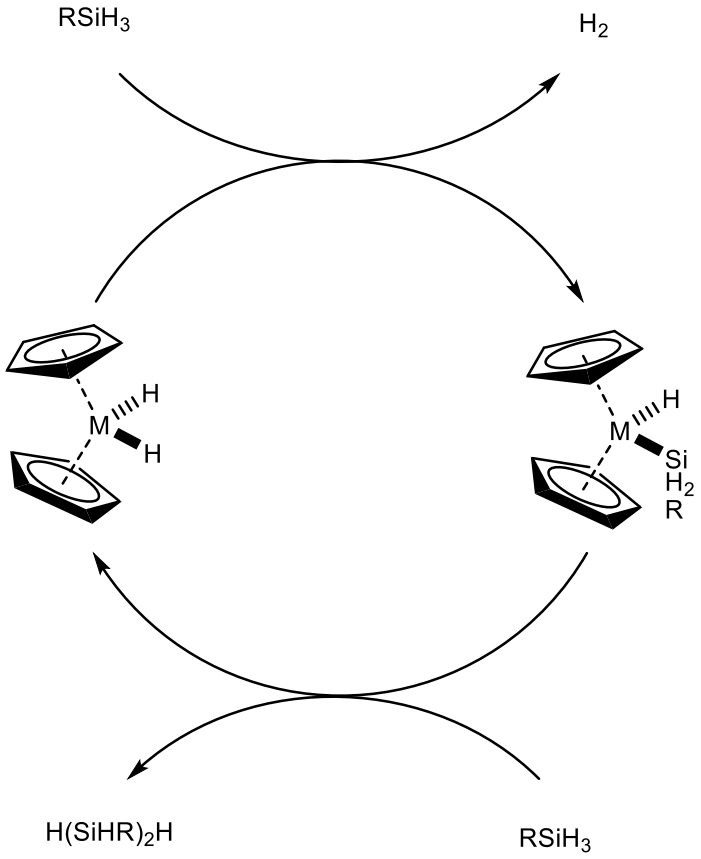

Scheme 1.14 *Metallocene-based dehydrocoupling catalytic cycle for the hydro-, silyl metallocene active catalyst.*[57,100]

1.5.3 Secondary Dehydrocoupling Mechanisms

Alternative secondary mechanisms have been proposed for hydrosilane dehydrocoupling with both late transition metal catalysts and early transition metal metallocenes. α-Elimination reactions have been proposed as viable mechanisms, due to their frequent appearance for Sn and As dehydrocoupling mechanisms.[101] α-Elimination favours sterically bulky elements and it is postulated the relatively small steric bulk of silicon prevents silane dehydrocoupling through α-elimination methods. However, Jackson et al.[86] reported potential evidence for a possible α-elimination dehydrocoupling reaction for Si-Si formation. This was concluded from the observation of H_2 loss from the $P_2Rh(H)Cl(SiHR_2)$ complex. However, it was not confirmed whether this H_2 loss proceeded through alpha-elimination or oxidation addition of a silane to a Rh=Si complex before release of a Si-Si compound.

One mechanism with has experienced persistent support without conclusive synthetic evidence is the silylene-intermediate based mechanism. This relies on a metal-silylene intermediate as the active catalyst. This unsaturated metal-silylene intermediate is then able to react to a second hydrosilane

equivalent, whereby the hydride is coordinated to the metal centre and the silyl species bonds to the silylene intermediate to create a silylene-silyl intermediate species. This proposed mechanism has experienced continued support as probing of catalyst dehydrocoupling mechanism through ESI-MS revealed the formation of metal-silylene complexes.[86]

The major criticism for this silylene-based mechanisms is distinct absence of silylene-silyl intermediate species have yet to be reported from dehydrocoupling reaction conditions. Additionally, the silylene-intermediate mechanism would be limited to primary and secondary hydrosilane substrates. While requiring extreme reaction conditions, late transition metal catalysts have been reported capable tertiary dehydrocoupling catalyst. This seems to indicate this mechanism is not viable for late transition metal catalysts or at least occurs concurrently with another disilane synthesis mechanism**.** Metal-silylene mechanisms have been favoured for metallocene catalysts, even though limited by the rarity of metal-silylene for early transition metals.[94] One example utilises a dihydro-metallocene complex to catalyse disilane formation through a silylene-intermediate mechanism (Scheme 1.15).

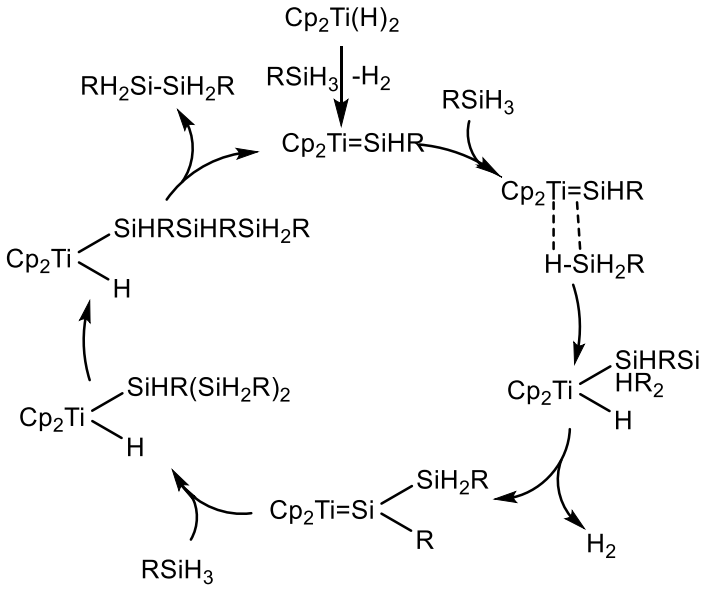

Scheme 1.15 *Catalyst dehydrocoupling of silanes by a titanocene catalyst through silylene intermediates.*[91]

Radical-based mechanisms have also been proposed for both late transition and metallocene catalysts. While radical-based mechanisms have potential, a lack evidence of radical intermediates eliminate radical-based dehydrocoupling reactions being the dominant mechanisms for transition metal catalysts.

1.6 Covalent Bridging of Disilanes

Investigations into catalytic dehydrocoupling for polysilane synthesis have revealed a plethora of highly efficient potential catalysts capable of selective Si-Si formation. However, without additional factors stabilising the Si-Si backbone, homolytic cleavage of the Si-Si with results in subsequent polysilane degradation. Attempts to prevent polysilane degradation have focused on non-synthetic approaches, ensuring the polysilane is maintained under inert atmospheres in the absence of moisture. Research conducted by the Leitao Research group has investigated a potential synthetic route to stabilising Si-Si bonds from homolytic cleavage. The incorporation of molecular bridges between disilane bonds was proposed to act as secondary reinforcement of the Si-Si backbone[102] (Figure 1.8).

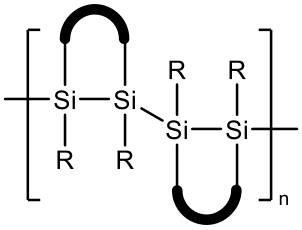

Figure 1.8 *Bridged polysilane, solid line represents a covalent bridge.*

Reinforcement is proposed to proceed through decreasing the rate of non-reforming silyl radical reactions. Through spatially localising the silyl radical nearby the silylene centre, the probability of disilane bond reformation is increased[102] (Scheme 1.16).

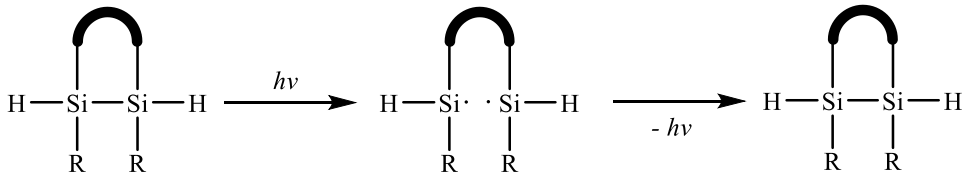

R = Alkyl, aryl

Scheme 1.16 *Photolytic degradation of a bridged disilane Si-Si bond and subsequent bridged supported disilane reformation*

Research have focused on the development of a library of disilyl precursors which undergo dehydrocoupling to synthesise bridged-disilane monomers. Previous synthetic work has developed a library of disilane monomers with disubstituted disilane monomers (Figure 1.9).

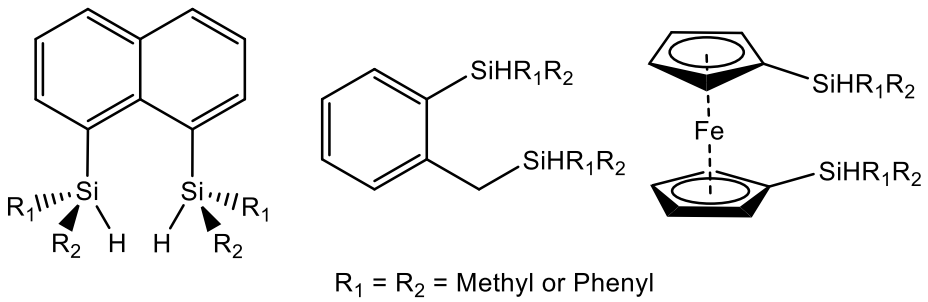

Figure 1.9 *Structures of bridged disilyl precursors synthesised during previous research*[102,103].

The incorporation of aryl-based bridges was shown to optimise the electronic properties of the disilane.[27] The introduction of π-conjugation into the polysilane allows for σ-π mixing.[104,105] For the incorporation of naphthalene bridges, π-conjugation contribution is significantly greater than the contribution by single phenyl rings. This was observed through red-shifts in polysilane UV absorption and suggests the incorporation of naphthalene bridges to polysilanes would further the lowering of the band gap of the polysilane, optimising the application of the polysilane within electronic semiconductors.[106]

The development of bridged polysilanes from the library of disubstituted silane building blocks is not possible, as the bridged disilanes lack the terminal Si-H ends required for dehydropolymerisation and chain growth. Attempts to synthesise a naphthalene-bridged disilane capable of polysilane formation produced the naphthalene-bridged di(phenyl)silyl precursor which underwent successful dehydrocoupling to form the disilane (Scheme 1.18).

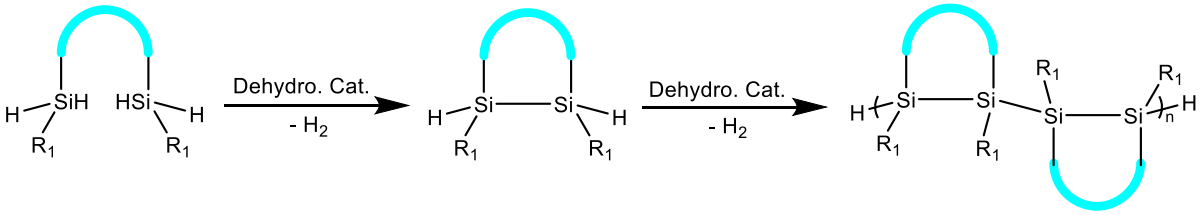

Scheme 1.17 *Dehydrocoupling of a covalently bridged disilyl monomer to the formation of the disilane and subsequent dehydropolymerisation.*

Dehydrocoupling conditions were performed using Wilkinson's catalyst under literature-based approaches ($Rh(PPh_3)_3Cl$) at 5 mol % for 3 days at 90 °C.[107] While disilane formation proceeded under the mentioned reaction conditions, dehydrocoupling was limited to disilane formation without polysilane formation. A series of catalysts were investigated to identify catalysts capable of dehydropolymerisation for bridged-disilanes. Zirconocene-based catalysts were unable to catalyse intramolecular disilane synthesis, let alone dehydropolymerisation.[103] However, the chloro(1,5-cyclooctadiene)rhodium(I) dimer ($[Rh(cod)Cl]_2$) complex was shown to be an effective dehydrocoupling catalyst for both disubstituted and monosubstituted silanes. The rhodium dimer

catalyst was capable of (dehydrocoupling going to completion) after 24 h under mild conditions (at room temperature at 5 mol %). However, $^{29}Si\{^{1}H\}$ NMR spectroscopy displayed two signal peaks, the *cis* and *trans* isomers of the disilane, indicating dehydropolymerisation had not occur and dehydrocoupling was limited to disilane synthesis.

Chapter 2: Aims of the Research

The application of polysilane materials within modern semiconductors arises from the unique electronics properties associated with the σ-conjugation present throughout the Si-Si backbone. However, the weak nature of the Si-Si bond allows for facile cleavage and degradation of the polysilane backbone, limiting industrial application in modern electronics. Attempts to reinforce the disilane bonds through the incorporation of molecular bridges have yielded great promise. A library of disubstituted disilane monomers have been created through synthesis of bridged disilyl precursors followed by successive dehydrocoupling. However, these monomers are unable to form polysilanes as they lack terminal Si-H ends necessary for dehydropolymerisation.

This project aims to continue development of bridged disilanes and expand the synthetic library of tethered polymerizable building blocks for polysilane chain synthesis. This will entail the successful synthesis of bridged disilane substrates possessing terminal Si-H ends for polysilane dehydropolymerisation. Focus will be given towards the formation of bridged di(phenylsilyl) precursors before catalytic dehydropolymerisation reactions towards polysilane synthesis (Figure 2.1).

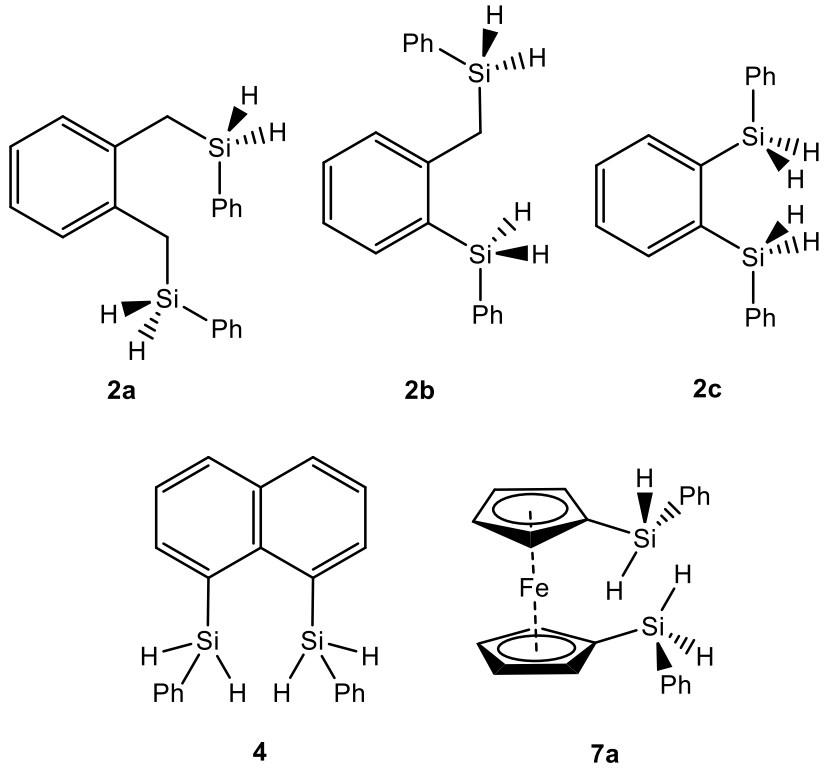

Figure 2.1 *Structures of the bridged disilyl precursors that are the focus of the research in this thesis.*

The first aspect of the project will investigate the synthesis of benzyl silane possessing bridged disilyl monomers. Previous work has identified selectivity regarding the use of chloro(aryl)silanes for benzyl silane synthesis. This research aims to identify a suitable synthetic procedure for benzyl silane synthesis with chloro(phenyl)silane. The monosubstituted chlorophenyl)silanes was selected to ensure the

bridged disilyl precursors may act as polymerizable building blocks for the synthesis of a bridged polysilane through dehydropolymerisation. The synthetic strategies will involve stepwise activation of the bridge substrate through lithiation and Grignard reactions before installation of the silyl species through chlorosilane and salt elimination (Scheme 2.1).

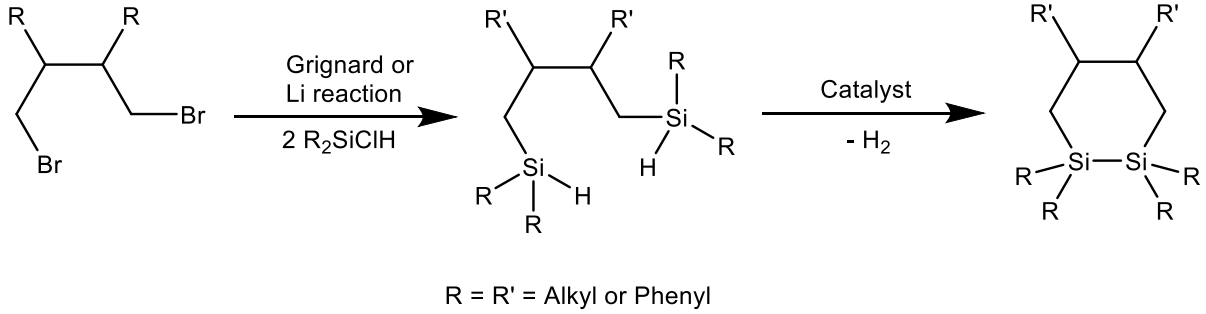

Scheme 2.1 *Stepwise strategy of bridged disilane synthesis through Grignard or lithiation methods, followed by dehydrocoupling.*

The second aspect of this project will involve an investigation into the use of four different dehydrocoupling catalysts with the disilyl precursors of the naphthalene and ferrocene bridges. The naphthalene-bridged precursors were selected due to previous success in synthesising the disilane monomer. The ferrocene-bridged precursors were selected as dehydrocoupling under previously investigated catalysts have failed to yield disilane formation (Scheme 2.2). It was hoped identification of a more efficient dehydrocoupling catalysts may allow for disilane synthesis.

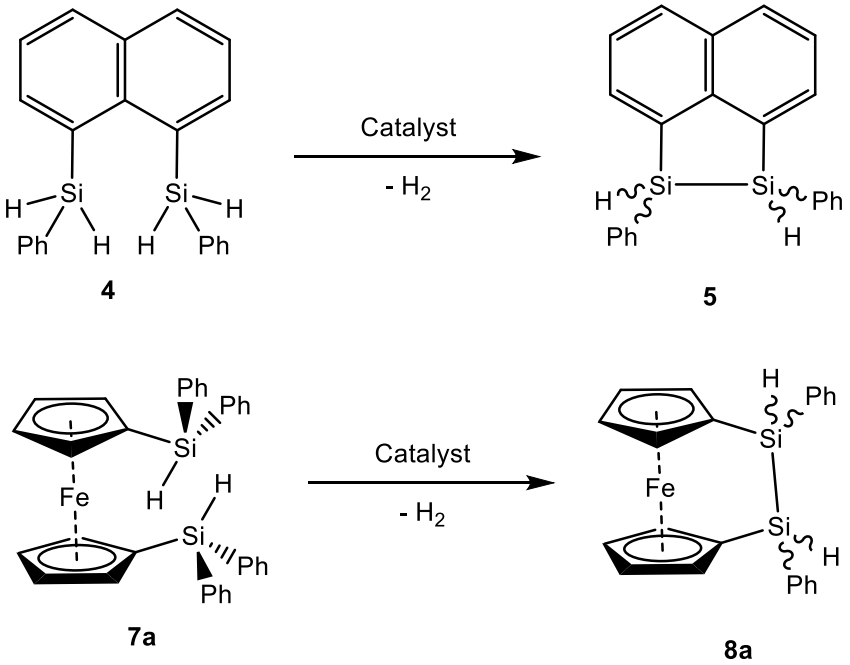

Scheme 2.2 *Catalytic dehydrocoupling reactions to be investigated.*

Four dehydrocoupling catalysts were investigated suitability towards intramolecular dehydrocoupling of bridged disilanes. The $[Rh(cod)Cl]_2$ dimer catalyst was selected due to previous investigations identifying the complex as high potential for successful dehydropolymerisation under mild reaction conditions. Wilkinson's catalyst was selected alongside $[Rh(cod)Cl]_2$ as it also a Rh(I) catalyst with greater mechanistic support detailing the dehydrocoupling of hydrosilanes with the Rh(I) catalyst. Zirconocene-based catalysts (Cp_2ZrCl_2/2*n*BuLi) were (re-investigated) after previous (attempts) failed to yield disilane products. It was proposed in situ generation of the zirconocene catalyst may favour dehydrocoupling, as in situ generated metallocenes favour secondary silane substrates. For comparison to the Cp_2ZrCl_2/2*n*BuLi system, dimethyl zirconocene (Cp_2ZrMe_2) was investigated due to its activity and literature precedent for primary silane dehydrocoupling. The efficiency and stereoselectivity for all four dehydrocoupling catalysts were analysed with mechanistic postulations derived from reaction observations and results.

Chapter 3: Results and Discussion

3.1 Benzyl Silane Synthesis

Previous work surrounding the expansion of bridging moieties investigated a series of benzene-ring motif substrates, α,α'-dibromo-*o*-xylene (**1a**) and 2-bromobenzylbromide (**1b**), for their potential application within the development of a synthetic library of tethered polymerizable building blocks for polysilane chain synthesis. Both substrates were selected for their potential formation of benzyl silane monomers. Synthesis of the molecular bridges experienced mixed degrees of success with regards to the successful installation of silane species at the benzyl bromide position. Limitations were observed for the substrates with regards to selectivity of the chlorosilane. Grignard approaches with **1a** and chloro(aryl)silanes failed to yield successful silane attachment. Only chloro(dimethyl)silane was observed to successfully attachment to the **1a** bridge (Scheme 3.1). In contrast, **1b** did not exhibit any selectively with ready addition of the chloro(disubstituted)silanes under Grignard conditions.

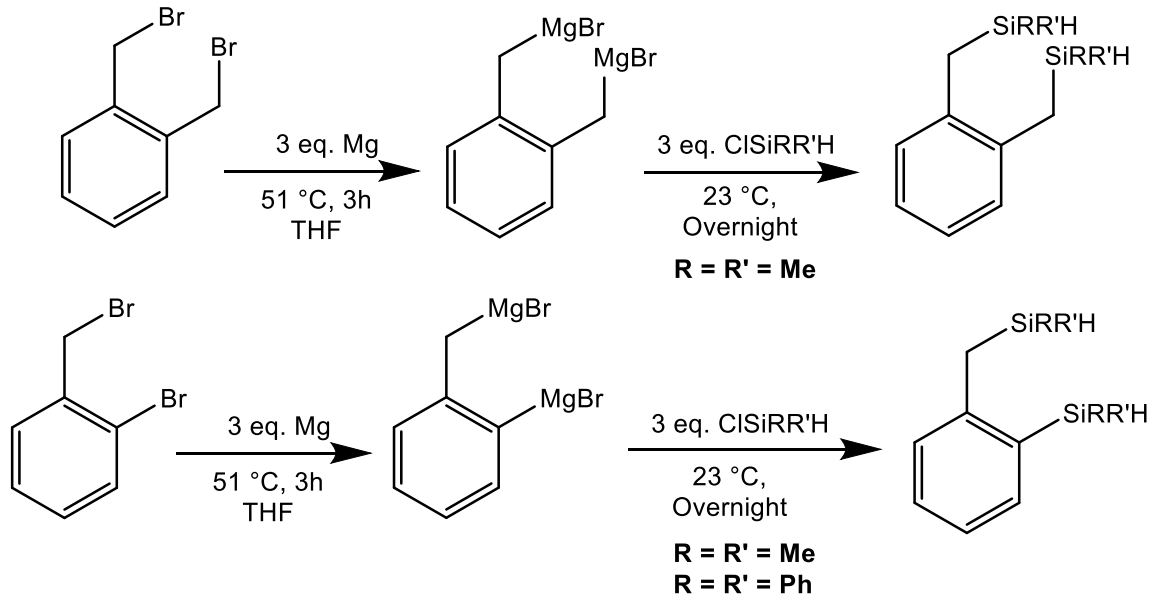

Scheme 3.1 *Synthesis of the bridged disilyl compounds possessing benzyl silane functionalities conducted in previous research.*

Experimental attempts to synthesise the monosubstituted disilyl precursor product were not investigated in detail. Initial attempts to produce the disilyl precursors **2a** and **2b** did not proceed cleanly through the previously established Grignard reaction conditions. It was postulated the selectivity observed by the **1a** substrate for chloro(aryl)silanes in for chloro(disubstituted)silanes was once again present. However, this selectivity was more pronounced with **1b** unable to form **2b** through the previous Grignard approach. This selectivity is reported within literature, whereby attachment of chloro(aryl)silanes to benzyl bromide Grignard substrates for benzyl(aryl)silane synthesis is very difficult. However, the success of the **2a** substrate to with chloro(diphenyl)silane indicated this selectivity may be overcome under specific conditions.

The incorporation of the phenylsilane species within a disilyl precursors presents greater future potential over the previously synthesised disubstituted silanes. The synthesis of a disilyl precursor with terminal Si-H ends allows for potential dehydropolymerisation and polysilane synthesis. Additionally, the incorporation of aryl species on the silane would further aid the electronic properties of the synthesised polysilane. Thus, it was decided to re-investigate the potential application of phenylsilane onto the molecular bridges. To overcome the difficulty associated with the reaction of chloro(phenyl)silane and the benzyl bromide Grignard substrates, a focus was placed on the identification of a reaction procedure which would facilitate benzyl silane formation with chloro(phenyl)silane to the **1a** and **1b** bridge substrates. In addition to **1a** and **1b**, 1,2-dibromobenzene (**1c**) was investigated alongside the two substrates (Figure 3.1). The **1c** does not possess the benzyl bromide functionality associated with the selectivity issue observed previously and **2c** does not possess a benzyl silane functionality. Selection of this bridge allowed for better understanding of the effect of each approach and the efficiency of each respective procedure.

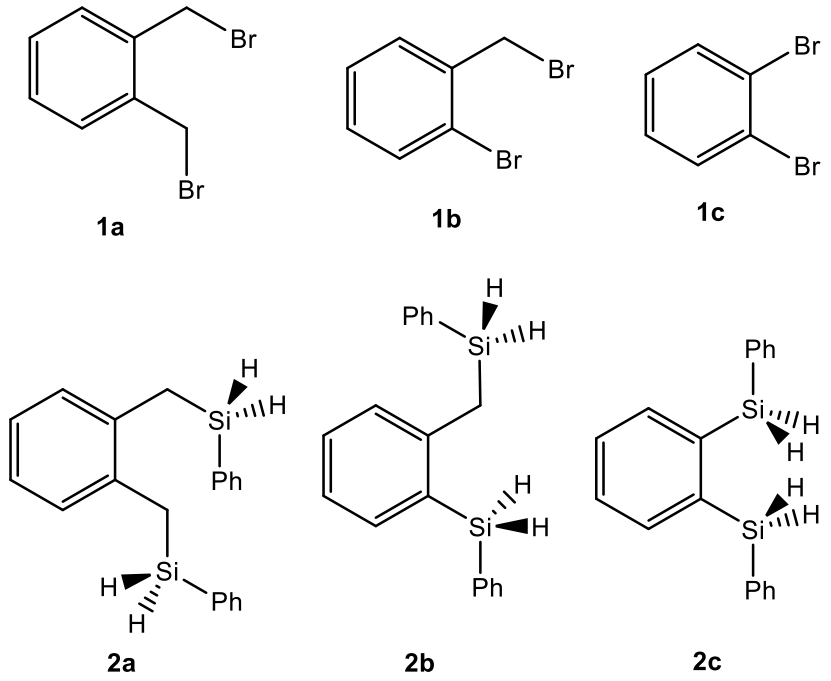

Figure 3.1 *Structures of the desired bridged disilyl precursors (**2a-c**) and their dibromo- substrates (**1a-c**) from which the synthesis of **2a-c** will proceed.*

Previously established bridge substrate activation utilised a Grignard approach with reflux under inert atmospheric conditions. Magnesium was added in slight excess to the bridge substrate in a 3:2 ratio. The generation of the Grignard-substrate occurred through boiling the solution of THF for 3 h. The chloro(disubstituted)silanes was then added in excess and the reaction was left overnight to stir at room temperature. Given the difficulties associated with benzyl silane formation, it was determined best to investigate ways to avoid Grignard conditions entirely. Synthetic approaches for other successfully synthesised bridged disilyl precursors exhibited lithiation of dibromide substrates as an efficient method

for substrate activation before chlorosilane addition. Lithiation approaches were successful for the activation of di-aryl substrates. An experimental attempt was set up to confirm if the lithiation pathway was viable pathway for benzyl bromide functionality activation. This approach involved the treatment of **1a** with *n*BuLi before the addition of chloro(phenyl)silane (Scheme 3.2).

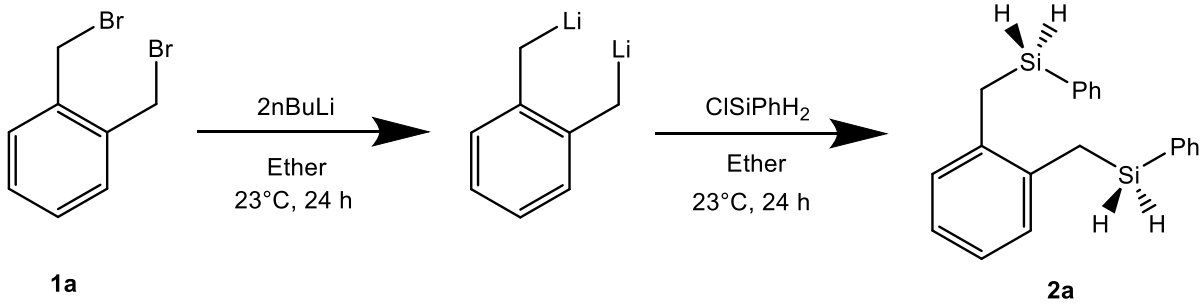

Scheme 3.2 *Proposed synthesis of the di(benzyl silane)* ***2a*** *product with* ***1a*** *through lithiation.*

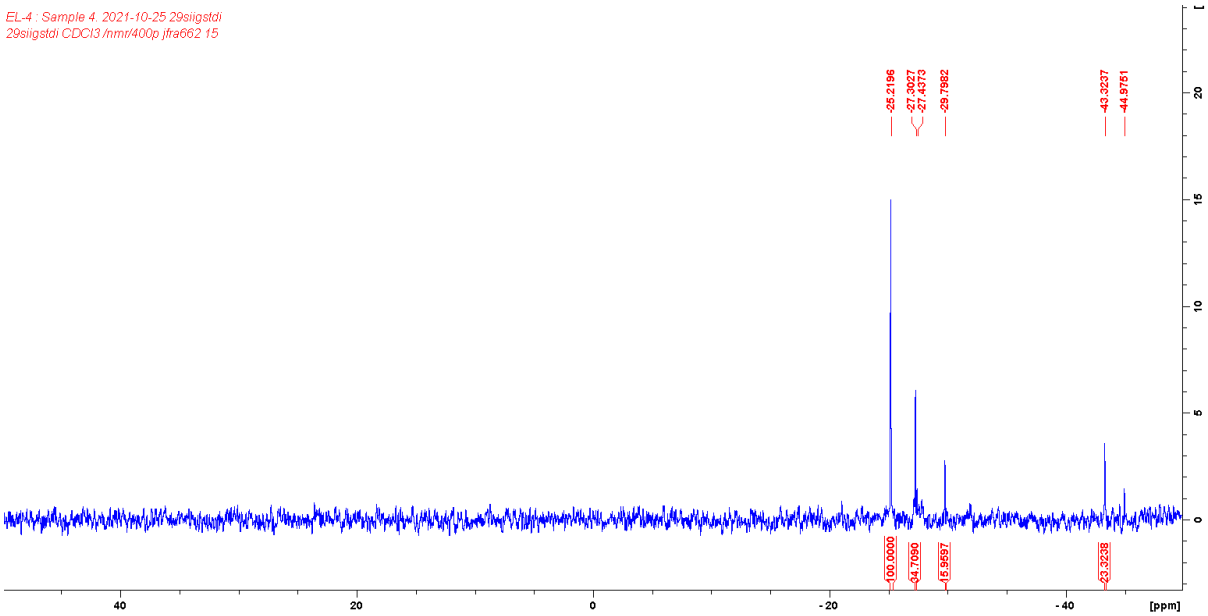

Figure 3.2 *$^{29}Si\{^{1}H\}$ NMR spectrum of the reaction of* ***1a*** *and chloro(phenyl)silane through lithiation.*

^{1}H and $^{29}Si\{^{1}H\}$ NMR spectroscopy did not indicate a clean synthesis of a major product with a series of silicon peaks observed (Figure 3.2). ESI-MS investigation failed to indicate the formation of any disilyl precursors, or benzyl silanes species. It was noticed post-workup the formation of tiny white solids suspended within the solution. The addition of pentanes increased the formation of this solid. Isolation of the solid revealed the solid was not soluble in any common organic solvent.

It is proposed this solid are the hydrolysed products of the litihiated **1a** substrate, litihiated at the non-bromide positions. The strength of the *n*BuLi reagent means that there is a mixture of lithiation products, where *n*BuLi may lithiation the benzene ring and leave the bromide functionality untouched. The addition of pentanes facilitates hydrolysation through the small quantities of water present in the organic

solvents. It was determined the silicon products observed are siloxane-based, arising from the quenching of free chlorosilanes post-workup. It was concluded from the results the *n*BuLi reagent is too strong for the benzyl bromide functionality, whereby addition of a chloro(phenyl)silane fails to produce the **2a** product. Due to this result, lithiation approaches were no longer investigated for subsequent investigations surrounding benzyl silane synthesis.

While it was hoped to avoid Grignard methods for the synthesis of the benzyl silane containing **2a** and **2b**, the inability of the lithiation experiment to facilitate silane attachment directed research back towards Grignard methods. No literature approach was identified for the activation of di(benzyl bromide) substrates. However, two approaches were identified with great potential for the **1a-c** substrates. Future attempts to synthesis the disilyl-bridge compounds were conducted through Grignard-style approaches.

The two selected approaches differed about the nature of Grignard substrate prepared by each procedure. The first procedure reported by Visco et al[108] uses Barbier-type coupling to allow for the reaction of a chloro(phenyl)silane with a single benzyl-bromide functionality for benzyl(aryl)silane formation (Scheme 3.3).[108] It is hoped through increasing the equivalents of chloro(phenyl)silane this procedure may facilitate the successful reaction of a second benzyl bromide functionality with chloro(phenyl)silane.

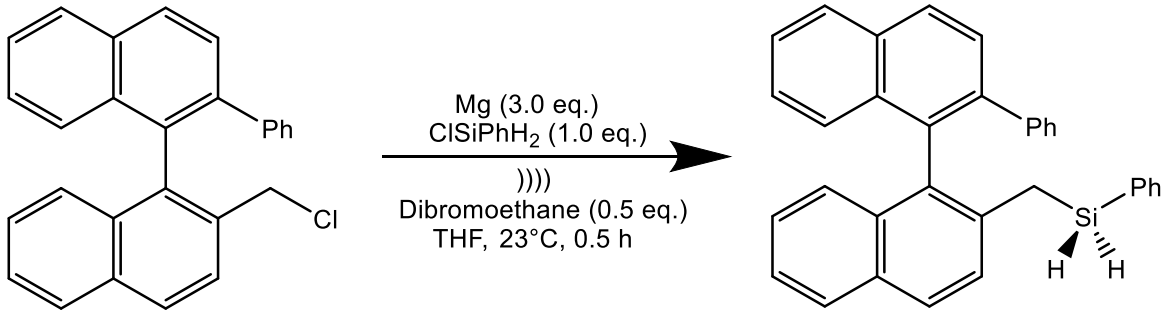

Scheme 3.3 *Reported Grignard procedure for the synthesis of benzyl silanes through chloro phenylsilane in a Barbier-type coupling step.*[108]

In contrast, a second Grignard procedure reported by Schrock et al[109] was identified where dibromo benzene substrates were successful treated through Grignard conditions and chloro(aryl)silanes for the synthesis of a di(aryl silyl)benzene (Scheme 3.4). While not specifically focused on benzyl silane synthesis, the reported activation of the dibromide substrates for disilylation shows potential for our selected dibromide substrates.

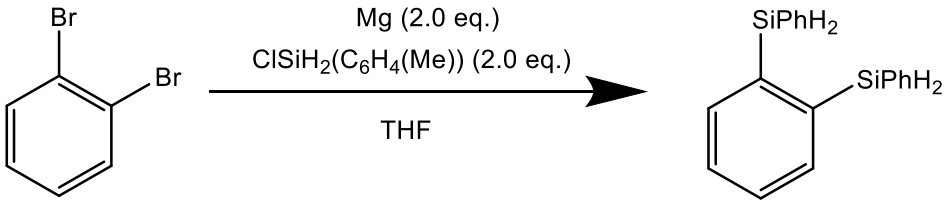

Scheme 3.4 *Reported Grignard procedure for the synthesis of disilylbenzene compounds from Schrock et al.*[109]

Experimental procedures were adopted from both literature procedures for potential suitability towards the synthesis of **2a-c** from the **1a-c** substrates. The major difference the Visco and Schrock adopted procedures is the general reaction conditions facilitating reaction success. The Visco procedure uses sonication for 30 min with 1,2-dibromoethane. In contrast, the Schrock procedure relies on an 8 h reflux. The **1c** substrate was investigated first for two reasons. Given the **1c** substrate does not possess the benzyl bromide functionalities which present selectivity issues for chloro(aryl)silanes, the 1c substrate is being used to establish the general efficiency of both Grignard procedures. Additionally, as the **1c** substrate was utilised within the reported Schrock et al. experiment, it is proposed the adopted Schrock procedure should produce the **2c** product in high yields (Scheme 3.5).

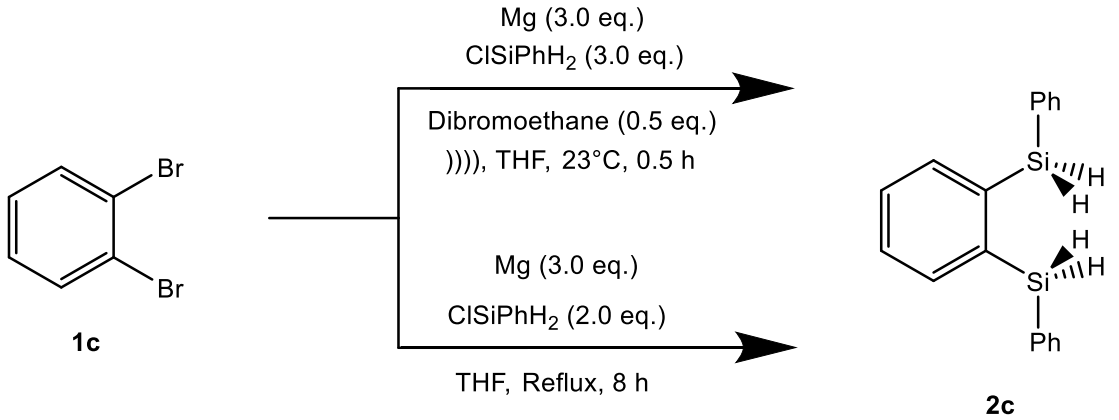

Scheme 3.5 *Proposed synthesis of the **2c** disilyl precursor from the **1c** substrate through the Visco (Top) and Schrock (Bottom) Grignard reaction conditions.*

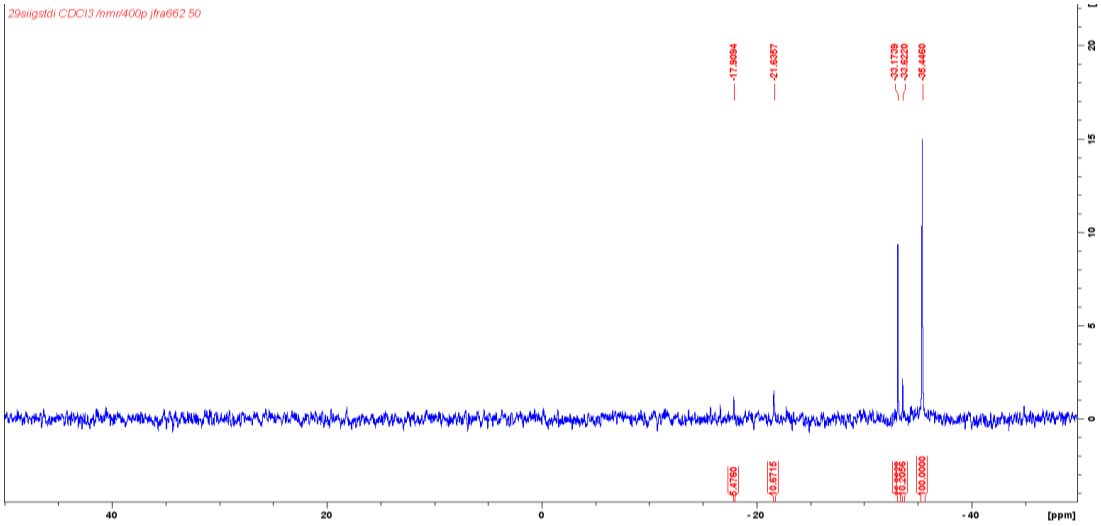

Figure 3.3 *$^{29}Si\{^{1}H\}$ NMR spectrum of the Grignard reaction of **1c** towards **2c** using the Schrock procedure.*

As expected, the Schrock et al. procedure produced a clean reaction mixture with $^{29}Si\{^{1}H\}$ NMR spectroscopy revealing the dominant formation of two silicon products at -33.2, -35.5 ppm (Figure 3.3). ESI-MS results were unable to confirm the presence of **2c** product in the reaction. However, a series of disilyl-benzene products were observed, indicating successful silane attachment. It was proposed these two product peaks correspond to monosilylated (-33.2 ppm) and the **2c** (-35.5 ppm) products from the successful Grignard reaction. Attempts to purify the product mixture to confirm assignment through column chromatography were unsuccessful. In contrast, the Visco procedure produced a series of silicon peaks in $^{29}Si\{^{1}H\}$ NMR spectroscopy (Figure 3.4). The two assigned signal peaks corresponding to **2c** and the monosilylated product were observed. However, it rapidly identified the series of peaks observed were identical to the signal peaks observed for the lithiation reaction procedure for the **1a** substrate.

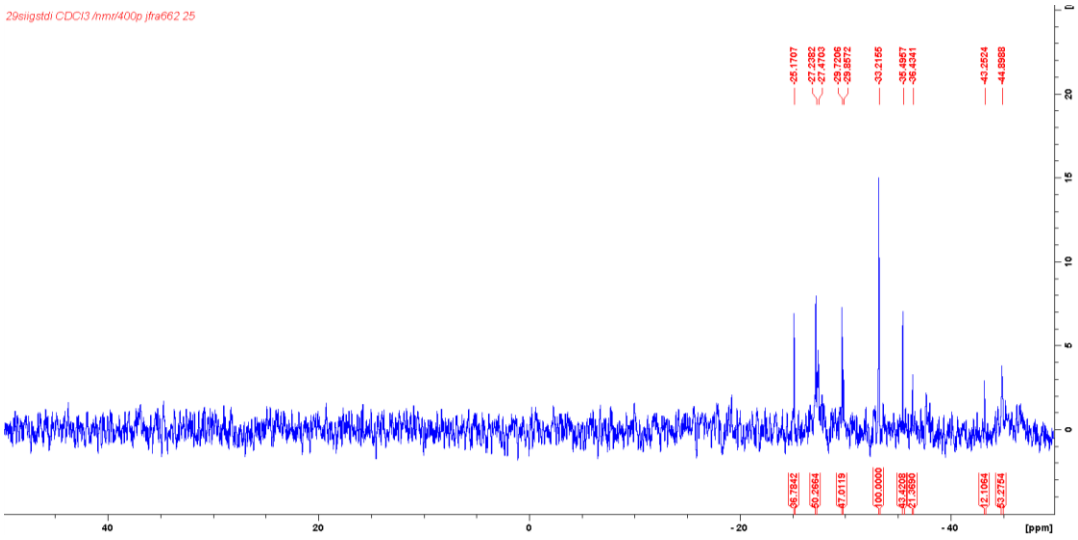

Figure 3.4 *$^{29}Si\{^{1}H\}$ NMR spectrum of the Grignard reaction of **1c** towards **2c** using the Visco procedure.*

Given that both experiments utilised different substrates (**1a** vs **1c**) and utilised different reaction conditions (Lithiation vs. Grignard), it was confidently determined the peaks were free siloxane-based products. This confirmed the conclusions achieved previously for the lithiation reaction. It was noted the monosilylated signal peak was the major product of the reaction instead of **2c** by a ratio of 2:1. It was concluded while the **2c** product was formed by the Visco procedure, it confirmed the Schrock procedure is a viable reaction procedure for **2c** synthesis. Given that both procedures were shown to successfully facilitate **2c** synthesis, the **1b** substrate was investigated next (Scheme 3.6). This was to determine the capability of each procedure towards benzyl silane formation with one benzyl bromide functionality present. Experimental conditions were maintained the same between the **1c** and **1b** substrate experiments.

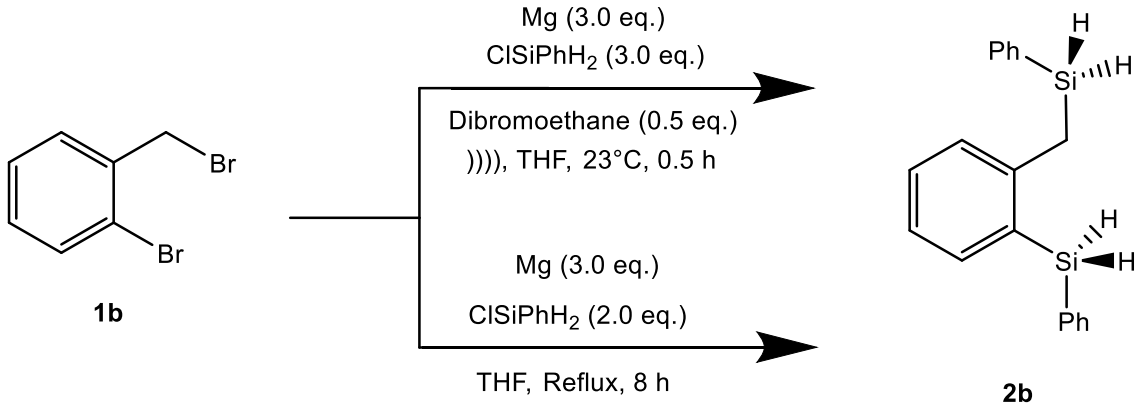

Scheme 3.6 *Proposed synthesis of the* ***2b*** *disilyl precursor from the* ***1a*** *substrate through the Visco (Top) and Schrock (Bottom) Grignard reaction conditions.*

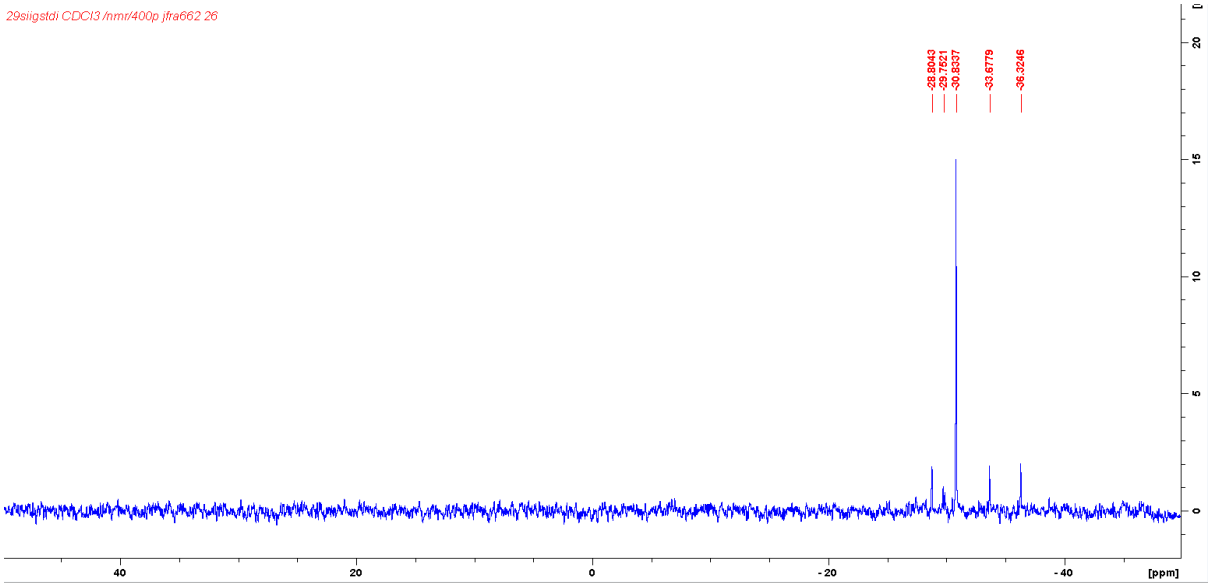

Figure 3.5 *$^{29}Si\{^{1}H\}$ NMR spectrum of the Grignard reaction of* ***1b*** *towards* ***2b*** *using the Visco procedure.*

In contrast to the **1c** substrate, $^{29}Si\{^{1}H\}$ NMR spectroscopy for the Visco procedure indicated the clean formation of one silicon-based major product (-30.8 ppm) (Figure 3.5). No free siloxane signals were observed in the NMR spectrum. However, presence of one major Si signal is undesirable, as the **2b** product is expected two signal peaks with a 1:1 ratio. ESI-MS failed to indicate the presence of the **2b** product with the expected product m/z not observed. Additionally, no disilyl-precursors were reliably observed within ESI. It was hoped the Schrock procedure would provide more information surrounding the product mixture. observed. However, the Schrock procedure produced a significant quantity of free siloxane products, confirmed through $^{29}Si\{^{1}H\}$ NMR.

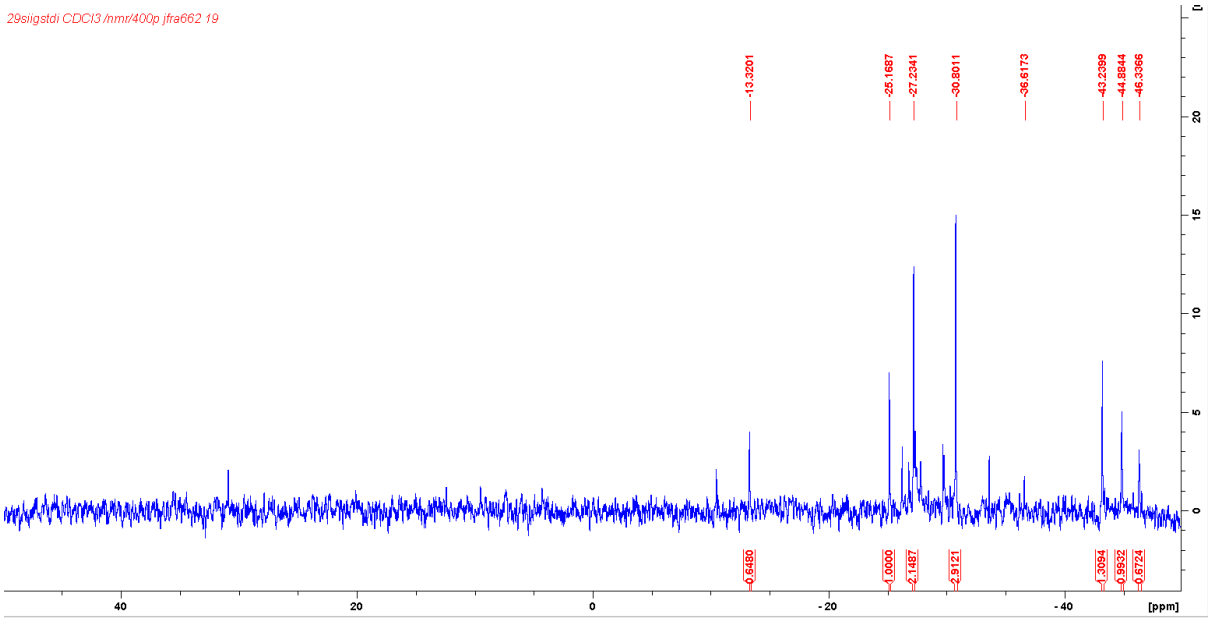

Figure 3.6 *$^{29}Si\{^{1}H\}$ NMR spectrum of the Grignard reaction of **1b** towards **2b** using the Schrock procedure.*

The two signal peaks at -30.8 ppm and -36.6 ppm were observed in both experiments (Figure 3.6). It is proposed the -30.8 ppm signal peak corresponds to the monosilylated product where the bromide functionality is successfully displaced with a silane species. However, without confirmation through ESI, it is unknown whether benzyl silane formation occurs within the reaction. Although the results of both experiments proved inconclusive for the synthesis of the **2b** product, it was determined unlikely either experiment was able to synthesis the **2b** product. The presence of two different bromide functionalities prevented clear understanding of the reaction. To confirm the ability or inability of the Grignard procedures to facilitate a successful reaction with the benzyl bromide functionality, the **1a** substrate was selected with its two benzyl bromide functionalities (Scheme 3.7).

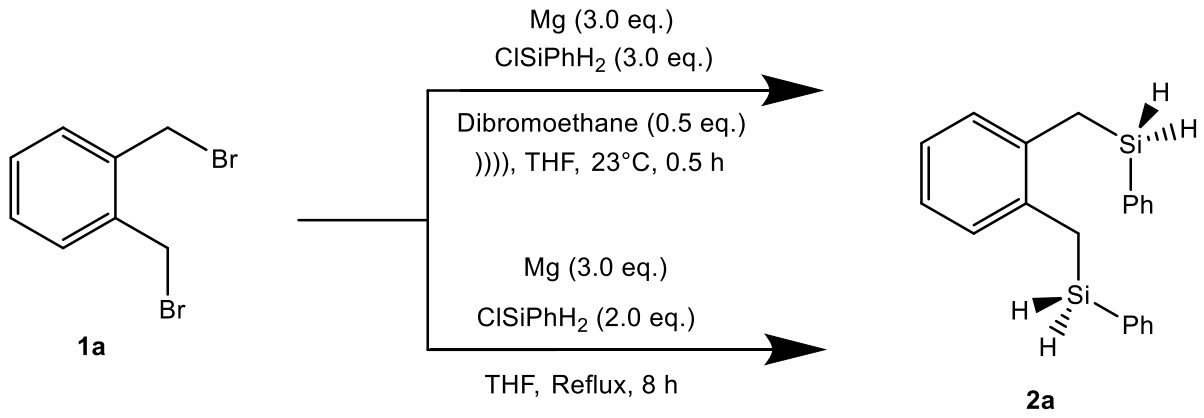

Scheme 3.7 *Proposed synthesis of the* ***2a*** *disilyl precursor from the* ***1a*** *substrate through the Visco (Top) and Schrock (Bottom) Grignard reaction conditions.*

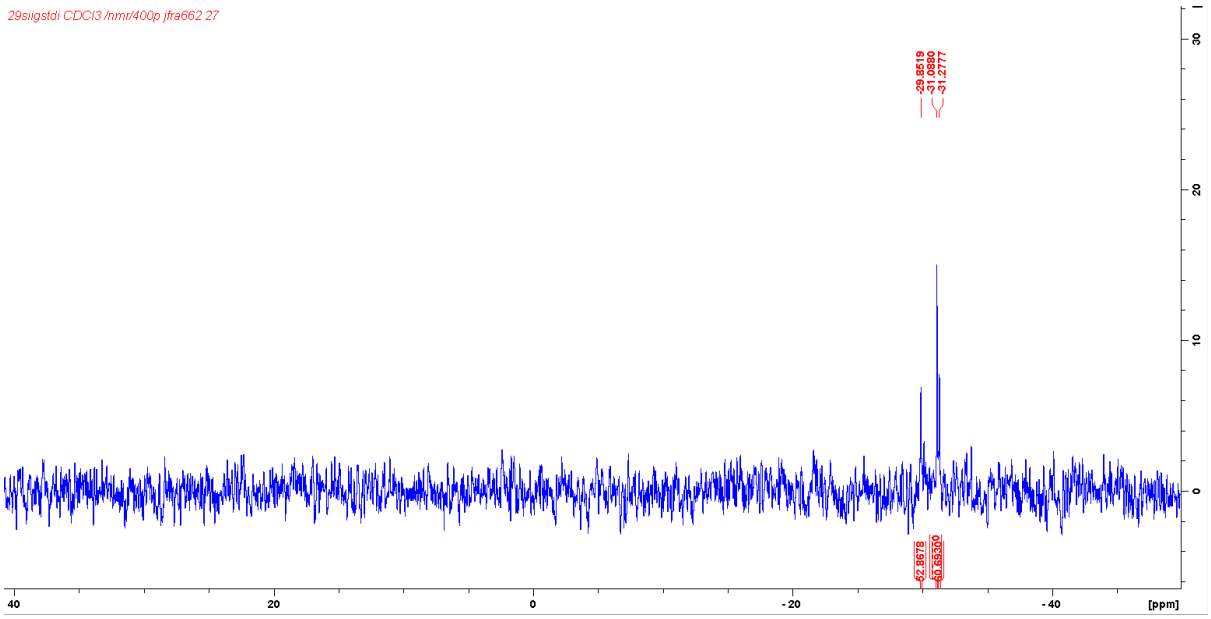

Figure 3.7 *$^{29}Si\{^{1}H\}$ NMR spectrum of the Grignard reaction of* ***1a*** *towards* ***2a*** *using the Visco procedure.*

In contrast to the previous experimental results, the Visco procedure displayed a clean reaction mixture with 3 major signal peaks in $^{29}Si\{^{1}H\}$ NMR spectroscopy (Figure 3.7). The signal peak of -29.8 ppm was rapidly assigned to a free siloxane-based product, observed during previous reactions. Attempts to confirm the identity of the -31.0 and -31.3 ppm signal peaks were hampered by difficulties encountered during purification of the reaction mixture through silica chromatography. ESI-MS was unable to confirm the formation of the **2a** product with the expected product m/z not observed. Additionally, no disilyl-precursors products were observed within ESI-MS. The Schrock procedure failed to provide any new information surrounding the identity of the two peaks, with a series of free-siloxane peaks observed throughout the $^{29}Si\{^{1}H\}$ NMR spectrum. This was in addition to the two peaks at -31.0 and -31.3 ppm.

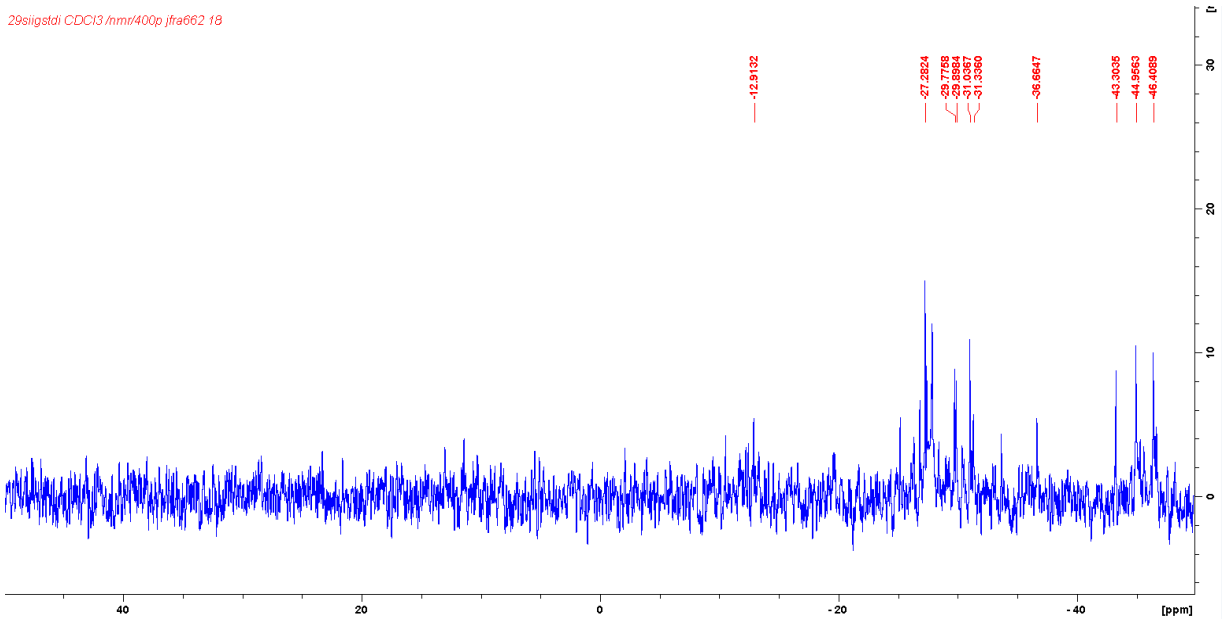

Figure 3.8 *$^{29}Si\{^{1}H\}$ NMR spectrum of the Grignard reaction of **1b** towards **2b** using the Schrock procedure.*

The identity of the two silicon-based products remains unclear after post-reaction analysis. The two signal peaks may correspond to the **2a** (-31.0 ppm) and monosilylated product (-31.3 ppm) (Figure 3.8). This assignment is based on the integral ratios where the signal at -31.0 ppm is observed at a greater intensity. However, without clear evidence of **2a** formation, it was determined both procedures were unable to synthesis the **2a** product. The results from the Grignard procedures were disappointing in that simple and straightforward addition of chloro(phenyl)silane for benzyl silane synthesis were not observed. While synthesis and purification of the **2a** and **2b** precursors were not achieved, the **2c** disilane was successfully synthesised and is ready for future dehydrocoupling investigations.

3.2 Naphthalene-Bridged Dehydrocoupling Catalyst Investigation

In contrast to the synthetic attempts to install chloro(aryl)silanes to benzyl bromide substrates for benzyl silane synthesis, the 1,8-dibromonaphthalene substrate has been showed capable of ready addition of silane species through lithiation methods. As discussed, in section 1.6.1, previous work has developed a library of naphthalene-bridged di(disubstituted)silyl precursors which are capable of dehydrocoupling to form bridged disilane building blocks. However, the absence of the terminal Si-H ends for the disilane monomers prevents dehydropolymerisation and synthesis of polysilane chains**.** Initial attempts to develop naphthalene-bridged disilanes capable of polymerisation has resulted in the synthesis of the 1,8-bis(phenylsilyl)naphthalene (**4**) precursor. Treatment of **4** with Wilkinson's catalyst ($Rh(PPh_3)_3Cl$) produced the disilane product (**5**) after 3 days at 90 °C. A small investigation into dehydrocoupling catalysts capable of disilane formation was conducted (Scheme 3.8).

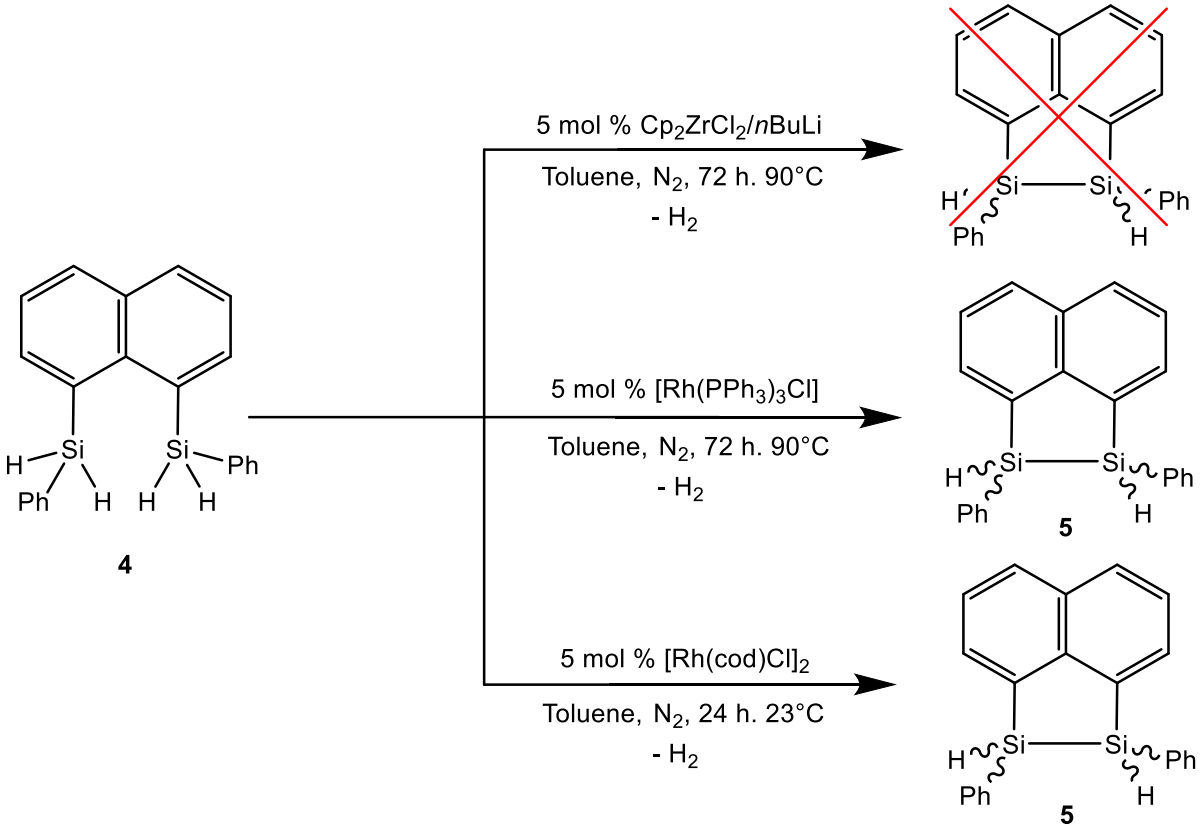

Scheme 3.8 *Catalyst investigation results from previous research on the synthesis of the naphthalene-bridged disilane* ***5*** *from dehydrocoupling reaction with* ***4****.*

Two major conclusions were achieved from the results. The zirconocene-based catalyst failed to yield the **5** disilane under the given conditions and the Rh(I) catalyst, chloro(1,5-cyclooctadiene)rhodium(I) dimer ($[Rh(cod)Cl]_2$), produced **5** with yields superior to $Rh(PPh_3)_3Cl$. Additionally, the $[Rh(cod)Cl]_2$ catalyst was shown to go to completion after 24 h at room temperature. The observation of the extreme efficiency of the $[Rh(cod)Cl]_2$ catalyst for dehydrocoupling under mild reaction conditions led to

potential hope the catalyst may be able to catalyst tertiary intermolecular dehydrocoupling reactions between the bridged disilane units. Previous research within the Leitao research group was unable to thoroughly investigate the capability of the $[Rh(cod)Cl]_2$ catalyst for tertiary silane dehydrocoupling.[102] It was determined beneficial to further investigation into the $[Rh(cod)Cl]_2$ catalyst, to confirm the inability of the catalyst to conduct dehydropolymerisation. It was proposed through increasing the catalytic loading and increasing the reaction temperature tertiary dehydrocoupling may be catalysed (Scheme 3.9).

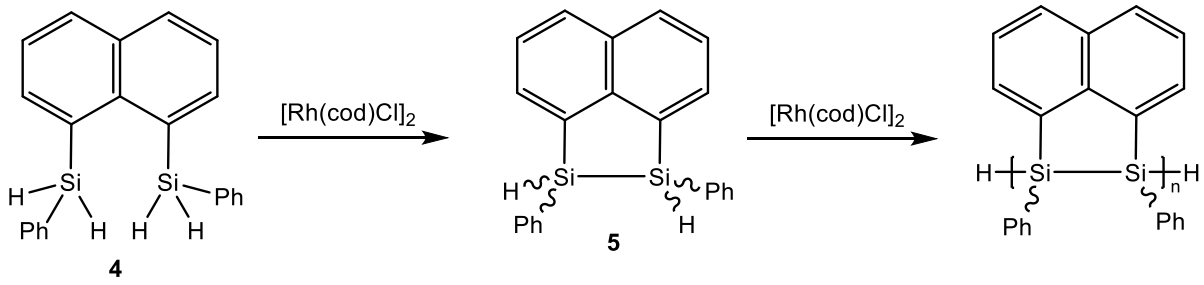

Scheme 3.9 *Proposed $[Rh(cod)Cl]_2$ catalysed dehydropolymerisation of 1,8-bis(phenylsilyl)naphthalene (**4**) for the synthesis of a bridged polysilane*

To allow for investigation of the $[Rh(cod)Cl]_2$ catalyst, the disilyl precursor 1,8-bis(phenylsilyl)naphthalene (**4**) was synthesised for subsequent dehydrocoupling investigations. It was also decided to re-investigation the Wilkinson's catalyst alongside$[Rh(cod)Cl]_2$. The synthetic strategy for **4** has been optimised from previous investigations. This strategy involved the formation of chloro(phenyl)silanes from the treatment of phenylsilane and the reaction with a 1,8-dilithionaphthalene under inert conditions (Scheme 3.10). Product confirmation was done according to comparison of ^{1}H and $^{29}Si\{^{1}H\}$ NMR values to literature.

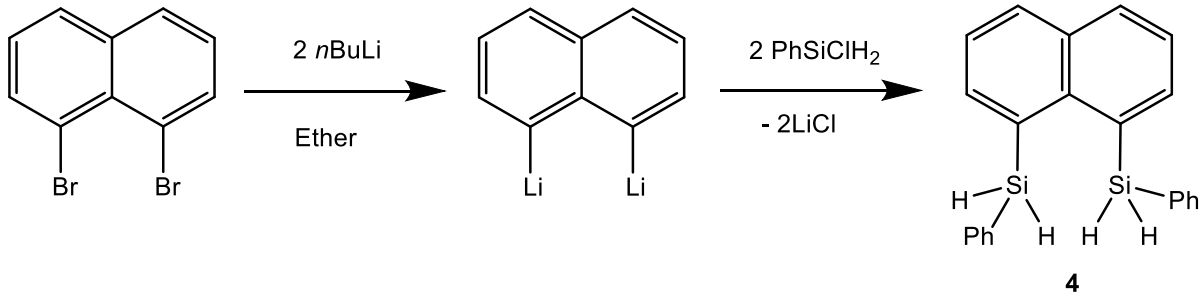

Scheme 3.10 *Synthetic strategy for the synthesis of 1,8-bis(phenylsilyl)naphthalene (**4**).*

Standard catalytic dehydrocoupling reaction conditions were utilised for both catalysts (5 mol % cat, @ 23 °C). Several silicon-based products were observed through the $^{29}Si\{^{1}H\}$ NMR spectra of both reaction mixtures. The two distinct Si peaks, corresponding to the meso (**5a**) and chiral (**5b**) diastereomers of 5, were observed for both catalysts at 37.3 ppm and -40.2 ppm (Figure 3.2.1). Formation of the disilane product, 5, was further confirmed via ESI-MS.

Sadly, both Rh(I) catalysts were unable to catalyse tertiary dehydropolymerisation, with no change in signal peaks observed in $^{29}Si\{^{1}H\}$ NMR for the $[Rh(cod)Cl]_2$ catalyst on increasing the reaction temperature above room temperature (50 °C and 80 °C). It was noted during catalytic loading investigation the increase in catalyst concentration does not increase the **5** disilane yield linearly. Notably, high catalytic loading (25 mol %) reactions were shown to proceed significantly slow, with the hydrosilane substrate **4** re-obtained from the product mixture (Figure 3.9)

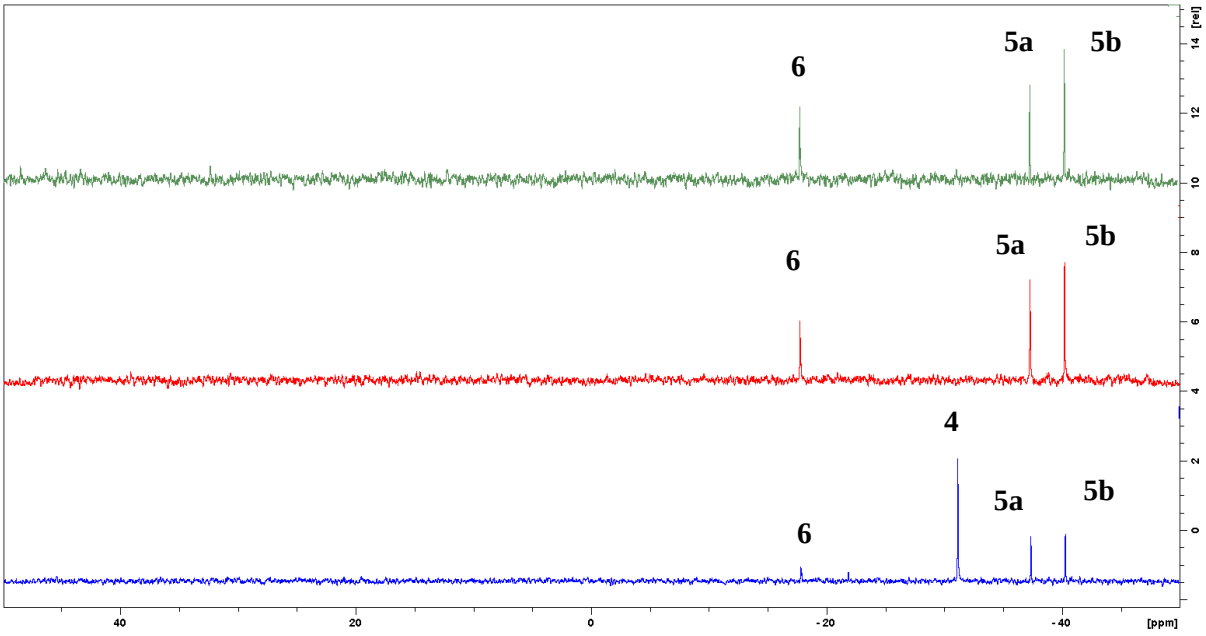

Figure 3.9 *$^{29}Si\{^{1}H\}$ NMR spectra for $[Rh(cod)Cl]_2$ catalysed dehydrocoupling of 4 with different catalytic loadings. (Green = 5 mol %, Red = 10 mol %, Blue = 25 mol %).*

It was evident through comparison between the $Rh(PPh_3)_3Cl$ and $[Rh(cod)Cl]_2$ reaction mixtures disilane formation produces the meso (**5a**) and chiral (**5b**) diastereomers (Scheme 3.11). However, it was evident ratio of **5a**:**5b** observed in $^{29}Si\{^{1}H\}$ NMR differed significantly between the Rh(I) catalyst used. The $Rh(PPh_3)_3Cl$ catalyst favoured the chiral **5b** diastereomer by a ratio of approximately 4:1. The $[Rh(cod)Cl]_2$ catalyst produced a near 50:50 ratio of **5a**:**5b**, where **5b** was slightly favoured by a ratio of 1.3:1.

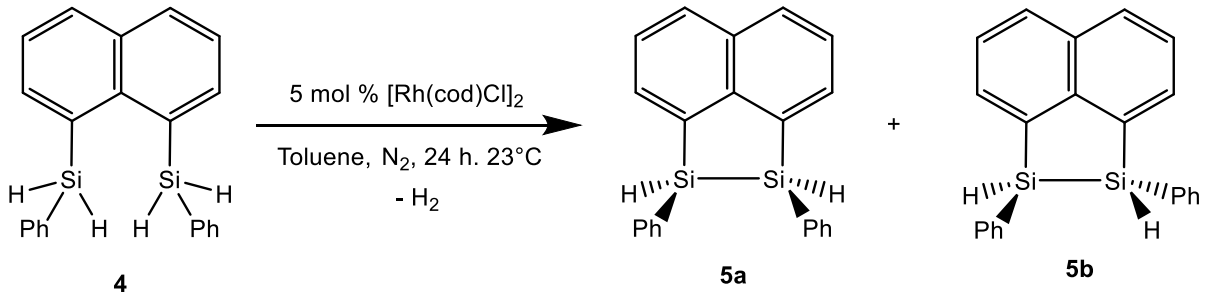

Scheme 3.11 *Synthesis of the meso (**5a**) and chiral (**5b**) through dehydrocoupling of **4** with the [Rh(cod)Cl]$_2$ catalyst.*

Literature surrounding the dehydrocoupling ability of the [Rh(cod)Cl]$_2$ dimer has yet to be reported for disilane synthesis. However, due to its nature as a Rh(I) catalyst, it is presumed as a Rh(I) catalyst it follows a similar mechanistic pathway to Rh(PPh$_3$)$_3$Cl, which has had a plethora of reliable mechanistic investigations for the dehydrocoupling of silanes towards polysilanes. Based on the same assumption both Rh(I) catalysts utilise similar activation methods and catalytic cycles, it is proposed the stereoselectivity is directly correlated to the catalytic design and choice of ligand for the catalyst.

Control over the stereoselectivity of the dehydrocoupling catalyst is vital for subsequent plans relating to the application of polysilanes within semiconductors and electronic materials. Selective synthesis of the chiral **5b** is optimal for post-synthetic stages of polysilane application. During dehydropolymerisation of **4**, the selective synthesis of only **5b** within the polysilane chain would optimise the electronic properties of the bridged polysilane. The incorporation of the chiral-**5b** disilanes would allow for maximal adoption of transoid conformations throughout the bridged-polysilane. This transoid conformation will enable σ-conjugation to proceed along the Si-Si backbone of the bridged polysilane. As discussed in section 1.3.1, the presence of cisoid configurations within the polysilane fail to extend σ-conjugation throughout the length of the polysilane.[25] It is thus proposed the incorporation of the meso isomer **5a** into a polysilane would fail to enhance the electronic properties of the polysilane and purification of the chiral **5b** diastereomer vital towards the synthesis of semi-conducting bridged polysilanes.

It was determined the best strategy to achieve isolated and pure **5b** would involve the identification of high activity dehydrocoupling catalysts that selectivity produced the **5b** without the **5a** and goes to completion under mild conditions. This strategy is validated through attempts to purify and isolate the **5a** and **5b** disilanes through silica-gel chromatography. The moisture sensitivity of disilane compounds presents a significant difficulty in maintaining disilane purity during the purification stages. Repeated chromatography attempts to separate the diastereomers failed with separation of small-scale reaction mixtures silica chromatography resulted in disilane degradation within the column. It is proposed the presence of the Si-Si bond allows for facile cleavage of the disilane whereby the **5a**/**5b** compounds attach to the silica column and are degraded. Separation attempts involving larger scale reaction mixtures were able to elute the **5a** and **5b** products from the column. However, no separation was observed between the **5a**, **5b** diastereomers and **4** disilyl precursor. Attempts to crystallise the disilanes with n-hexanes and pentanes through slow evaporation failed to facilitate crystal formation**.** Successive crystallisation attempts through freezing at -5 °C overnight and -20 °C in pentanes failed to facilitate the formation of any solids either.

During investigative studies into the literature of potential dehydrocoupling catalysts, it was identified a potential variation of the metallocene-based dehydrocoupling reactions which may yield more promising results. Previous attempts using metallocene catalysts used zirconocene dichloride (5 mol %) with n-BuLi (5 mol %) in toluene for 90 h at 90 °C. The mechanism for dehydrocoupling in this catalytic system relies on the formation of the Schwartz reagent ([$Cp_2Zr(H)Cl$]) as the active catalyst (Scheme 3.12). Activation of the zirconocene dichloride occurs through the addition of one equivalent of *n*BuLi. The *n*BuLi reagent is then responsible for substitution of the chloride ligand with a hydride ligand.

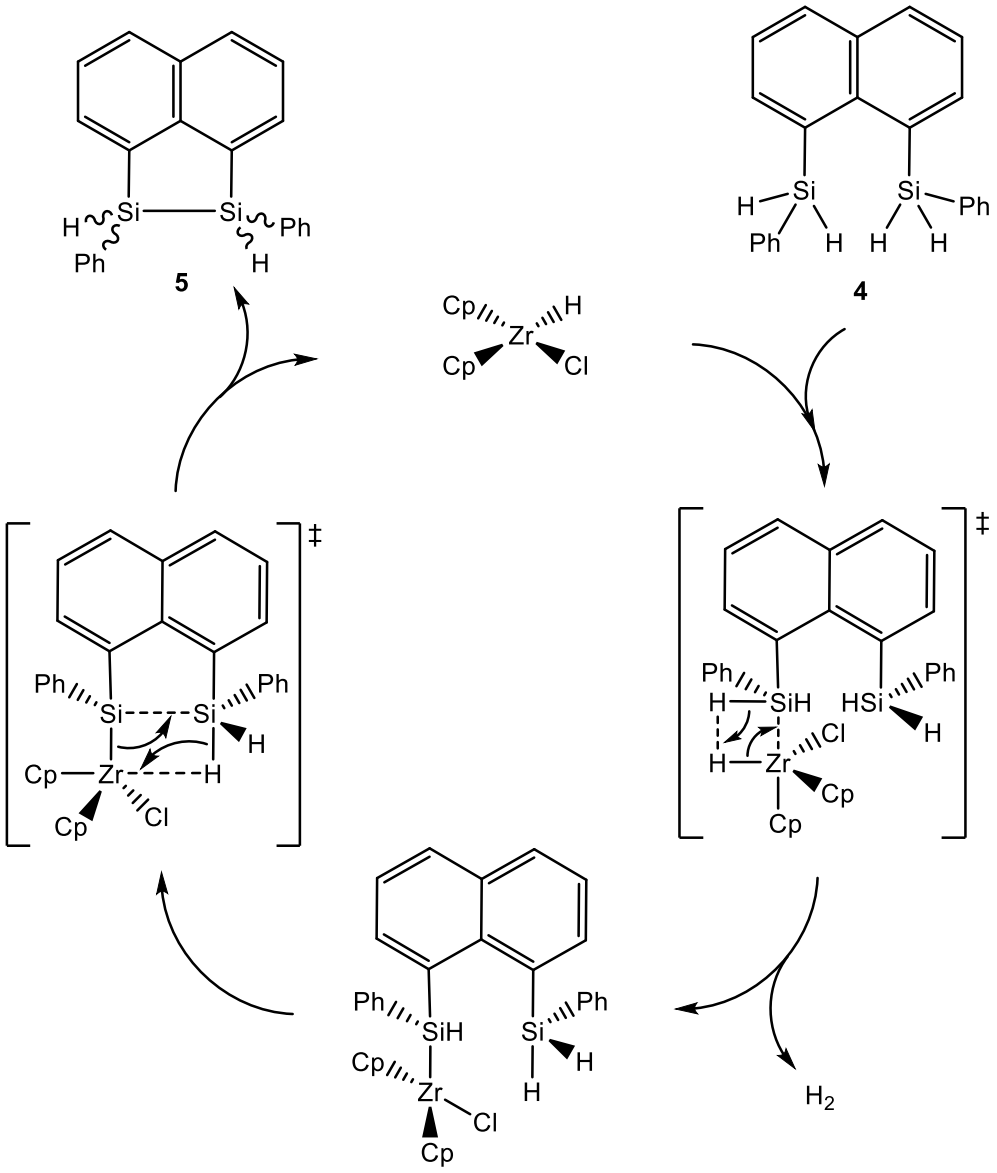

Scheme 3.12 *Proposed dehydrocoupling mechanism for the [$Cp_2Zr(H)Cl$] active catalyst with the (**4**) substrate through σ-bond* metathesis reactions.

While the Schwartz reagent ([$Cp_2Zr(H)Cl$]) has literary precedent as an efficient dehydrocoupling catalyst,[110] its efficiency is limited to primary silanes. This limitation is additionally shared with dialkylmetallocenes (Cp_2MR_2, R = alkyl), which are shown to be incapable of dehydropolymerisation with secondary silanes. In contrast, *in situ* generation of the metallocene catalysts have been repeatedly

reported as capable secondary silane dehydrocoupling catalysts. Standard approaches for *in situ* metallocene catalysts utilise 2 equivalents of alkyllithium for catalytic activation. The best example is the $Cp_2ZrCl_2/2n$BuLi catalytic system reported by Corey et al.[97] While unable to synthesis long polysilanes chains (n > 5), in situ generated metallocenes present a high potential for dehydrocoupling of our secondary silane **4** disilyl precursor. It was thus determined necessary to use the $Cp_2ZrCl_2/2n$BuLi catalytic system for our bridged disilanes (Scheme 3.13).

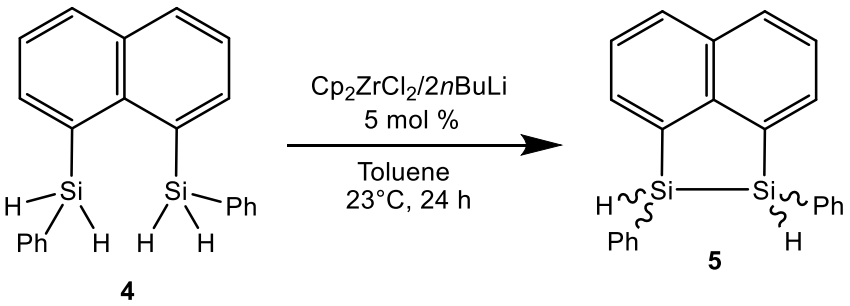

Scheme 3.13 *Catalytic dehydrocoupling of* ***4*** *using* $Cp_2ZrCl_2/2n$BuLi

To confirm the capability of *in situ* metallocene catalysts, an experimental reaction was set up based on the reported $Cp_2ZrCl_2/2n$BuLi catalytic system. This utilised zirconocene dichloride (5 mol %) and n-BuLi (10 mol %) in toluene for 24 h at 25 °C. The n-butyllithium reagent was added to the Cp_2ZrCl_2 before the addition of the hydrosilane to allow for Cp_2ZrBu_2 formation. Observation of the reaction mixture through $^{29}Si\{^1H\}$ NMR spectroscopy showed no reaction had taken after 24 h. However, after 90 h, $^{29}Si\{^1H\}$ NMR signal peaks were present correlating to the **5a** and **5b** isomers. The absence of the **4** signal peak indicated the reaction had gone to completion (Figure 3.10).

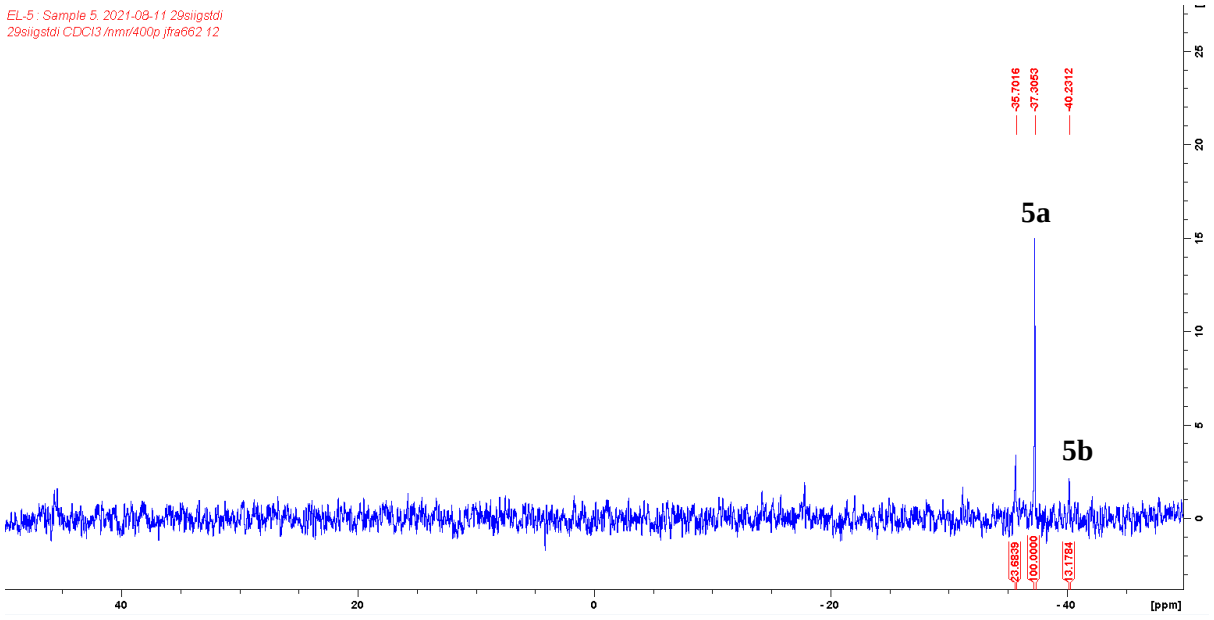

Figure 3.10 *$^{29}Si\{^1H\}$ NMR spectrum of Cp_2ZrBu_2 catalysed dehydrocoupling of* ***4*** *after 90 h.*

The successful observation of the **5** disilane supports the hypothesis that metallocene-based catalysts are capable of bridged disilyl precursor dehydrocoupling. The formation of **5** and reaction completion achieved after 90 h at room temperature indicates the Cp_2ZrCl_2/2*n*BuLi catalytic system as a capable dehydrocoupling catalyst, like $Rh(PPh_3)_3Cl$, which requires 90 h at 90 °C for completion. However, the most important observation from the Cp_2ZrCl_2/2*n*BuLi catalytic system experiment is the new stereoselectivity associated with **5a**, **5b** products. Both disilanes were observed in $29^{29}Si\{^1H\}$ NMR with the dominant formation of the *meso* **5b** disilane with a **5a:5b** ratio of approximately 1:7. This contrasting selectively towards the **5b** disilane is opposite to the selectivity observed for the Rh(I) catalysts. With the evident reaction success of the Cp_2ZrCl_2/2*n*BuLi catalyst, reactions were conducted to identify the impact of each catalyst component on the reaction. The vitalness of *n*BuLi reagent for **5** formation was confirmed as the absence of *n*BuLi from the reaction conditions of Cp_2ZrCl_2 and **4** failed to yield any reaction. However, it was observed increasing the catalyst concentration to 10 mol % drastically decreased the time taken for reaction completion. Significant quantities of **5** was formed (63 % yield) after 24 h with 10 mol % Cp_2ZrCl_2/2*n*BuLi at room temperature, with reaction completion achieved after 48 h (Figure 3.11). However, further increase to catalytic yield proved detrimental to the purity of the product mixture. While the reaction with 25 mol % Cp_2ZrCl_2/2*n*BuLi went to completion after 24 h, an extreme variety of silicon products were observed within the product mixture. It was confirmed the majority of products were **4**, **5a**, **6** or litihiated products of **5a**. It was additionally noted that under these conditions only the *meso* **5a** product was observed with no chiral **5b** product.

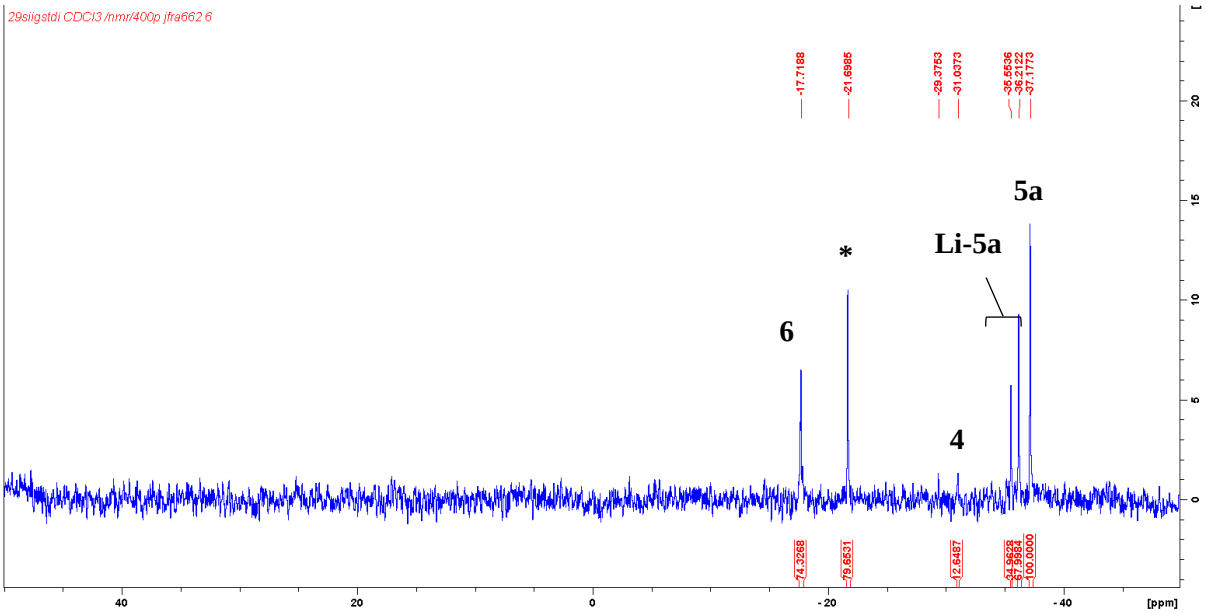

Figure 3.11 *$^{29}Si\{^1H\}$ NMR spectrum of dehydrocoupling reaction of **4** with the Cp_2ZrBu_2 catalyst at 25 mol % catalytic loading after 24 h (* = Grease).*

It is proposed reaction success is reliant on the formation of the [Cp_2Zr^{II}]. This observation further supported the hypothesis that higher concentrations of *n*BuLi facilitates the formation of **5**. Observation

of the Cp_2ZrCl_2/2*n*BuLi catalyst system before the addition of the hydrosilane (**4**) showed that addition of *n*BuLi to Cp_2ZrCl_2 changes the solution to a clear, dark brown solution. It is proposed this brown colour corresponds to) the formation of Zr^{II} complexes, postulated to be the [Cp_2Zr^{II}] active catalyst. This is supported by literature, where intense colour formation corresponds to the adoption of a lower oxidation state for zirconocene catalysts in dehydrocoupling reactions.[100] Generation of a [Cp_2Zr^{II}] complex proceeds through generation of the Cp_2ZrBu_2 complex, which undergoes a β-hydride elimination reaction to produce a Zr-allyl complex (Scheme 3.14). It is postulated the brown colour corresponds to the formation of the Zr^{II}-allyl complex.

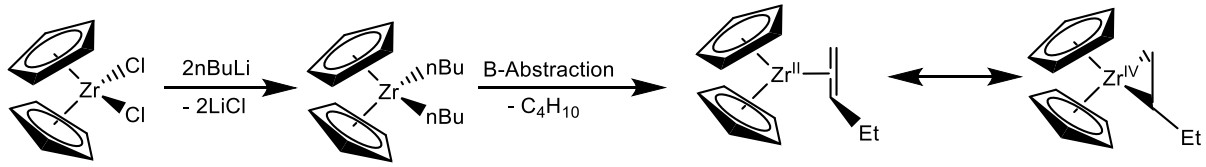

Scheme 3.14 *β-hydride abstraction elimination pathway for the formation of the zirconocene [Cp_2Zr^{II}] complex.*

The induction period associated with the Cp_2ZrBu_2 catalyst originates from the slow displacement of the allyl-ligand from the Zr^{II} metal. Displacement proceeds through oxidative addition of hydrosilane to the zirconocene complex. While there is a free olefin group present for potential hydrosilylation, there is no indication of this pathway with $^{29}Si\{^1H\}$ NMR spectroscopy confirmed the absence of hydrosilylation products from the reaction mixture.

At this stage, the precise nature by which the active catalyst is synthesised was undetermined and could not be reliability ascertained. However, a method by which the induction period for **5** synthesis could be reduced was identified without using high catalytic concentrations. The literature approach for the Cp_2ZrCl_2/2*n*BuLi catalytic system requires addition of Cp_2ZrCl_2 and *n*BuLi before the hydrosilane reagent, ensuring the formation of Cp_2ZrBu_2. However, conducting the experiment through a one-pot style reaction, where *n*BuLi is added to a solution of **4** and Cp_2ZrCl_2, produced more vigorous bubbling during the initial stages of the experiment. Analysis after 24 h revealed a greater yield for both **5a** and **5b** and indicated the reaction had gone to completion (Figure 3.12).

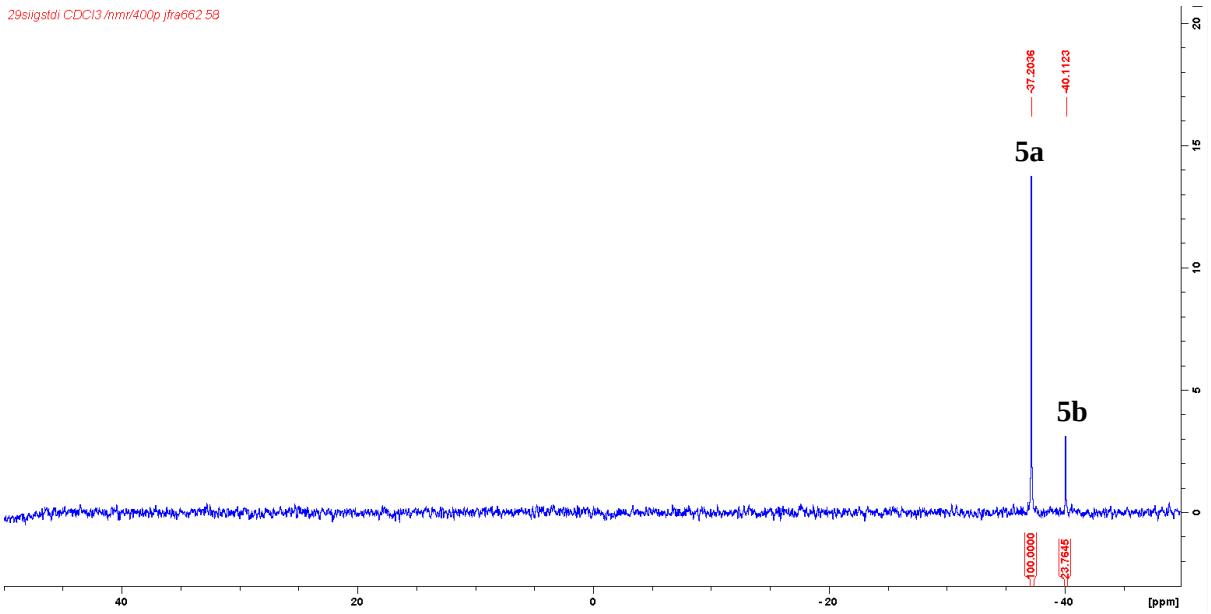

Figure 3.12 *$^{29}Si\{^{1}H\}$ NMR spectrum of dehydrocoupling reaction of **4** with the Cp_2ZrCl_2/2nBuLi catalytic system through one-pot style reaction conditions .*

It is evident the one-pot experimental approach facilitates the dehydrocoupling of **4** more efficiently than standard literature approach. As all the reaction components remain the same between the one-pot and Cp_2ZrBu_2 generated dehydrocoupling reactions, it was postulated the enhanced reactivity of the one-pot approach the presence of a different activation pathway for the catalyst. This is proposed to proceed through preferential lithiation of the hydrosilane over the zirconocene dichloride. This lithiation occurs via proton extraction from the hydrosilane by the butyl group of *n*BuLi. This activates the **4** hydrosilane through the formation of the extremely reactive litihiated-silane compound. Lithiation of **4** allows for direct addition of the silyl species to the zirconocene (Scheme 3.15).

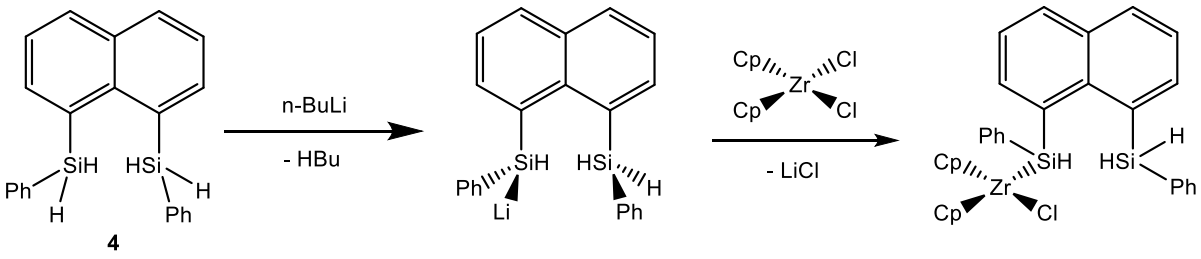

Scheme 3.15 *Reaction scheme for the lithiation of **4** and coordination to the zirconocene complex.*

This pathway avoids the formation of [Cp_2Zr^{II}-allyl] complex. Without having to displace the allyl ligand from the zirconocene, coordination of the hydrosilane proceeds rapidly through oxidative addition and may enter the dehydrocoupling catalytic cycle. The inability of the Schwartz catalyst reaction conditions to catalyst dehydrocoupling indicates the monohydride-zirconocene complex is not the active catalyst for the *in situ* generated metallocene catalysts. It is proposed the active catalyst is the monohydride-,monosilyl- zirconocene complex formed after oxidative addition of a hydrosilane.

Generation of this complex occurs through the reaction of the monosilyl-zirconocene with a second litihiated-silane to facilitate removal of the second chloride ligand. This disilyl complex is converted to the active catalyst) through reductive elimination of the **5** disilane and oxidative addition of the **4** hydrosilane (Scheme 3.16).

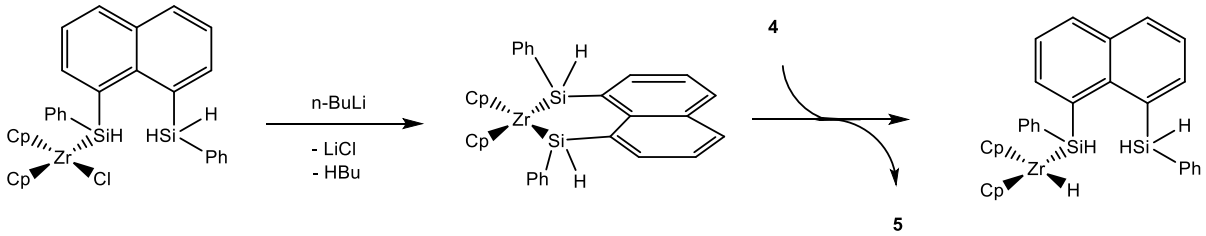

Scheme 3.16 *Conversion of the **4**-zirconocene complex monochloride, monosilyl-zirconocene catalyst to the catalytically active monohydride, monosilyl- zirconocene complex*

Based on the active catalyst being a monohydride-,monosilyl-zirconocene complex, it is proposed the dehydrocoupling of **4** proceeds through a catalytic cycle and reaction mechanism like early-transition-metal silyl-metallocenes catalysts. This proposed mechanism proceeds through a catalytic cycle containing two key stages (Scheme 3.17). The active catalyst undergoes σ-bond metathesis where the disilane is released and a dihydride- zirconocene complex is generated. This highly reactive complex reacts rapidly with another equivalent of hydrosilane to restore the catalyst through dehydrocoupling.

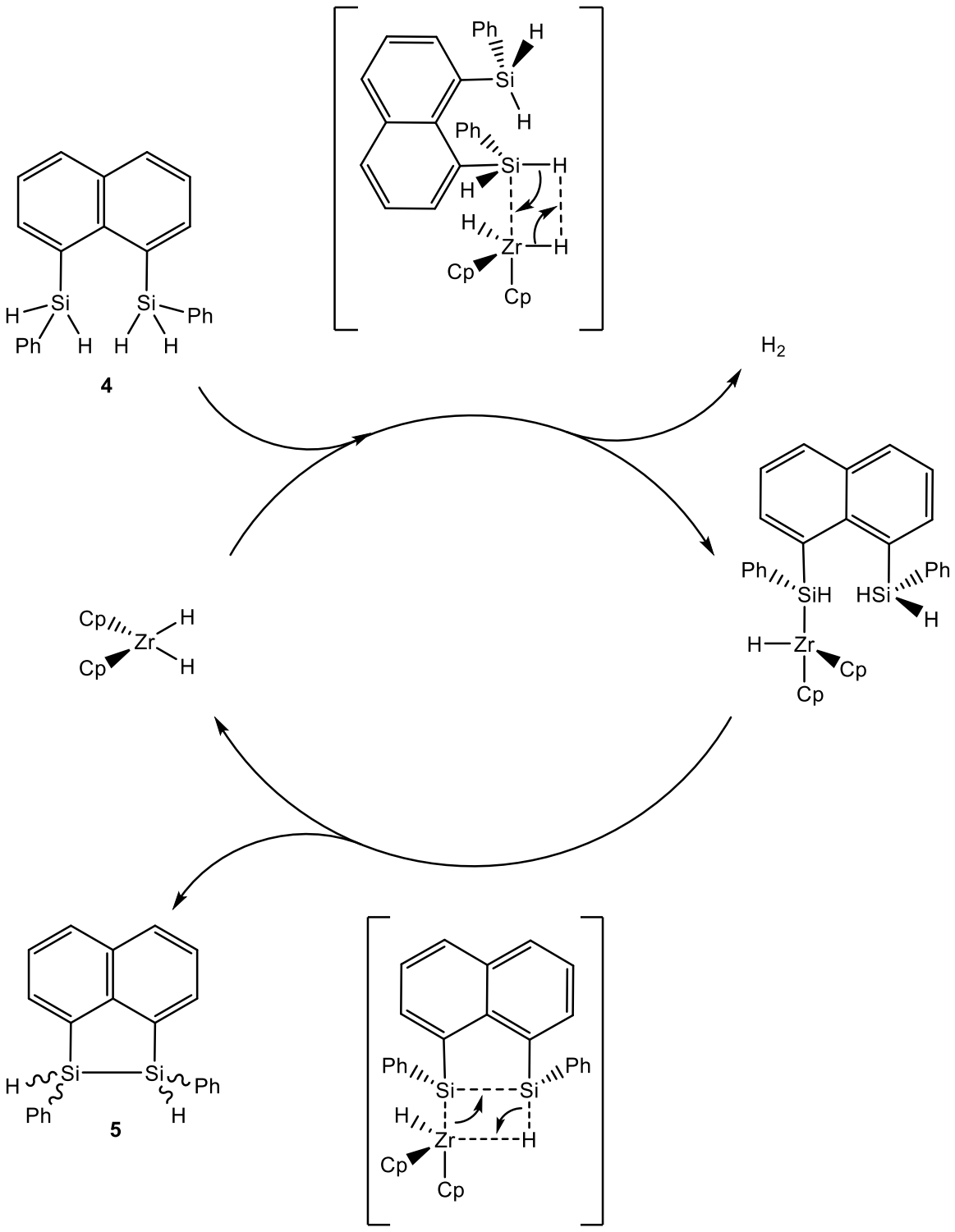

Scheme 3.17 *Catalytic mechanism by which the in situ zirconocene catalyst produces the* ***5a/5b*** *disilanes through the active hydride-, silyl-zirconocene catalyst.*

To confirm the conclusions achieved through the *in situ* Cp_2ZrCl_2/2*n*BuLi catalyst system, further investigation the intramolecular dehydrocoupling reactions into the capability of dialkylmetallocene catalysts was required for bridged disilyl precursor dehydrocoupling. Dimethyl zirconocene (Cp_2ZrMe_2) was identified as the most suitable catalyst due to the simple synthesis associated with

synthesis and mechanistic understanding for silane dehydrocoupling. Generation of the Cp_2ZrMe_2 was achieved through addition of two equivalents of methyllithium to zirconocene dichloride, under inert conditions. Catalytic dehydrocoupling conditions were maintained as identical to the Cp_2ZrBu_2 catalytic reaction (Scheme 3.18).

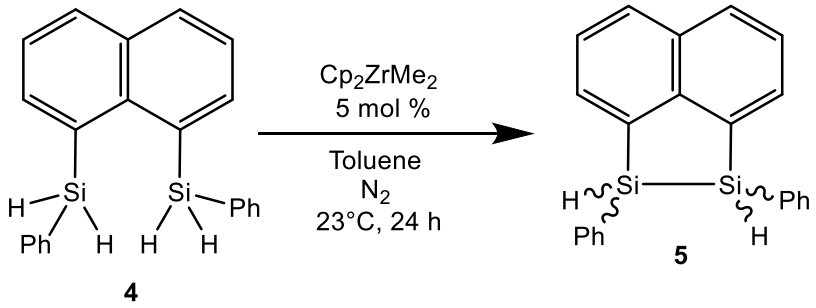

Scheme 3.18 *Catalytic dehydrocoupling of* ***4*** *using* Cp_2ZrMe_2

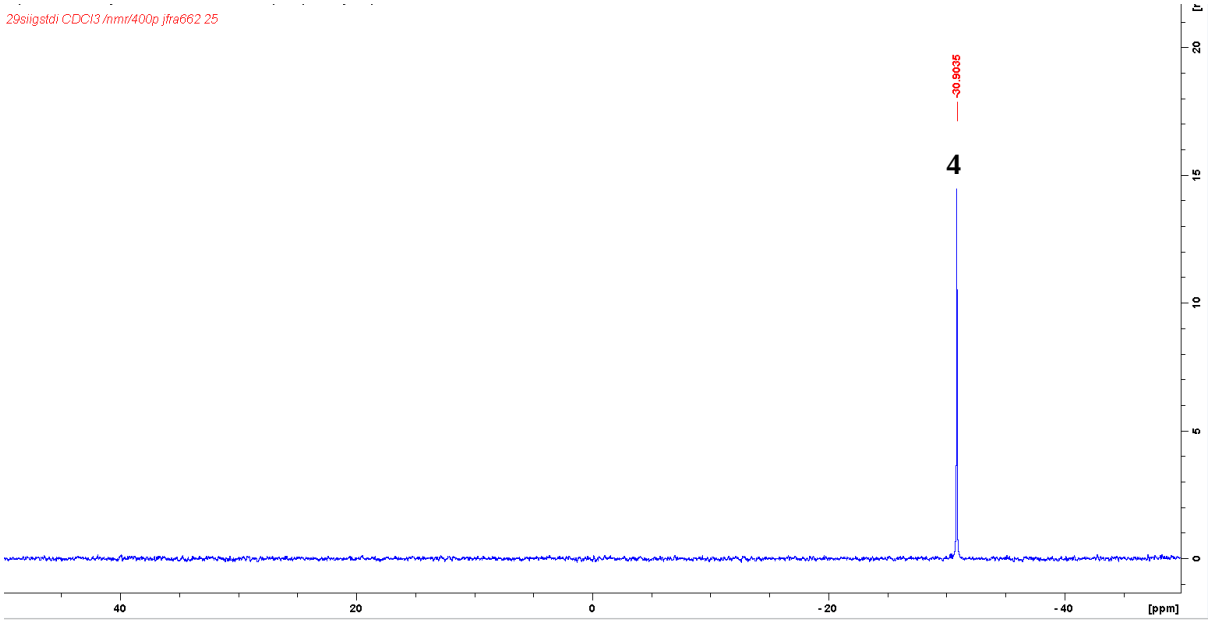

Figure 3.13 *$^{29}Si\{^1H\}$ NMR spectrum of the Cp_2ZrMe_2 dehydrocoupling reaction with* ***4*** *after 72 h.*

$^{29}Si\{^1H\}$ NMR spectroscopy of the post workup reaction mixture after 24 h revealed no reaction had occurred, with the **4** hydrosilane re-obtained from the reaction mixture (Figure 3.13). Allowing the reaction to continue for a week failed to facilitate any reaction. As predicted, the Cp_2ZrMe_2 catalyst was unable to successfully catalyse dehydrocoupling reactions. However, given the increased reactivity observed with Cp_2ZrCl_2/2*n*BuLi system through one-pot style reaction, a similar one-pot style experiment was set up for the Cp_2ZrMe_2 catalyst. This Cp_2ZrCl_2/2MeLi catalytic system was prepared through the direct addition of two equivalents of MeLi were added to a solution of Cp_2ZrCl_2 and **4**. Inspection of the reaction through $^{29}Si\{^1H\}$ NMR spectroscopy after 24 h revealed the majority of the hydrosilane remained unreacted (Figure 3.14). However, both the **5a** and **5b** disilanes were observed in

very minute quantities. ESI-MS was unbale to confirm the presence of **5a**/**5b** due to the low concentration of the product.

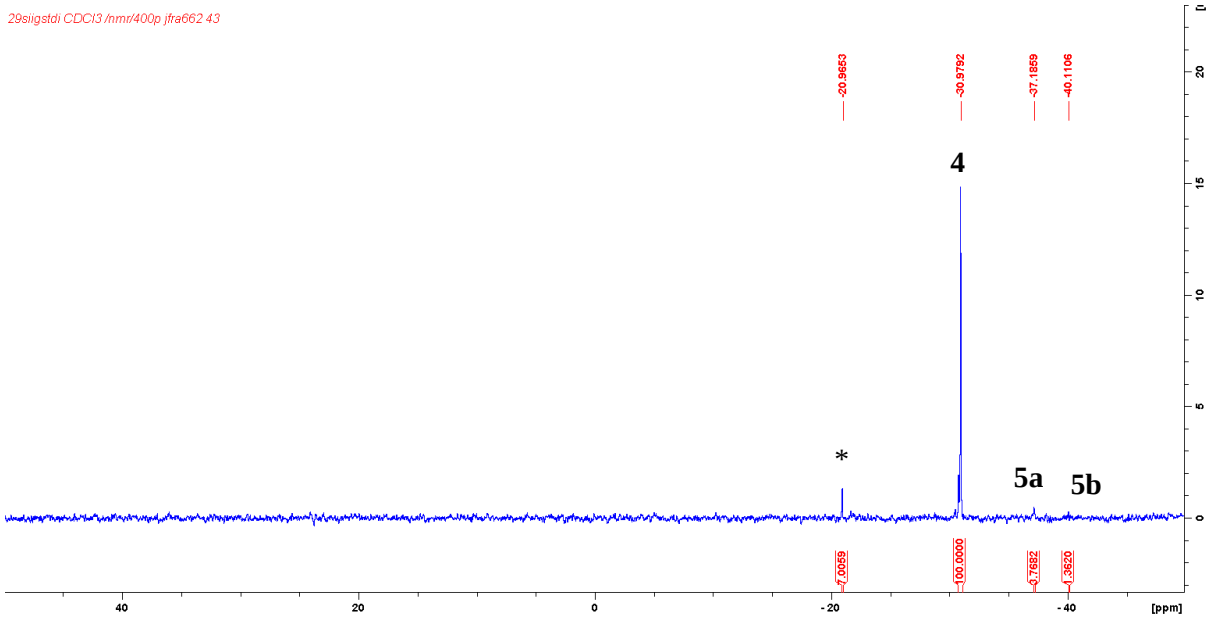

Figure 3.14 *$^{29}Si\{^{1}H\}$ NMR spectrum of the Cp_2ZrCl_2/2MeLi dehydrocoupling reaction with **4** after 72 h.*

The very minute presence of the **5a**/**5b** products through the *in situ* Cp_2ZrCl_2/2MeLi catalyst indicates while Cp_2ZrMe_2 in unable to catalyst the dehydrocoupling of 4, the in situ generated zirconocene catalyst through the above approach is capable. It is proposed disilane formation occurs through the same mechanistic pathway as discussed for the *in situ* Cp_2ZrCl_2/2*n*BuLi catalytic system, as coordination of the litihiated silane to zirconocene proceeds independently to the alkyl substituent for the alkyllithium reagent. The slower rate of reaction and minimal **5** formation observed with the use of MeLi is due to the formation of the catalytically inactive Cp_2ZrMe_2. While capable of catalysing dehydrocoupling for primary silanes, this complex is inactive for **4** dehydrocoupling. Through the direct lithiation of **4**, the active catalyst may be formed and catalyse dehydrocoupling.

With intramolecular dehydrocoupling reactions between the Rh(I) catalysts and zirconocene-based catalysts both favouring different diastereomers of the **5** disilane, it was determined necessary to investigate the mechanistic aspects of all the catalysts, to understand the stereoselectivity of each catalyst, especially given the ratio of **5a**:**5b** formed is heavily impacted by catalyst class and catalyst concentration. Observation of the silane products for the intramolecular dehydrocoupling catalytic reactions displays distinct stereoselectivity for the diastereomers **5a** and **5b**. It is proposed steric factors are the driving factor towards **5a** and **5b** selectivity for the Rh(I) catalysts and the *in situ* zirconocene catalysts. Electronic factors do not immediately present themselves as the dominant factor, with as the band gap difference between meso and chiral diastereomers is insignificant (4.07 vs 4.04 eV for **5a** vs **5b**).

The mechanistic aspects for silane dehydrocoupling for disilane synthesis using Wilkinson's' catalyst has been discussed previously in section 1.5.1. As both catalysts exist as Rh(I) catalysts, it is proposed the $[Rh(cod)Cl]_2$ dehydrocoupling mechanism proceeds through a similar catalytic cycle to $Rh(PPh_3)_3Cl$. It is proposed the active catalyst is the rhodium-hydride species (Figure 3.15).

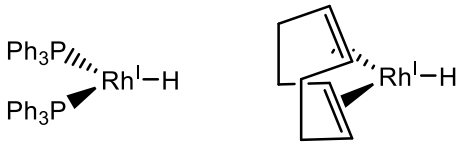

Figure 3.15 *Structure of the active Rh(I) catalysts for the $Rh(PPh_3)_3Cl$ (Left) and $[Rh(cod)Cl]_2$ (Right) catalysts.*

The high catalytic activity for the $[Rh(cod)Cl]_2$ catalyst is partially ascribed to the dimeric nature of the catalyst. Addition of the Rh(I) in a dimer state allows for the masking of a vacant coordination site, resulting in rapid coordination of the hydrosilane to the rhodium centre, hence more rapid catalyst activation. This dissociation of the dimer complex aids explanation why increasing the catalyst loading for the for $[Rh(cod)Cl]_2$ catalyst failed to increase the dehydrocoupling and disilane synthesis rate linearly. Solvation of the Rh(I) catalyst allows for dissociation, where the $[Rh(cod)Cl]_2$ catalyst exists in equilibrium between its dimeric and monomeric states. Increasing the concentration of the dimer pushes the equilibrium further towards dimerization, reducing the amount of free catalyst available to coordinate the hydrosilane substrates. Wilkinson's catalyst in contrast is reliant on the lability of a phosphine- ligand to create a vacant coordination site for hydrosilane coordination. This is driven from the *trans* effect brought about by the presence of the chloride ligand[87] and is comparatively very slow. After the formation of a vacant coordination site, oxidative addition of the hydrosilane (**4**) produces a 5-membered trigonal bipyramidal Rh(III) complex (Scheme 3.19). This complex is key for formation of the active catalyst. The rhodium complex may return to the Rh(I) oxidation state through the reductive elimination of two potential products. Elimination of the hydride and silyl ligands reproduce the original hydrosilane reagent. However, reductive elimination of a chlorosilane species allows for the formation of the active hydride-rhodium (Rh-H) catalyst and allows for dehydrocoupling to proceed.

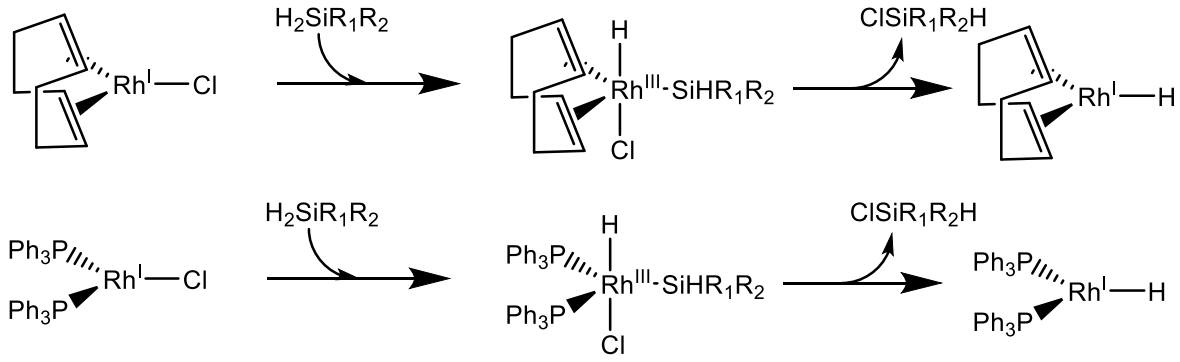

Scheme 3.19 *Formation of the active catalyst for the Rh(I) catalysts; [Rh(cod)Cl]$_2$ (Top) and Rh(PPh$_3$)$_3$Cl (Bottom).*

It is proposed dehydrocoupling proceeds through the catalytic cycles shown in Scheme 3.20 and Scheme 3.21 for [Rh(cod)Cl]$_2$ and Rh(PPh$_3$)$_3$Cl catalyst respectively.

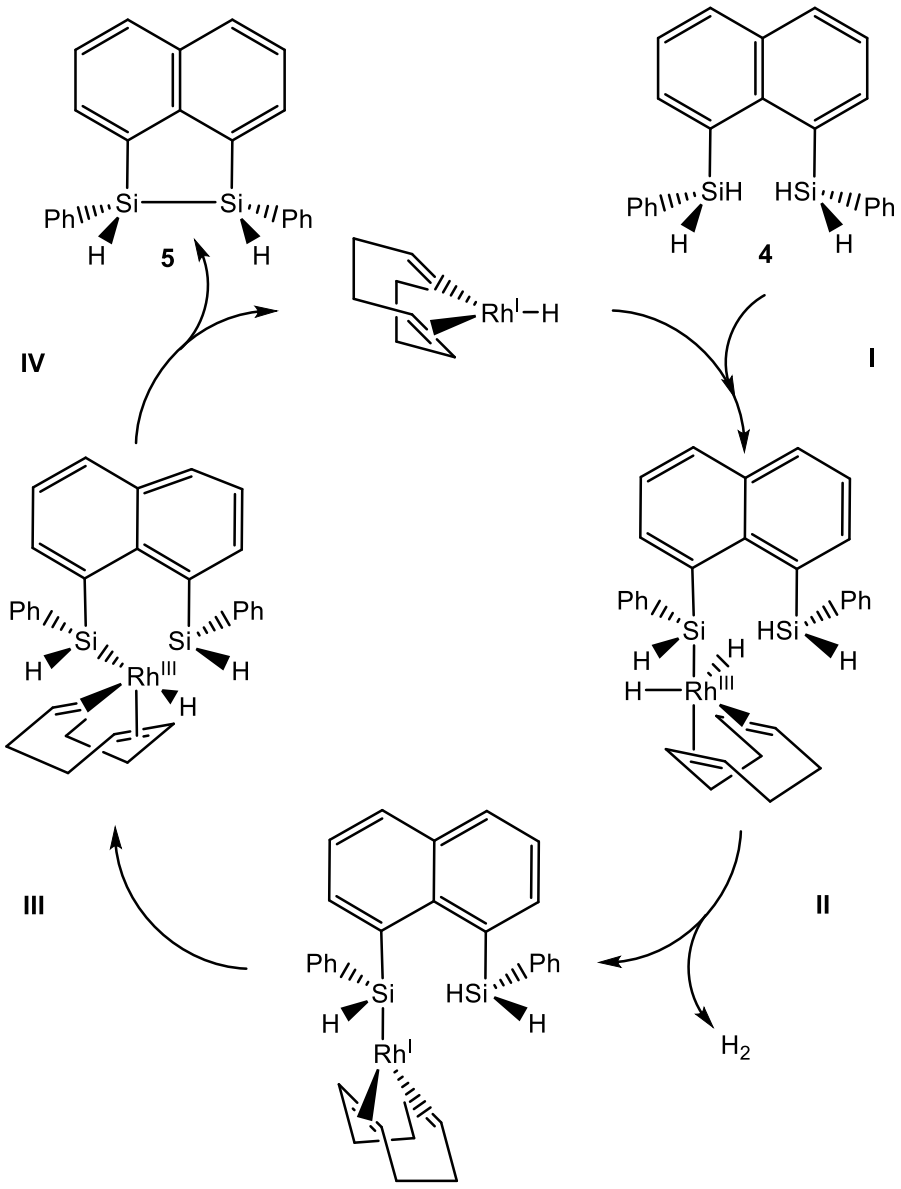

Scheme 3.20 *Proposed mechanism for dehydrocoupling* of **4** to **5** *using [Rh(cod)Cl]₂ via oxidative addition/reductive elimination*

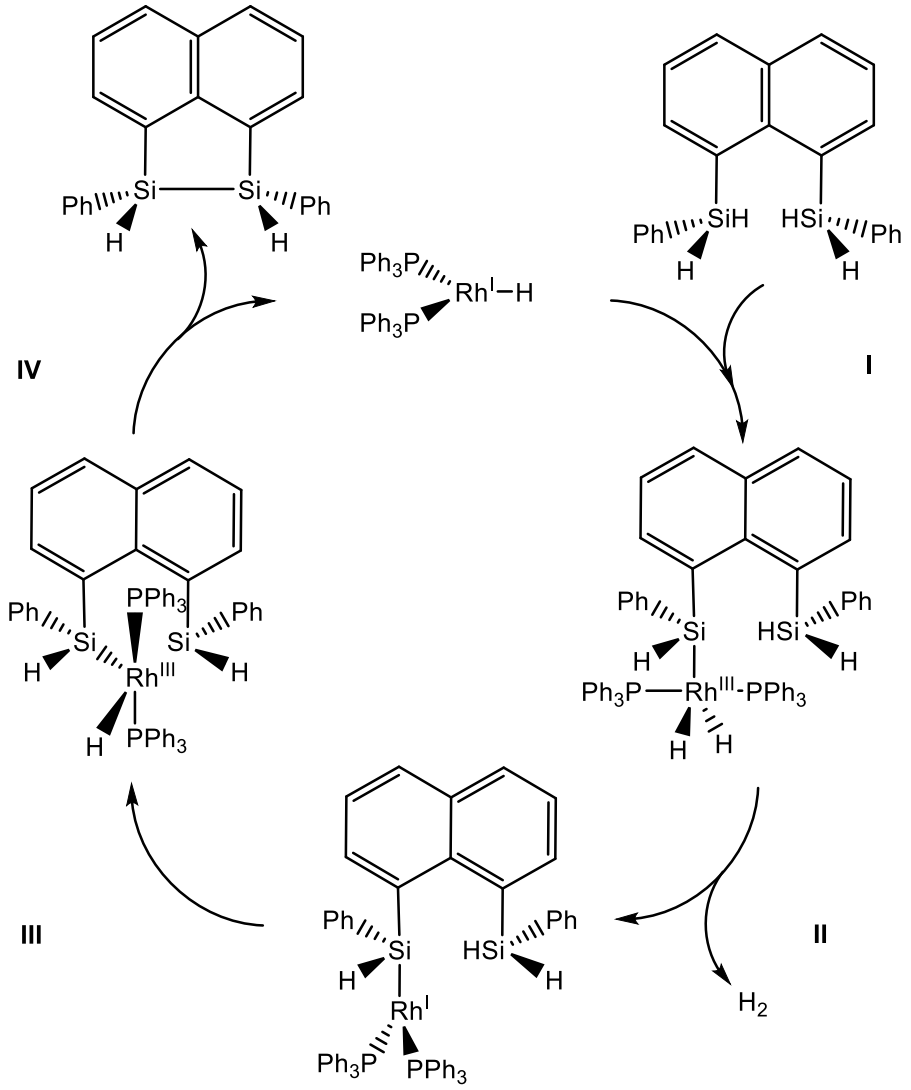

Scheme 3.21 *Proposed mechanism for dehydrocoupling of **4** to **5** using Rh(PPh₃)₃Cl via oxidative addition/reductive elimination.*

Before the dehydrocoupling (step I), configuration of the non-labile ligands has no effect on the stereochemistry of the disilane. However, the structure of the Rh^{III} complex formed after addition of the second hydrosilane (step III) is proposed to have a direct impact of the stereoselectivity of **5** synthesis. It is observed in trans-configuration of the 5-ccordinate disilyl complex possesses a degree of symmetry within the complex. This symmetry provides identical steric factors for both phenyl rings found within **4**. It is based on this assumption that stereoselectivity between the two isomers is dependent on the steric repulsions between each substituent species (i.e., phenyl ring). As steric repulsion between the phenyl rings favours the phenyl rings being *trans* relative to each other, this results in disilane synthesis whereby the phenyl rings are chiral relative to each other and the 2a disilane is produced favourably. The formation of the *trans*-configuration for this complex is supported by structural evidence within mechanistic investigations.

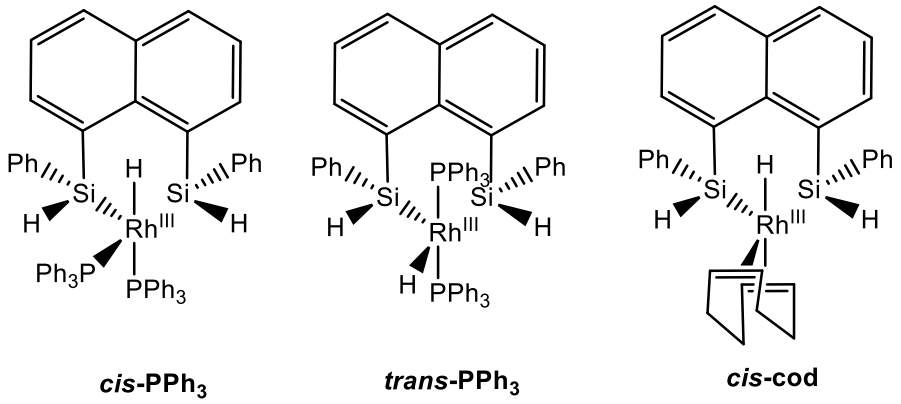

Figure 3.16 *Structure of the stereoselective-determining Rh(I) catalyst complex for each respective Rh(I) catalyst.*

In contrast to the $Rh(PPh_3)_3Cl$ catalysts, the 5-coordinate catalytic intermediates for the $[Rh(cod)Cl]_2$ catalyst are unable to adopt a *trans*-configuration. The bidentate cod ligand limits the complex structures to *cis* configurations. This allows for the selective formation of the cis-Rh^{III} disilyl complex (Figure 3.16). This contrasts structural evidence for the $Rh(PPh_3)_3Cl$ dehydrocoupling catalysts. This may indicate that while the trans-configuration is predominantly observed for the $Rh(PPh_3)_3Cl$ catalyst, both *cis*- and *trans*- configurations are capable of catalysing dehydrocoupling.

It is proposed the preferential formation of the *cis*-configuration 5-coordinate complex removes the selectivity of the Rh(I) catalyst towards chiral **5b** synthesis. The cis-configuration complex produces a complex whereby there is a relative absence of a bulky ligands around one of the axial regions. This provides a region of steric freedom, where the major steric repulsions are those from the cod ligand, a relatively non-bulky ligand. This provides a region which favours where the phenyl rings favourably adopt cis-conformations relative to each other, allowing for more favoured synthesis of the meso **5a** disilane. However, as the $Rh(cod)Cl_2$ catalysts still favour the chiral **5b** diastereomer, it is proposed this steric freedom is relatively low in impact, as the cod ligand is relatively small in bulk. The small bulk of the cod ligand likely allows for the chiral **5b** diastereomer to be formed in a slight majority.

For all the zirconocene catalyst reactions observed, the meso **5a** diastereomer was synthesised in greater quantities than the chiral **5b** diastereomer. It is proposed the stereoselectivity is a consequence of competing steric effects, where the steric bulk provided by the Cp rings overcomes any steric hindrance experienced within the bridged disilane. The σ-bond metathesis nature of zirconocene catalysts requires the zirconocene and the coordinating hydrosilane to occupy a very small tight space for reaction success. While the phenyl rings found within **4** are sterically bulky, the close tight nature of the reaction centre places the Cp rings of the zirconocene near the **4** substrate. The rings sterically repulse the two phenyl rings towards a cis conformation, allowing for more selective **5a** synthesis (Scheme 3.22).

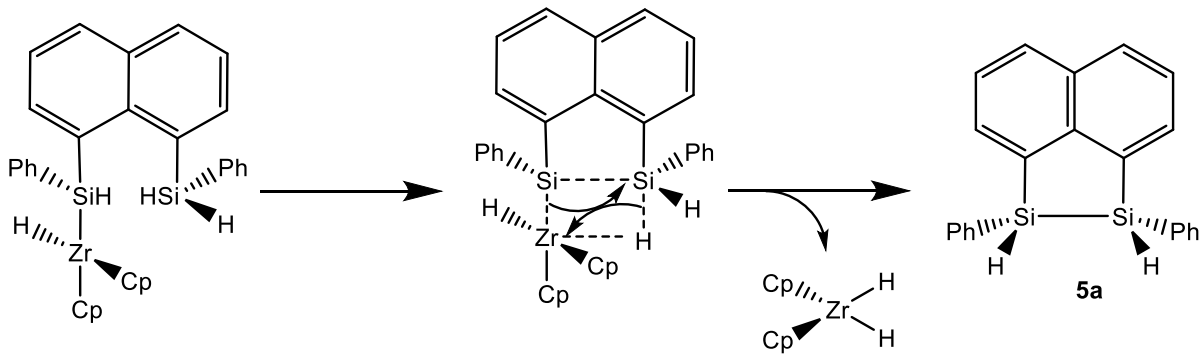

Scheme 3.22 *Proposed σ-bond metathesis mechanism step for the formation of the* ***5a****/****5b*** *disilane.*

The other successful zirconocene catalyst, Cp_2ZrCl_2/2MeLi displays the same stereoselectivity towards meso **5a** synthesis. As reaction success is proposed to occur through lithiation of the **4** hydrosilane, the dehydrocoupling mechanism for the Cp_2ZrCl_2/2MeLi catalyst proceeds through the same dehydrocoupling catalytic cycle as the Cp_2ZrCl_2/2*n*BuLi catalyst. This would agree with the observation where both zirconocene catalysts stereoselectively synthesis the meso disilane at a similar ratio of **5a**:**5b**.

3.3 Ferrocene-Bridged Dehydrocoupling Catalyst Investigation

The relative success observed with the $[Rh(cod)Cl]_2$ and $Cp_2ZrCl_2/2nBuLi$ intramolecular dehydrocoupling catalysts provided a degree of optimism towards the potential application of these dehydrocoupling catalysts for disilane synthesis of non-naphthalene bridged disilanes. During attempts to develop the synthetic library of bridged disilanes and expand the potential scope of bridge substrates, ferrocene was identified as a high-potential molecular bridge. It was proposed incorporation of the ferrocene along the polysilane chain would introduce and organometallic nature to the bridged polysilane chain in addition to introducing redox capabilities. It was postulated attachment of the silyl groups on the Cp rings of ferrocene followed by disilane formation may produce a disilane monomer with favourable electronic effects, arising through the σ-π mixing effects present from disilane (σ) and Cp rings (π). Experimental work confirmed an electronic effect is observed on attachment of the silyl-groups into the Cp rings, producing a new peak in UV/vis spectroscopy in the 450 – 440 nm region. This effect was observed regardless of the nature of the silyl group, silyl species or siloxane.

As the synthesis and investigations into the ferrocene-bridged disilanes were conducted during the initial stages of research into bridged disilanes, the scope of successful dehydrocoupling catalysts remained limited to $Rh(PPh_3)_3Cl$. Intramolecular dehydrocoupling experiments with $Rh(PPh_3)_3Cl$ under extreme conditions (90 °C for 1 week) failed to produce the disilane compound, favouring siloxane formation. Although conducted under inert conditions in a glovebox, siloxane formation was consistent observed across a series of ferrocene disilyl precursors, such as the bis(phenylsilyl)ferrocenes) (**7a**) and 1,1-bis(diphenyl silyl)ferrocenes) (**7b**) precursors (Scheme 3.23).

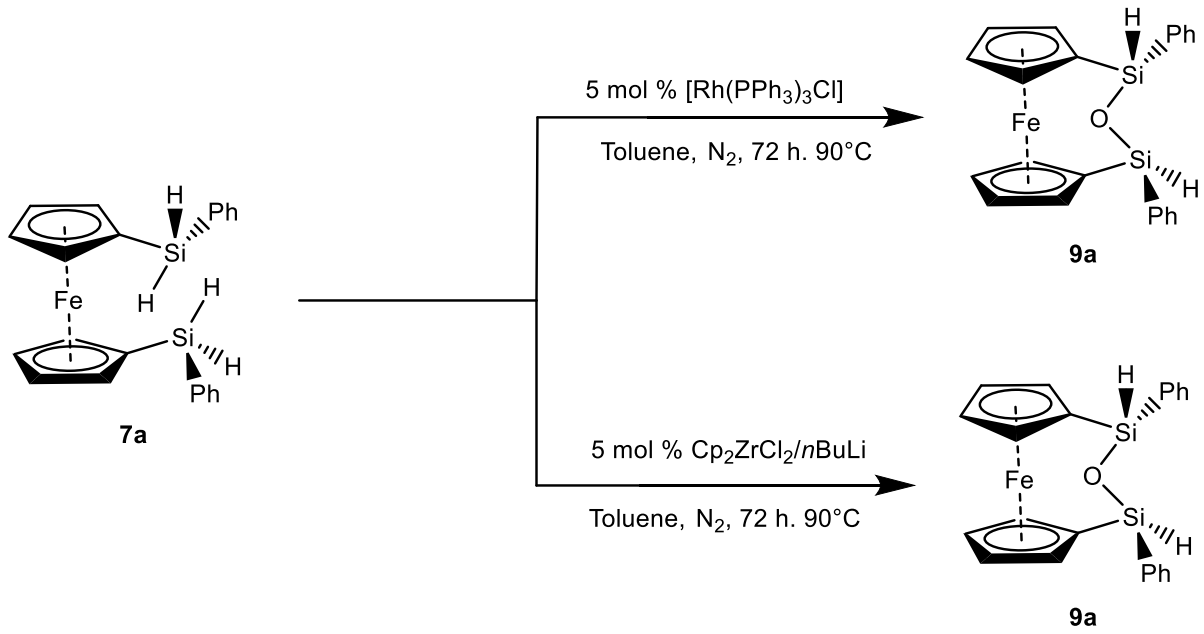

Scheme 3.23 *Catalytic intramolecular dehydrocoupling reaction results of previous research for the bis(phenylsilyl)ferrocene) (**7a**) disilyl precursor with the $Rh(PPh_3)_3Cl$ and $Cp_2ZrCl_2/2nBuLi$ catalysts.*

Previous investigations were unable to confirm source of siloxane formation. Two siloxane synthetic pathways are present within the dehydrocoupling reaction conditions. Dehydrocoupling catalysts are well-known to facilitate selective siloxane formation in the presence of water, at the cost of disilane formation (Scheme 3.24, step I). This is especially true late transition metal catalysts such as rhodium-based catalysts. However, facile oxidation of the disilane compound allows for a degradation based pathway, where siloxane formation is dependent on disilane formation by the dehydrocoupling catalysts (Scheme 3.24, step II).

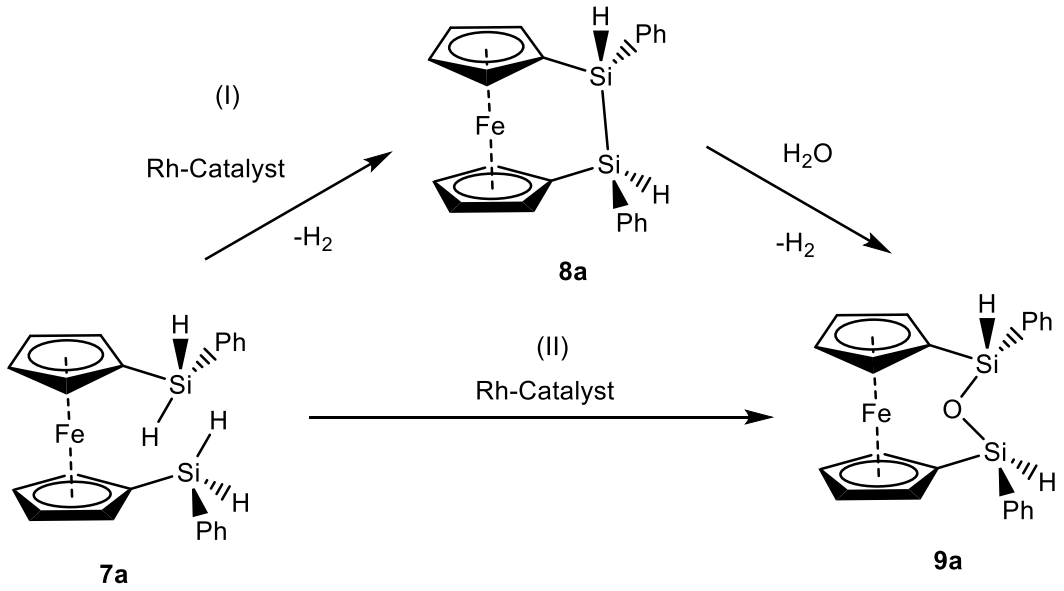

Scheme 3.24 *Depiction of two pathways for siloxane synthesis; through facile insertion of H_2O to a disilane (**8**) (I) or through rhodium-catalysed siloxane formation (II).*

It was unknow and unconfirmed whether the disilane degradation pathway was present within the reaction mixture due to the uncertainty present whether the disilane was present within the reactions at all. Since the initial dehydrocoupling investigations surrounding ferrocene disilyl precursors, a wider range of dehydrocoupling catalysts have been found capable of efficient disilane synthesis. Theses catalysts, specifically the $[Rh(cod)Cl]_2$ dimer and the *in situ* Cp_2ZrCl_2/2*n*BuLi catalysts have exhibited greater dehydrocoupling activities than the previously utilised catalysts. It was determined vital to investigate the intramolecular dehydrocoupling reactions with the two catalysts mentioned before, to provide more information surrounding ferrocene-bridge disilane formation. It is postulated treatment of the ferrocene-bridged disilyl precursors with these more active catalysts may yield successful disilane synthesis in small quantities (Scheme 3.25).

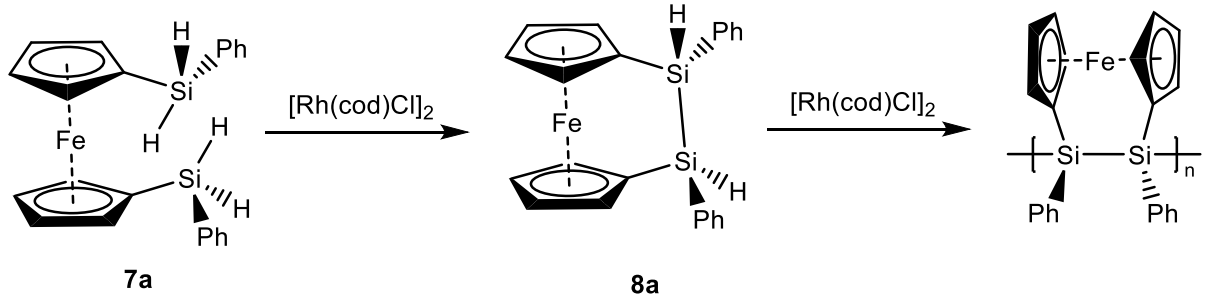

Scheme 3.25 *[Rh(cod)Cl]$_2$ catalysed dehydropolymerisation of the ferrocene-bridge **7a** substrate.*

Synthesis of ferrocene-bridged disilyl precursors **7a** and **7b** has been established in previous work supported by literature approaches. Synthesis of the disilyl-ferrocene compounds follows a di-lithiation of the ferrocene substrate, whereby addition of a 2 chlorosilanes allowed for successful synthesis of **7a** and **7b** (Scheme 3.26).

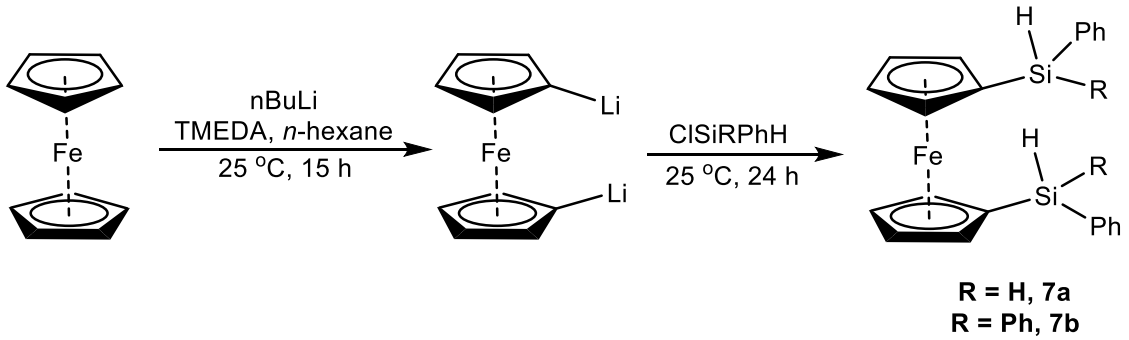

Scheme 3.26 *Synthetic approach for the synthesis of the **7a** and **7b** disilyl precursors.*

Intramolecular dehydrocoupling of the **7b** disilyl precursor was conducted under the same experimental conditions as for the **4** disilyl precursor. Experiments of the **7b** disilyl precursor with the [Rh(cod)Cl]$_2$ dimer and Cp$_2$ZrCl$_2$/2*n*BuLi catalysts after 24 h under mild conditions indicated no reaction had taken place through ^{29}Si{^{1}H} NMR spectroscopy. Leaving the reaction for one week failed to produce any reaction, with the **7b** precursors re-obtained from the reaction.

The inability of the Cp$_2$ZrCl$_2$/2*n*BuLi catalyst to synthesis **8b** is predictable, with the literature precedent of metallocenes being incapable of tertiary silane dehydropolymerisation. In contrast, the [Rh(cod)Cl]$_2$ dimer has been shown to be capable of intramolecular dehydrocoupling of tertiary silanes for disilane synthesis. This one example of this is for the naphthalene-bridged disilyl precursor

(tetramethyl, disilyl-naphthalene). The inability of the $[Rh(cod)Cl]_2$ dimer to catalyse any reaction may indicate higher temperatures are required to facilitate siloxane synthesis.

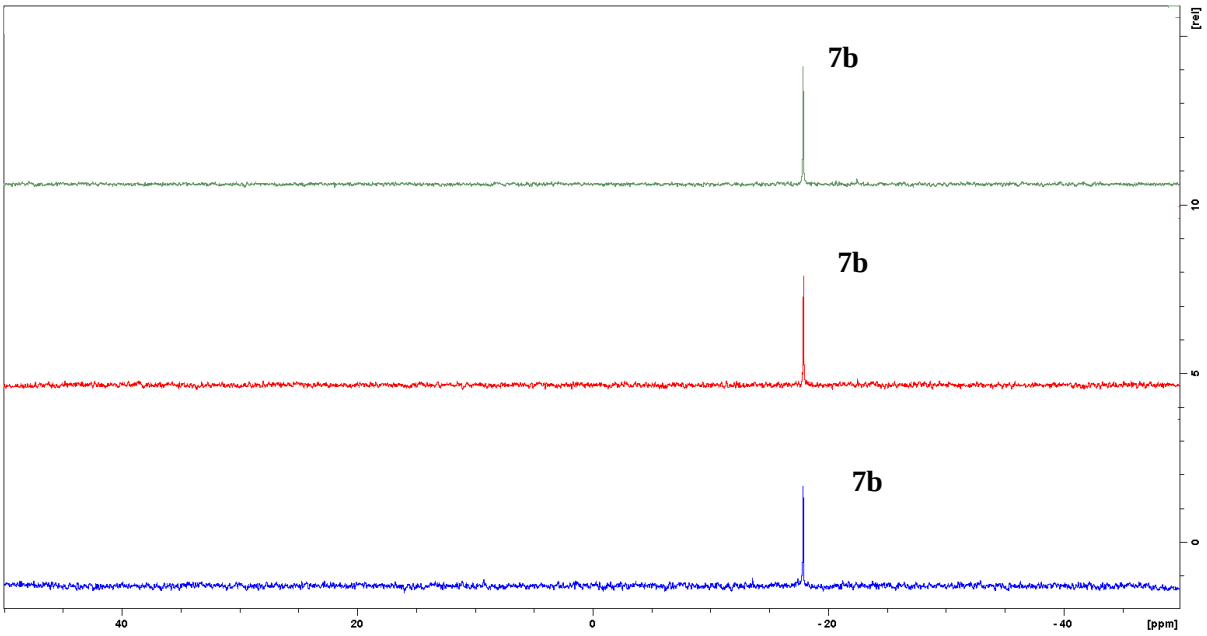

Figure 3.17 *$^{29}Si\{^1H\}$ NMR spectra for the dehydrocoupling catalyst reactions with **7b** (Green = purified **7b**, Red = $[Rh(cod)Cl]_2$, Blue = Cp_2ZrCl_2/2nBuLi).*

In contrast to the **7b** dehydrocoupling experiments, **7a** dehydrocoupling was predicted to catalyst disilane formation. Initial attempts to observe the reaction after 24 h were complicated through the apparent absence of silicon species in $^{29}Si\{^1H\}$ NMR spectroscopy (Figure 3.17). Subsequent analysis revealed work-up of the reaction mixture through florasil pipettes resulted in the degradation of our silyl-based products. It is presumed addition of the reaction mixture to the florasil pipette resulted in the attachment of the ferrocene-bridged products to the silica layers, where they are unable to be eluted from the florasil column. This resulted in a series of silyl-cleaved products being observed through NMR and ESI techniques. Subsequent analysis of the reaction mixtures was not worked up, with the catalyst remaining the analysed mixture.

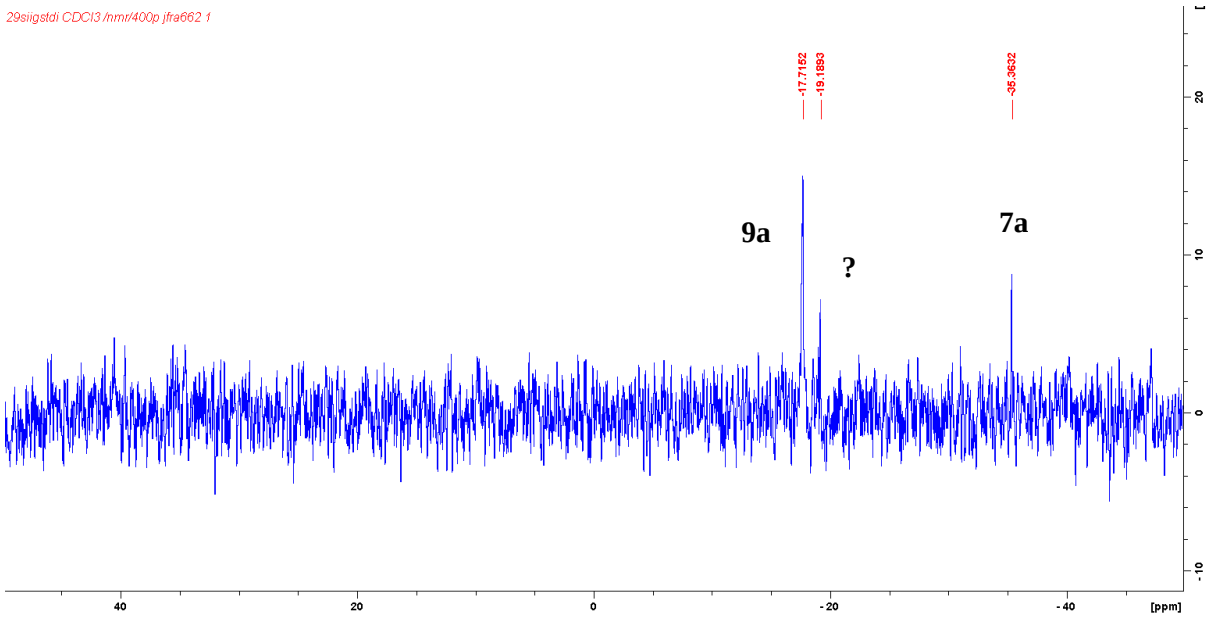

Figure 3.18 *$^{29}Si\{^{1}H\}$ NMR spectrum of the dehydrocoupling reaction between 1,1-bis(phenylsilyl)ferrocene (**7a**) and the $[Rh(cod)Cl]_2$ catalyst.*

For the $[Rh(cod)Cl]_2$ catalysed reaction, two main products were observed in the $^{29}Si\{^{1}H\}$ NMR spectrum after 24 h alongside unreacted **7a** (Figure 3.18). The peak at -17.7 ppm corresponded to the siloxane product (**9a**). The identity of the signal peak at – 19.2 ppm is unknown, with ESI unable to provide conclusive evidence as to its identity. ESI-MS was unable to confirm the presence of the **8a** disilane. It is proposed the -19 ppm signal does not correspond to the **8a** disilane. This is supported by the observation that the signal for **8a** is expected further up field in the $^{29}Si\{^{1}H\}$ NMR spectrum. It was hoped the catalytic reaction of **7a** with the $Cp_2ZrCl_2/2n$BuLi catalyst would shed more information on the reaction products observed above. In contrast the $Cp_2ZrCl_2/2n$BuLi system failed to catalyse any reaction for the **7a** dehydrocoupling experiment (Figure 3.19). Analysis of the ESI-MS results explains the inability of the catalyst to yield any reaction.

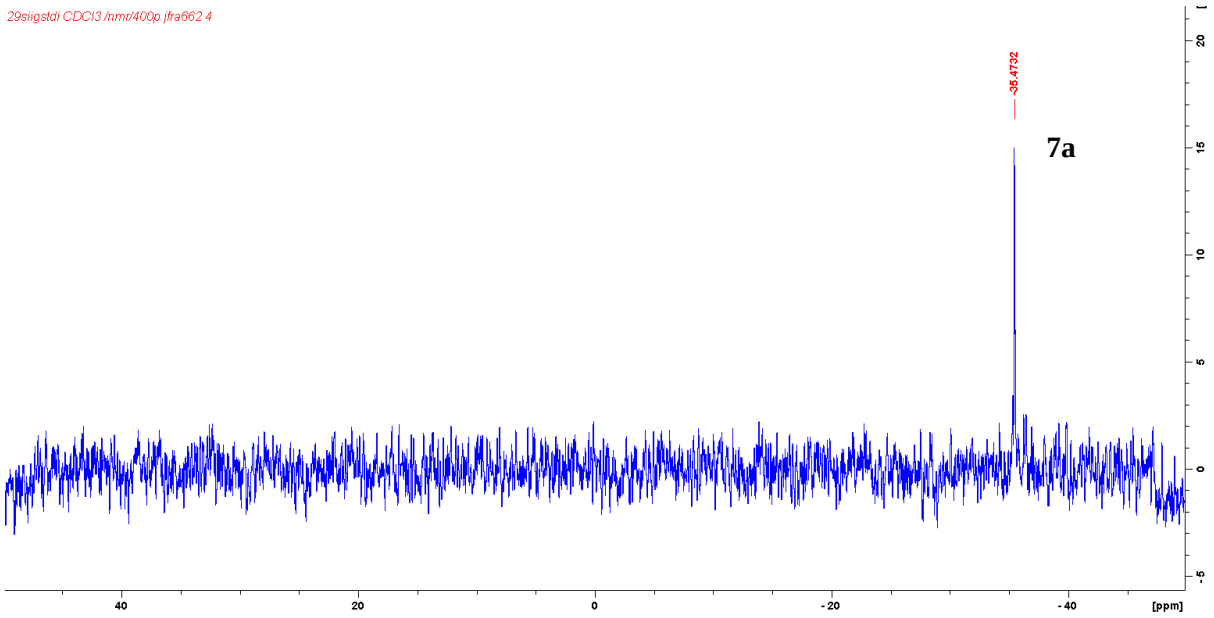

Figure 3.19 *$^{29}Si\{^{1}H\}$ NMR spectrum of the dehydrocoupling reaction between 1,1-bis(phenylsilyl)ferrocene (**7a**) and the Cp_2ZrCl_2/2nBuLi catalyst.*

As discussed earlier for the **4** hydrosilane**,** the mechanism for the Cp_2ZrCl_2/2*n*BuLi catalyst system relies on lithiation of the hydrosilane for rapid activation of the metallocene catalyst. For the naphthalene precursors, lithiation occurs preferentially at the hydrosilane. However, ferrocene-bridged disilyl precursors present an additional site for lithiation, the protons on the Cp rings. Synthesis of the **7a** and **7b** reagent rely on lithiation of the Cp ring for silyl attachment. It is proposed the addition of an alkyllithium reagent fails to react with the zirconocene dichloride or hydrosilane functionalities, instead preferential lithiation of the Cp ring occurs (Scheme 3.27). This means the active catalyst required for dehydrocoupling remains unformed and no dehydrocoupling reactions may proceed.

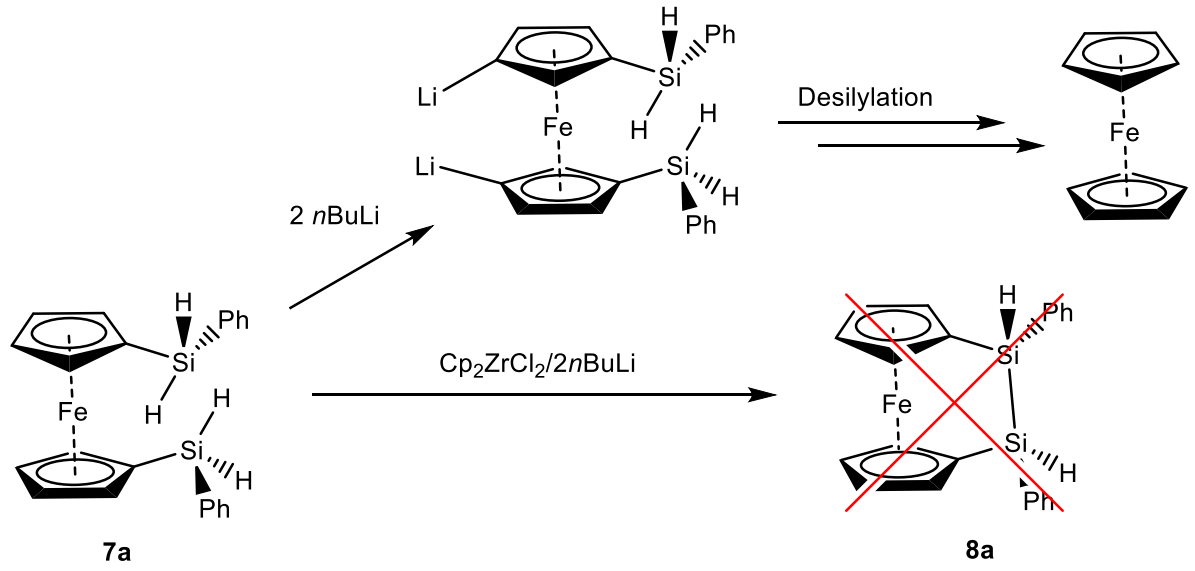

Scheme 3.27 *Reaction scheme indicating the lithiation of the ring instead of the zirconocene*

The absence of the active zirconocene dehydrocoupling catalyst may explain the complete absence of reaction, specifically the absence of siloxane formation. Sadly, preparation of the active catalyst before the addition of the hydrosilane was not identified as a viable approach. Lithiation of the hydrosilane for **4** dehydrocoupling was the reason behind the reduction of the observed induction period for dehydrocoupling with the Cp_2ZrCl_2/2*n*BuLi catalyst. The addition of Cp_2ZrCl_2 and *n*BuLi reagent before the addition of the **7** hydrosilane would prevent lithiation of the Cp rings. However, this would generate the Cp_2ZrBu_2 complex, which would require the extreme temperatures to undergo dehydrocoupling and has been previously show unable to for disilane formation, favouring siloxane synthesis.

Thus, it is concluded the Cp_2ZrCl_2/2*n*BuLi catalyst system is capable of efficient dehydrocoupling for the naphthalene-bridged disilanes. However, further application of the *in situ* generated Cp_2ZrCl_2/2*n*BuLi system should be limited to disilyl precursors which do not possess functionalities capable lithiation. Given the ability of the $[Rh(cod)Cl]_2$ catalyst to catalyse siloxane formation under mild conditions, it is proposed siloxane formation for the above conditions proceeds entirely through the rhodium-catalysed siloxane synthetic pathway, instead of facile degradation of the **8a** disilane. Confirmation of the identity of the signal at -19.2 ppm may prove otherwise. However, this is unlikely.

Chapter 4: Conclusion and Future Work

4.1 Summary & Conclusions

This thesis details continued attempts to develop bridged-disilanes towards the synthesis of robust polysilane chains. The identification of a synthetic procedure capable of benzyl silane synthesis with chloro(phenyl)silanes was not identified. Two Grignard procedures for reported benzyl silane synthesis were investigated and reaction success was unconfirmed. Lithiation approaches were confirmed as non-viable for benzyl silanes, where preferential lithiation of the benzene ring prevents reaction success. The $[Rh(cod)Cl]_2$ catalyst was identified and confirmed as a highly efficient dehydrocoupling catalyst for the synthesis of the chiral **5b** bridged disilane. The other Rh(I) catalyst, $Rh(PPh_3)_3Cl$, was shown possess relatively lower dehydrocoupling activity with greater selectivity towards the **5b** diastereomer. In contrast, the Cp_2ZrCl_2/2*n*BuLi catalyst was identified as a highly efficient dehydrocoupling catalyst for the synthesis of the meso **5a** bridged disilane. The addition of the *n*BuLi to the **4** hydrosilane allows for lithiation of the hydrosilane, increasing the reaction rate from days to hours. The stereoselectivity for the two dehydrocoupling catalyst classes was explained through investigation into the dehydrocoupling mechanisms for **4** to **5**. Dehydrocoupling investigations with the ferrocene-bridged disilyl precursors (**7a** & **7b**) were unable to synthesis the **8** disilane through the $[Rh(cod)Cl]_2$ or Cp_2ZrCl_2/2*n*BuLi catalysts. The $[Rh(cod)Cl]_2$ catalyst was shown to be capable of siloxane (**9a**) synthesis under mild conditions. Use of the Cp_2ZrCl_2/2*n*BuLi catalyst was determined to be substrate-dependent, where addition of *n*BuLi may allow for degradation of the hydrosilane.

4.2 Future Work

4.2.1 Synthesis of benzyl silane bridge monomers

Attempts to produce disilyl precursors possessing benzyl silane functionalities were unsuccessful with the use of chloro(phenyl)silane determined to be the limiting factor. Future work should in this area should focus on the use of chloro(alkyl)silanes within Grignard approaches for the synthesis of bridged-(alkyl)disilanes. Through avoiding the presence of the aryl species, this allows for the use of a more reactive chlorosilane species for benzyl silane synthesis, as observed in previous work surrounding benzyl silane synthesis for chloro(disubstituted)silanes. The use of chloro(alkyl)silanes is proposed to proceed readily for benzyl silane synthesis and would allow for better confirmation surrounding the effectiveness of the two Grignard procedures for the synthesis of benzyl silanes. It is proposed chloro(methyl)silane (Scheme 4.1) and chloro(hexyl)silane should be utilised during initial studies. Both selected chlorosilanes possess two hydride functionalities, allowing for the presence of terminal Si-H ends in the dehydrocoupled bridged disilane monomer to allow for subsequent

dehydropolymerisation.

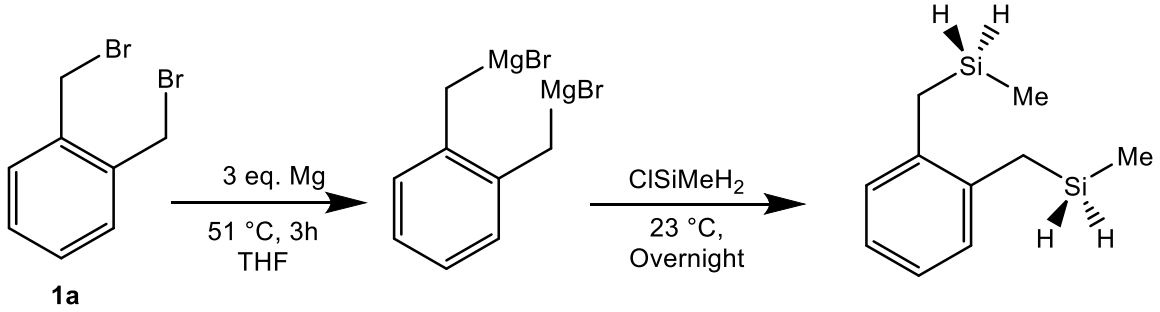

Scheme 4.1 *Proposed synthesis of a di(benzyl silane) precursor through Grignard methods with a chloro(methyl)silane reagent.*

4.2.2 Naphthalene-Bridged Dehydrocoupling Catalyst Investigation

Investigation into the $[Rh(cod)Cl]_2$ catalyst confirmed the catalyst as a highly efficient dehydrocoupling catalyst the intramolecular dehydrocoupling of **4** to the **5** disilane. However, increased catalytic loading and higher temperatures failed to exhibit the presence of tertiary dehydrocoupling between the bridged disilane **5** monomers. Future work should investigate deeper into dehydrocoupling catalyst design with specific attention provided towards the preparation of the bridged disilane monomers through intramolecular dehydrocoupling of secondary silanes, and the intermolecular dehydrocoupling of the **5** monomers through tertiary silane dehydrocoupling.

Given the increased reactivity required for tertiary dehydrocoupling, it is likely catalysts capable of intramolecular dehydrocoupling for bridged disilane synthesis will not be suitable or able to catalyse intermolecular dehydrocoupling between the bridged disilane monomers. Given the increased reactivity requirement, it is proposed catalyst investigation should proceed alongside the idea of identifying two different dehydrocoupling catalysts. one catalyst would be optimal for intramolecular dehydrocoupling of the disilyl precursors, with a second catalyst capable of tertiary dehydrocoupling and polymerisation for polysilane synthesis (Scheme 4.2).

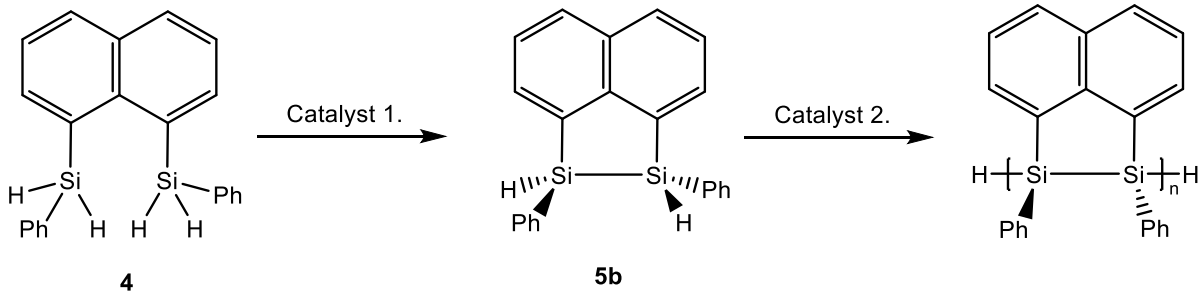

Scheme 4.2. *Proposed dehydropolymerisation scheme whereby two catalysts; 1 & 2, are utilised for poly(5b) synthesis. Catalyst 1. = Intramolecular dehydrocoupling catalyst and Catalyst 2. = Intermolecular dehydrocoupling catalyst.*

Stereoselective formation of the chiral diastereomers by both dehydrocoupling catalysts would prove favourable for subsequent electronic application. As discussed previously, the chiral diastereomers allow for maximum σ-conjugation throughout the polysilane Si-Si backbone, providing the desirable semiconducting properties associated with polysilane electronic application. Catalyst selection needs to consider the stereoselectivity of each catalyst, ensuring the synthesis of the chiral disilanes (i.e., **5b**) in high yields.

It is with this in mind, zirconocene catalysts are ruled out as potential dehydrocoupling catalysts for future work. Incapable of tertiary silane dehydrocoupling, the use of zirconocene catalysts through Cp_2ZrCl_2/2nBuLi or Cp_2ZrBu_2 are unsuitable, due to their stereoselective synthesis of the meso **5a** disilane.[91] However, non-zirconocene metallocenes may yet prove more successful for intramolecular dehydrocoupling. Titanocene catalysts have been reported to possess great stereoselectivity towards all-*trans* cyclic polysilanes.[111] While cyclisation is unlikely to proceed, intramolecular dehydrocoupling towards the chiral disilane synthesis presents a great potential option for future investigation.

Alongside the titanocene catalysts, it is proposed nickel-based catalysts and lanthanide based dehydrocoupling catalysts be investigated for intramolecular dehydrocoupling. The $[(dppe)Ni(\mu\text{-}H)]_2$ and $[Ni(dmpe)_2]$ dehydrocoupling catalysts were both identified as capable secondary silane dehydrocoupling catalysts.[73,74,112] The use of lanthanide-based catalysts may prove limited for control over the stereoselectivity of the disilane product. Lanthanide dehydrocoupling catalysts proceed through σ-bond metathesis style reactions. The precise stereoselectiveness of lanthanide complexes varies significantly between metal complex and may prove suitable of chiral disilane synthesis.

Identifying potential intermolecular dehydrocoupling catalysts is the greater challenge, with all potential catalyst needing to be capable of tertiary silane dehydrocoupling. This required reactivity limits catalyst selection to late transition metals, specifically rhodium and platinum catalysts. Given rhodium dehydrocoupling catalysts have been investigated in the present work, initial studies should focus on platinum catalysts, specifically Karstedt's catalyst and the $Pt(cod)_2$ catalyst. Both platinum catalysts have reported success with regards to polysilane synthesis. Karstedt's catalyst is the only report catalyst capable of tertiary dehydropolymerisation under room temperature conditions.[76] The $Pt(cod)_2$ catalyst likewise was reported to catalyse the dehydropolymerisation of a silafluorene substrate.[65] While polysilane synthesis through Pt catalysts are limited by relatively molecular weight distributions (PDI > 2)[63,65] the high reactivity of the Pt catalysts may be required to observe successful polymerisation of our bridged disilanes (**5**).

Additional future work surrounding the naphthalene-bridged disilanes should prioritise the identification purification methods using non-silica means. Silica gel chromatography has been shown unreliable for separation of **5a**, **5b** and **4** from a product mixture, with degradation of 5a and 5b

observed. The ability to purify the diastereomers would reduce the pressure for the dehydrocoupling catalysts to produce only chiral disilanes.

It would prove insightful to synthesis the methyl-substituent variant of the **4** precursor and **5** disilane, to investigate the potential difference in stereoselectivity and efficiency of the previously discussed dehydrocoupling catalysts (Scheme 4.3). This would additionally be interesting to compare the difference in electronic properties through non-computational means.

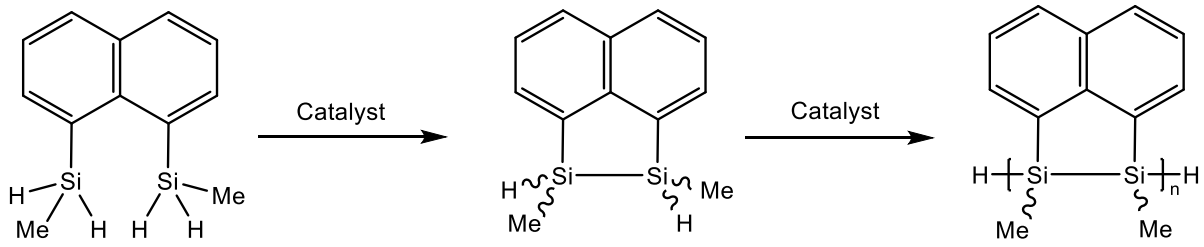

Scheme 4.3 *Proposed dehydropolymerisation scheme for the naphthalene-bridged disilane with methyl species bound to each silicon.*

4.2.3 Ferrocene-Bridged Dehydrocoupling Catalyst Investigation

Future work surrounding the disilane formation of the ferrocene disilyl precursors should proceed after attempts to identify suitable intermolecular dehydrocoupling catalysts for the **4** substrate are complete. Current catalysts have been shown as unable to synthesis the **8** disilane. Until more reactive dehydrocoupling catalysts are identified, disilane synthesis is unlikely to be observed with the current selection of catalysts. Until the catalysts are identified, probing of the siloxane formation mechanism with NMR and ESI-MS techniques with the $[Rh(cod)Cl]_2$ catalyst may provide confirmation surrounding the source of siloxane synthesis.

Chapter 5: Experimental

5.1 Instrumental

Dry solvents were obtained using a solvent purification system. Reagents were purchase from Sigma-Aldrich, AK-Scientific, Gelest and Acros Organics. All glassware was oven-dried overnight in a 135 °C oven. ^{1}H, ^{13}C, $^{29}Si\{^{1}H\}$ NMR were recorded on a Bruker DPX-400 (400 MHz) spectrometer. Chemical shifts for protons are reported in parts per million (ppm) downfield from tetramethylsilane and are referenced to the residual protium in the NMR solvent (e.g., CHCl3 at 7.26 ppm). Chemical shifts for silicon are reported in parts per million (ppm) downfield from tetramethylsilane (TMS δ = 0.0). The silicon NMR resonances were determined with an inverse gated coupled pulse sequence. High resolution mass spectrometry measurements were performed on a Bruker microTOF-QII mass spectrometer, equipped with a KD Scientific syringe pump, in positive ion ESI mode.

5.2 Synthesis

5.1 Benzyl Silane Synthesis

Synthesis of 1,2-bis((phenylsilyl)methyl)benzene) (2a) through the Visco et al. adopted procedure:

To an oven dried Schlenk flask was added magnesium turnings (0.292 g, 12 mmol, 3.0 eq.) and purged with N_2, followed by addition of THF (20 mL). A secondary Schlenk flask was purged with a solution of *α,α'*-dibromo-*o*-xylene (**1a**) (1.273 g, 4 mmol, 1.0 eq.), chloro(phenyl)silane [6 mmol, generated by treating $PhSiH_3$ (12 mmol, 2.96 mL) in dry hexane (30 mL), with BCl_3 (1.0 M in Et_2O, 0.4 eq. 2.4 mmol, 2.4 mL)] at 0°C, and allowed to stir at room temperature for 24 h] in THF (30 mL). The primary Schlenk flask containing magnesium was placed in a sonicator water bath at room temperature. Upon subject of the flask to sonication, dibromoethane (0.172 mL) was added immediately, followed by the addition of the reaction mixture of the secondary flask. The reaction mixture was sonicated for 30 min, followed by quenching with a saturated $NH_4Cl_{(aq.)}$. The product was extracted with diethyl-ether three times and dried over $NaSO_4$ and concentrated in vacuo.

Synthesis of 1-(benzyl silyl), 2-(phenylsilyl)benzene) (2b) through the Visco et al. adopted procedure:

To an oven dried Schlenk flask was added magnesium turnings (0.292 g, 12 mmol, 3.0 eq.) and purged with N_2, followed by addition of THF (20 mL). A secondary Schlenk flask was purged with a solution of 2-bromobenzyl bromide (**1b**) (1.216 g, 4 mmol, 1.0 eq.), chloro(phenyl)silane [6 mmol, generated by treating $PhSiH_3$ (12 mmol, 2.96 mL) in dry hexane (30 mL), with BCl_3 (1.0 M in Et_2O, 0.4 eq. 2.4 mmol, 2.4 mL)] at 0°C, and allowed to stir at room temperature for 24 h] in THF (30 mL). The primary Schlenk flask containing magnesium was placed in a sonicator water bath at room temperature. Upon subject of the flask to sonication, dibromoethane (0.172 mL) was added immediately, followed by the addition of the reaction mixture of the secondary flask. The reaction mixture was sonicated for 30 min,

followed by quenching with a saturated $NH_4Cl_{(aq.)}$. The product was extracted with diethyl-ether three times and dried over $NaSO_4$ and concentrated in vacuo.

Synthesis of 1,2-bis(phenylsilyl)benzene (2c) through the Visco et al. adopted procedure:

To an oven dried Schlenk flask was added magnesium turnings (0.292 g, 12 mmol, 3.0 eq.) and purged with N2, followed by addition of THF (20 mL). A secondary Schlenk flask was purged with a solution of 1,2-dibromobenzene (**1c**) (0.582 mL, 1.160 g, 4 mmol, 1.0 eq.), chloro(phenyl)silane [6 mmol, generated by treating $PhSiH_3$ (12 mmol, 2.96 mL) in dry hexane (30 mL), with BCl_3 (1.0 M in Et_2O, 0.4 eq. 2.4 mmol, 2.4 mL)] at 0ºC, and allowed to stir at room temperature for 24 h] in THF (30 mL). The primary Schlenk flask containing magnesium was placed in a sonicator water bath at room temperature. Upon subject of the flask to sonication, dibromoethane (0.172 mL) was added immediately, followed by the addition of the reaction mixture of the secondary flask. The reaction mixture was sonicated for 30 min, followed by quenching with a saturated $NH_4Cl_{(aq.)}$. The product was extracted with diethyl-ether three times and dried over $NaSO_4$ and concentrated in vacuo.

Synthesis of 1,2-bis((phenylsilyl)methyl)benzene) (2a) through the Schrock et al. adopted procedure:

A solution of α,α'-dibromo-*o*-xylene (**1a**) (1.273 g, 4.0 mmol) in THF (5mL) was added to a slurry of Magnesium turnings (0.292 g, 12.0 mmol in a refluxing solution of chloro(phenyl)silane [6 mmol, generated by treating $PhSiH_3$ (12 mmol, 2.96 mL) in dry hexane (30 mL), with BCl_3 (1.0 M in Et_2O, 0.4 eq. 2.4 mmol, 2.4 mL)] at 0 °C, and allowed to stir at room temperature for 24 h] in THF (10 mL). After refluxing the mixture for 8 h, the mixture was cooled to room temperature. Pentane (60 mL) was added, and the magnesium salts were filtered off. The filtrate was poured onto crushed ice and neutralised with Na_2CO_3. The organic layer was separated, washed three times with water (40 mL). The collected aqueous layer was washed three times with pentane (20 mL) and the organic extracts all combined and dried with $MgSO_4$. The solvent was evaporated to leave a clear, colorless oil.

Synthesis of 1-(benzyl silyl), 2-(phenylsilyl)benzene) (2b) through the Schrock et al. adopted procedure[109]:

A solution of 2-bromobenzyl bromide (**1b**) (0.658 mL, 1.216 g, 4.0 mmol) in THF (5mL) was added to a slurry of magnesium turnings (0.292 g, 12.0 mmol in a refluxing solution of chloro(phenyl)silane [6 mmol, generated by treating $PhSiH_3$ (12 mmol, 2.96 mL) in dry hexane (30 mL), with BCl_3 (1.0 M in Et_2O, 0.4 eq. 2.4 mmol, 2.4 mL)] at 0ºC, and allowed to stir at room temperature for 24 h] in THF (10 mL). After refluxing the mixture for 8 h, the mixture was cooled to room temperature. Pentane (60 mL) was added, and the magnesium salts were filtered off. The filtrate was poured onto crushed ice and neutralised with Na_2CO_3. The organic layer was separated, washed three times with water (40 mL). The

collected aqueous layer was washed three times with pentane (20 mL) and the organic extracts all combined and dried with $MgSO_4$. The solvent was evaporated to leave a yellow oil.

Synthesis of 1,2-bis(phenylsilyl)benzene (2c) through the Schrock et al. adopted procedure:

A solution of 1,2-dibromobenzene (**1c**) (0.582 mL, 1.160 g, 4.0 mmol) in THF (5mL) was added to a slurry of magnesium turnings (0.292 g, 12.0 mmol in a refluxing solution of chloro(phenyl)silane [6 mmol, generated by treating $PhSiH_3$ (12 mmol, 2.96 mL) in dry hexane (30 mL), with BCl_3 (1.0 M in Et_2O, 0.4 eq. 2.4 mmol, 2.4 mL)] at 0^oC, and allowed to stir at room temperature for 24 h] in THF (10 mL). After refluxing the mixture for 8 h, the mixture was cooled to room temperature. Pentane (60 mL) was added, and the magnesium salts were filtered off. The filtrate was poured onto crushed ice and neutralised with Na_2CO_3. The organic layer was separated, washed three times with water (40 mL). The collected aqueous layer was washed three times with pentane (20 mL) and the organic extracts all combined and dried with $MgSO_4$. The solvent was evaporated to leave a dark yellow oil.

5.2 Naphthalene-Bridged Dehydrocoupling Catalyst Investigation

Synthesis of 1,8-bis(phenylsilyl)naphthalene (4): In an oven dried 25 mL Schlenk flask phenylsilane (6.0 mmol, 0.74 mL) in dry hexanes (10 mL) was prepared and cooled to 0 °C. To the cooled mixture was added BCl3 (1.0 M in Et_2O, 0.4 eq., 2.4 mmol, 2.4 mL). The reaction mixture was warmed to room temperature and was stirred for 24 h. After 24 h, half of the volume of hexanes was removed using high vacuum. In another oven dried 100 mL flask equipped with a stir bar, was added dry ether and 1,8-dibromonapthalene. The solution was cooled to -78 °C and to it was added *n*BuLi (2.0 M in cyclohexane, 2.2 eq., 4.84 mmol, 2.4 mL). The mixture was warmed to room temperature and was stirred for 1 h. The mixture was again cooled to -78 °C and the phenyl(chloro)silane mixture was added. The reaction mixture was then stirred overnight at room temperature before filtering over florasil and the clear solution was subjected to vacuum evaporation to remove the solvents. The crude product obtained was purified by column chromatography (90:10/Hexane:DCM) to give the pure product **4**.The NMR characterisation data matched with the literature values.

^{1}H NMR (400 MHz, CDCl3): δ 7.96-7.16 (m, Ph, 32H), 5.26 (s, Si-H *cis*, 2H), 5.24 (d, Si-H *trans*, 2H). 13C{1H} NMR (100.6 MHz, CDCl3): δ 147.4 (Ph), 147.4 (Ph), 136.9 (Ph), 136.8 (Ph), 135.8 (Ph), 135.7 (Ph), 135.1 (Ph), 135.1 (Ph), 134.9 (Ph), 133.1 (Ph), 132.4 (Ph), 131.6 (Ph), 131.0 (Ph), 129.9 (Ph), 129.6 (Ph), 125.5 (Ph), 128.8 (Ph), 128.0 (Ph), 126.4 (Ph), 126.0 (Ph), 125.9 (Ph), 125.3 (Ph). ^{29}Si{^{1}H} NMR (79.5 MHz, CDCl3): δ -37.2, -40.3. HRMS-ESI: Found for $C_{24}H_{24}Si_2$: 363.0999 *m/z*, Cal'd.: 361.0839 *m/z*.

Synthesis of 5 via $[Rh(cod)Cl]_2$: To an oven-dried 25 mL Schlenk flask equipped with a stir bar and purged with N_2, was added $[Rh(cod)Cl]_2$ (5 mol%, 0.025 mmol, 12 mg), **4** (0.5 mmol, 0.16 g) and dry toluene (0.5 mL). The mixture was stirred an instant bubbling was observed for next few minutes. The reaction mixture was further stirred for 24 h at room temperature. The mixture was passed through a florasil pad with hexanes as eluent. After the removal of solvents under vacuum, the reaction mixture was characterised by NMR and ESI-MS.

Synthesis of 5 via $Rh(PPh_3)_3Cl$: To an oven-dried 25 mL Schlenk flask equipped with a stir bar and purged with N_2, was added $Rh(PPh_3)_3Cl$ (5 mol %, 0.025 mmol, 23 mg), **4** (0.5 mmol, 0.16 g) and dry toluene (0.5 mL). Consistent bubbling was observed after 5 min. The reaction mixture was further stirred for 24 h at room temperature. The mixture was passed through a florasil pad with hexanes as eluent. After the removal of solvents under vacuum, the reaction mixture was characterised by NMR and ESI-MS.

Synthesis of 5 via Cp_2ZrBu_2: To an oven-dried 25 mL Schlenk flask equipped with a stir bar and purged with N_2, was added Cp_2ZrCl_2 (5 mol %, 0.025 mmol, 8 mg), *n*BuLi (2.0 M in cyclohexane, 10 mol %, 0.050 mmol, 0.03 mL) and dry toluene (0.5 mL). After 20 min, **4** (0.5 mmol, 0.16 g) was added to the reaction under N_2. Slow bubbling was observed after 10 min. Gradually growing in intensity. The reaction mixture was further stirred for 24 h at room temperature. The mixture was passed through a

florasil pad with hexanes as eluent. After the removal of solvents under vacuum, the reaction mixture was characterised by NMR and ESI-MS.

Synthesis of 5 via Cp_2ZrMe_2: To an oven-dried 25 mL Schlenk flask equipped with a stir bar and purged with N_2, was added Cp_2ZrCl_2 (5 mol %, 0.025 mmol, 8 mg), MeLi (3.1 M in cyclohexane, 10 mol %, 0.050 mmol, 0.02 mL) and dry toluene (0.5 mL). After 20 min, **4** (0.5 mmol, 0.16 g) was added to the reaction under N_2. The reaction mixture was further stirred for 24 h at room temperature. The mixture was passed through a florasil pad with hexanes as eluent. After the removal of solvents under vacuum, the reaction mixture was characterised by NMR and ESI-MS.

Synthesis of 5 via Cp_2ZrCl_2/2*n*BuLi: To an oven-dried 25 mL Schlenk flask equipped with a stir bar and purged with N_2, was added Cp_2ZrCl_2 (5 mol %, 0.025 mmol, 8 mg), **4** (0.5 mmol, 0.16 g) and dry toluene (0.5 mL). Next *n*BuLi (2.0 M in cyclohexane, 10 mol %, 0.050 mmol, 0.03 mL) was added. Bubbling was observed 5 min after addition. The reaction mixture was further stirred for 24 h at room temperature. The mixture was passed through a florasil pad with hexanes as eluent. After the removal of solvents under vacuum, the reaction mixture was characterised by NMR and ESI-MS.

Synthesis of 5 via Cp_2ZrCl_2/2MeLi: To an oven-dried 25 mL Schlenk flask equipped with a stir bar and purged with N_2, was added Cp_2ZrCl_2 (5 mol %, 0.025 mmol, 8 mg), **4** (0.5 mmol, 0.16 g) and dry toluene (0.5 mL). Next MeLi (3.1 M in cyclohexane, 10 mol %, 0.050 mmol, 0.02 mL) was added. Mild bubbling was observed after 30 min. The reaction mixture was further stirred for 24 h at room temperature. The mixture was passed through a florasil pad with hexanes as eluent After the removal of solvents under vacuum, the reaction mixture was characterised by NMR and ESI-MS.

5.3 Ferrocene-Bridged Dehydrocoupling Catalyst Investigation

Synthesis of 1,1-bis(phenylsilyl)ferrocene (7a): To a Schlenk flask of ferrocene (2.2 mmol, 0.41 g) in dry n-hexane (30 mL) tetramethyl ethylenediamine (tmeda; 0.33 mL, 33 mmol) was slowly added. To this flask a solution of nBuLi solution (2.0 M, 4.8 mmol, 2.4 mL) was added. After 15 h at room temperature the stirred reaction solution was cooled to -78 °C and $ClSiPhH_2$ [6 mmol, generated by treating $PhSiH_3$ (12 mmol, 2.96 mL) in dry hexane (30 mL), with BCl_3 (1.0 M in Et_2O, 0.4 eq. 2.4 mmol, 2.4 mL)] at 0 °C, and allowed to stir at room temperature for 24 h] was added dropwise. The reaction mixture was warmed to room temperature and was allowed to stir at 25ºC for a further 20 h. The reaction mixture was then filtered through Florasil using n-hexane, and the solvent removed from the filtrate under vacuum. The product was purified by silica gel chromatography using DCM and hexanes (50:50 v/v). Removal of the solvent through vacuum produced crystals which were dissolved in $CDCl_3$ for NMR.

Synthesis of 1,1-bis (diphenyl silyl) ferrocene, (7b): To a Schlenk flask of ferrocene (2.2 mmol, 0.41 g) in hexanes (30 mL) containing tetramethylethylenediamine (tmeda; 0.33 mL, 33 mmol) was slowly added a solution of nBuLi solution (2.0 M, 4.8 mmol, 2.4 mL). After 15 h at room temperature the stirred reaction solution was cooled to -78 °C and $ClSiPhH_2$ [6 mmol, generated by treating $PhSiH_3$ (12 mmol, 2.96 mL) in dry hexane (30 mL), with BCl_3 (1.0 M in Et_2O, 0.4 eq. 2.4 mmol, 2.4 mL)] at 0 °C, and allowed to stir at room temperature for 24 h] was added dropwise. The reaction mixture was warmed to room temperature and was allowed to stir at 25ºC for a further 20 h. The reaction mixture was then filtered through Florasil using n-hexane, and the solvent removed from the filtrate under vacuum. The product was purified by silica gel chromatography using DCM and hexanes (50:50 v/v). Removal of the solvent through vacuum produced crystals which were dissolved in $CDCl_3$ for NMR.

Attempted synthesis of 8a via $[Rh(cod)Cl]_2$: To an oven-dried 25 mL Schlenk flask equipped with a stir bar and purged with N_2, was added $[Rh(cod)Cl]_2$ (5 mol %, 0.025 mmol, 12 mg), **7a** (0.5 mmol, 0.20 g) and dry toluene (0.5 mL). Limited bubbling was observed minutes after addition. The reaction mixture was further stirred for 24 h at room temperature. The mixture was passed through a florasil pad with hexanes as eluent. After the removal of solvents under vacuum, the reaction mixture was characterised by NMR and ESI-MS.

Attempted synthesis of 8a via Cp_2ZrCl_2/2*n*BuLi: To an oven-dried 25 mL Schlenk flask equipped with a stir bar and purged with N_2, was added Cp_2ZrCl_2 (5 mol %, 0.025 mmol, 8 mg), **7a** (0.5 mmol, 0.20 g) and dry toluene (0.5 mL). Next *n*BuLi (2.0 M in cyclohexane, 10 mol %, 0.050 mmol, 0.03 mL) was added. No bubbling was observed during the initial stages of the reaction. The reaction mixture was further stirred for 24 h at room temperature. The mixture was passed through a florasil pad with hexanes as eluent. After the removal of solvents under vacuum, the reaction mixture was characterised by NMR and ESI-MS.

Attempted synthesis of 8b via [Rh(cod)Cl]$_2$: To an oven-dried 25 mL Schlenk flask equipped with a stir bar and purged with N_2, was added [Rh(cod)Cl]$_2$ (5 mol %, 0.025 mmol, 12 mg), **7b** (0.5 mmol, 0.27 g) and dry toluene (0.5 mL). No bubbling was observed during the initial stages of the reaction. The reaction mixture was further stirred for 24 h at room temperature. The mixture was passed through a florasil pad with hexanes as eluent. After the removal of solvents under vacuum, the reaction mixture was characterised by NMR and ESI-MS.

Attempted synthesis of 8b via Cp$_2$ZrCl$_2$/2*n*BuLi: To an oven-dried 25 mL Schlenk flask equipped with a stir bar and purged with N_2, was added Cp_2ZrCl_2 (5 mol %, 0.025 mmol, 8 mg), **7b** (0.5 mmol, 0.27 g) and dry toluene (0.5 mL). Next *n*BuLi (2.0 M in cyclohexane, 10 mol %, 0.050 mmol, 0.03 mL) was added. No bubbling was observed during the initial stages of the reaction. The reaction mixture was further stirred for 24 h at room temperature. The mixture was passed through a florasil pad with hexanes as eluent. After the removal of solvents under vacuum, the reaction mixture was characterised by NMR and ESI-MS.

Chapter 6: References

(1) Merchant, B. Everything That's Inside Your iPhone. *Vice*. **2017**. https://www.vice.com/en/article/433wyq/everything-thats-inside-your-iphone.

(2) Ur Rehman, A.; Lee, S. H. Advancements in N-Type Base Crystalline Silicon Solar Cells and Their Emergence in the Photovoltaic Industry. *Sci. World J.* **2013**, *2013*. https://doi.org/10.1155/2013/470347.

(3) Wolf, M. The Influence of Heavy Doping Effects on Silicon Solar Cell Performance. *Sol. Cells* **1986**, *17* (1), 53–63. https://doi.org/10.1016/0379-6787(86)90058-X.

(4) Arakawa, Y.; Ueno, K.; Imabeppu, H.; Kobayashi, A.; Ohta, J.; Fujioka, H. Electrical Properties of Si-Doped GaN Prepared Using Pulsed Sputtering. *Appl. Phys. Lett.* **2017**, *110* (4). https://doi.org/10.1063/1.4975056.

(5) Xia, Z.; Song, H.; Kim, M.; Zhou, M.; Chang, T. H.; Liu, D.; Yin, X.; Xiong, K.; Mi, H.; Wang, X.; Xia, F.; Yu, Z.; Ma, Z.; Gan, Q. Single-Crystalline Germanium Nanomembrane Photodetectors on Foreign Nanocavities. *Sci. Adv.* **2017**, *3* (7), 1–9. https://doi.org/10.1126/sciadv.1602783.

(6) Sharpe, A.; Housecroft, C. *Housecroft and Sharpe, Inorganic Chemistry 5th Ed.*; 2018.

(7) Nagashima, T.; Hora, M.; Koike, T. Manufacture of Silicon Single Crystal Substrate for Semiconductor, 1992.

(8) Liu, W.; Shi, J.; Zhang, L.; Han, A.; Huang, S.; Li, X.; Peng, J.; Yang, Y.; Gao, Y.; Yu, J.; Jiang, K.; Yang, X.; Li, Z.; Zhao, W.; Du, J.; Song, X.; Yin, J.; Wang, J.; Yu, Y.; Shi, Q.; Ma, Z.; Zhang, H.; Ling, J.; Xu, L.; Kang, J.; Xu, F.; Liu, J.; Liu, H.; Xie, Y.; Meng, F.; De Wolf, S.; Laquai, F.; Di, Z.; Liu, Z. Light-Induced Activation of Boron Doping in Hydrogenated Amorphous Silicon for over 25% Efficiency Silicon Solar Cells. *Nat. Energy* **2022**, *7* (5), 427–437. https://doi.org/10.1038/s41560-022-01018-5.

(9) Hayase, S. Polysilanes for Semiconductor Fabrication. *Prog. Polym. Sci.* **2003**, *28* (3), 359–381. https://doi.org/10.1016/S0079-6700(02)00034-5.

(10) Kumar, V. B.; Leitao, E. M. Properties and Applications of Polysilanes. *Appl. Organomet. Chem.* **2020**, *34* (3), 1–16. https://doi.org/10.1002/aoc.5402.

(11) Kepler, R. G. Electronic Properties of σ-Conjugated Polysilanes. *Synth. Met.* **1989**, *28*, 573–580.

(12) Richter, R.; Roewer, G.; Böhme, U.; Busch, K.; Babonneau, F.; Martin, H. P.; Müller, E. Organosilicon Polymers - Synthesis, Architecture, Reactivity and Applications. *Appl. Organomet. Chem.* **1997**, *11* (2), 71–106. https://doi.org/10.1002/(SICI)1099-0739(199702)11:2<71::AID-AOC562>3.0.CO;2-N.

(13) Michl, J. Relationship of Bonding to Electronic Spectra. *Acc. Chem. Res.* **1990**, *23* (5), 128–134. https://doi.org/10.1021/ar00173a002.

(14) Cypryk, M. *Polymerization of Cyclic Siloxanes, Silanes, and Related Monomers*; Elsevier B.V., 2012; Vol. 4. https://doi.org/10.1016/B978-0-444-53349-4.00112-6.

(15) Fujino, M. Photoconductivity in Organopolysilanes. *Chem. Phys. Lett.* **1987**, *136* (5), 451–453. https://doi.org/10.1016/0009-2614(87)80285-3.

(16) Kepler, R. G.; Zeigler, J. M.; Harrah, L. A.; Kurtz, S. R. Photocarrier Generation and Transport in -Bonded Polysilanes. *Phys. Rev. B* **1987**, *35* (6), 2818–2822. https://doi.org/10.1103/PhysRevB.35.2818.

(17) Fujiki, M. A Correlation between Global Conformation of Polysilane and UV Absorption Characteristics. *J. Am. Chem. Soc.* **1996**, *118* (31), 7424–7425. https://doi.org/10.1021/ja953835w.

(18) Fujiki, M. *Si–Si Bond Polymers, Oligomers, Molecules, Surface, and Materials*; 2014.

(19) Tachibana, H.; Matsumoto, M.; Tokura, Y.; Moritomo, Y.; Yamaguchi, A.; Koshihara, S.; Miller, R. D.; Abe, S. Spectra of One-Dimensional Excitons in Polysilanes with Various Backbone Conformations. *Phys. Rev. B* **1993**, *47* (8), 4363–4371. https://doi.org/10.1103/PhysRevB.47.4363.

(20) Yashima, E.; Maeda, K.; Lida, H.; Furusho, Y.; Nagai, K. Helical Polymers: Synthesis, Structures, and Functions. *Chem. Rev.* **2009**, *109* (11), 6102–6211. https://doi.org/10.1021/cr900162q.

(21) Marschner, C.; Baumgartner, J.; Wallner, A. Structurally and Conformationally Defined Small Methyl Polysilanes. *Daltan Trans.* **2006**, No. 48, 5667–5674. https://doi.org/10.1039/b613642g.

(22) Michl, J.; West, R. Conformations of Linear Chains. Systematics and Suggestions for Nomenclature. *Acc. Chem. Res.* **2000**, *33* (12), 821–823. https://doi.org/10.1021/ar0001057.

(23) Sohail, M.; Panisch, R.; Bowden, A.; Bassindale, A. R.; Taylor, P. G.; Korlyukov, A. A.; Arkhipov, D. E.; Male, L.; Callear, S.; Coles, S. J.; Hursthouse, M. B.; Harrington, R. W.; Clegg, W. Pentacoordinate Silicon Complexes with Dynamic Motion Resembling a Pendulum on the SN2 Reaction Pathway. *J. Chem. Soc. Daltan Trans.* **2013**, *42* (30), 10971–10981. https://doi.org/10.1039/c3dt50613d.

(24) Liu, J.; Zhong, Y.; Lam, J. W. Y.; Lu, P.; Hong, Y.; Yu, Y.; Yue, Y.; Faisal, M.; Sung, H. H. Y.; Williams, I. D.; Wong, K. S.; Tang, B. Z. Hyperbranched Conjugated Polysiloles: Synthesis, Structure, Aggregation-Enhanced Emission, Multicolor Fluorescent Photopatterning, and Superamplified Detection of Explosives. *Macromolecules* **2010**, *43* (11), 4921–4936. https://doi.org/10.1021/ma902432m.

(25) Tsuji, H.; Terada, M.; Toshimitsu, A.; Tamao, K. Σσ* Transition in Anti, Cisoid Alternating Oligosilanes: Clear-Cut Evidence for Suppression of Conjugation Effect by a Cisoid Turn. *J. Am. Chem. Soc.* **2003**, *125* (25), 7486–7487. https://doi.org/10.1021/ja034500e.

(26) Carberry, E.; West, R. Cyclic Polysilanes. III. The Preparation of Permethylcyclopolysilanes by Coupling, Pyrolysis, and Redistribution Reactions. *J. Am. Chem. Soc.* **1969**, *91* (20), 5440–5446. https://doi.org/10.1021/ja01048a007.

(27) Kagawa, T.; Fujino, M.; Takeda, K.; Matsumoto, N. Photoluminescence of Organo-Polysilane. *Solid State Commun.* **1986**, *57* (8), 635–637. https://doi.org/10.1016/0038-1098(86)90339-X.

(28) Chen, J.; Cao, Y. Silole-Containing Polymers: Chemistry and Optoelectronic Properties. *Macromol. Rapid Commun.* **2007**, *28* (17), 1714–1742. https://doi.org/10.1002/marc.200700326.

(29) Sanji, T.; Takase, K.; Sakurai, H.; Chemistry, A. Helical-Sense Programming through Polysilane-Poly (Triphenylmethyl Methacrylate) Block Copolymers Department of Pure and Applied Chemistry Science Uni V Ersity of Tokyo and CREST-JST Ming through Synthetic Block Copolymers , Polysilane- b -Poly- Poly (. **2001**, No. 14, 12690–12691.

(30) Sanji, T.; Sakamoto, K.; Sakurai, H. Thermochromic Behavior of Polysilanes Concerning the Dependence on the Sequence Length. *Bull. Chem. Soc. Jpn.* **1995**, *68*, 1052–1055.

(31) Gahimer, T.; Welsh, W. J. Theoretical Investigation of the Origins of Abrupt Thermochromism in the Polysilanes. *Polymer (Guildf).* **1996**, *37* (10), 1815–1823. https://doi.org/10.1016/0032-3861(96)87297-1.

(32) Bukalov, S. S.; Leites, L. A.; West, R. Thermochromism of Poly(Di-n-Hexylsilane) in Solution Revisited. *Macromolecules* **2001**, *34* (17), 6003–6004. https://doi.org/10.1021/ma0101714.

(33) Jamison, G.; Simmons-Potter, K. *Photosensitive Polysilane Thin Films for Write-as-Needed Optical Devices.*; Tucson, 2007.

(34) van Der Laan, G. P.; De Haas, M. P.; Frey, H.; Möller, M. Charge Carrier Mobilities in Liquid Crystalline Mesomorphic Poly(DI-n-Alkylsilylene)s; Influence of Backbone Conformation. *Macromol. Symp.* **1995**, *96* (1), 219–228. https://doi.org/10.1002/masy.19950960120.

(35) Abkowitz, M.; Knier, F. E.; Yuh, H.; Weagley, R. J.; Stolka, M. ELECTRONIC TRANSPORT IN AMORPHOUS SILICON BACKBONE POLYMERS. **1987**, *62* (8), 547–550.

(36) Jovanovic, M.; Michl, J. Understanding the Effect of Conformation on Hole Delocalization in Poly(Dimethylsilane). *J. Am. Chem. Soc.* **2018**, *140* (36), 11158–11160. https://doi.org/10.1021/jacs.8b05829.

(37) Sumiya, Y.; Maeda, S. Designing the Backbone of Hexasilabenzene Derivatives with a High Unimolecular Kinetic Stability. *Eur. J. Chem.* **2018**, *24* (47), 12264–12268. https://doi.org/10.1002/chem.201801699.

(38) Li, H.; Garner, M. H.; Shangguan, Z.; Zheng, Q.; Su, T. A.; Neupane, M.; Li, P.; Velian, A.; Steigerwald, M. L.; Xiao, S.; Nuckolls, C.; Solomon, G. C.; Venkataraman, L. Conformations of Cyclopentasilane Stereoisomers Control Molecular Junction Conductance. *Chem. Sci.* **2016**, *7* (9), 5657–5662. https://doi.org/10.1039/c6sc01360k.

(39) Emanuelsson, R.; Löfås, H.; Wallner, A.; Nauroozi, D.; Baumgartner, J.; Marschner, C.; Ahuja, R.; Ott, S.; Grigoriev, A.; Ottosson, H. Configuration- and Conformation-Dependent Electronic-Structure Variations in 1,4-Disubstituted Cyclohexanes Enabled by a Carbon-to-Silicon Exchange. *Chem. - A Eur. J.* **2014**, *20* (30), 9304–9311. https://doi.org/10.1002/chem.201402610.

(40) Fukushima, M.; Hamada, Y.; Tabei, E.; Aramata, M.; Mori, S.; Yamamoto, Y. Effects of Dopants and Polymer Structures on Electrical Conductivity of Organosilicon Polymers. *Synth. Met.* **1998**, *94* (3), 299–306. https://doi.org/10.1016/s0379-6779(98)00025-3.

(41) Oku, T.; Nakagawa, J.; Iwase, M.; Kawashima, A.; Yoshida, K.; Suzuki, A.; Akiyama, T.; Tokumitsu, K.; Yamada, M.; Nakamura, M. Microstructures and Photovoltaic Properties of Polysilane-Based Solar Cells. *Jpn. J. Appl. Phys.* **2013**, *52* (4 PART 2). https://doi.org/10.7567/JJAP.52.04CR07.

(42) Suzuki, H.; Hoshino, S.; Furukawa, K.; Ebata, K. Polysilane Light-Emitting Diodes. **2000**, *467* (December 1999), 460–467.

(43) Rulkens, R.; Resendes, R.; Verma, A.; Manners, I.; Murti, K.; Fossum, E.; Miller, P.; Matyjaszewski, K. Ring-Opening Copolymerization of Cyclotetrasilanes and Silicon-Bridged [1]Ferrocenophanes: Synthesis and Properties of Polysilane-Poly(Ferrocenylsilane) Random Copolymers. *Macromolecules* **1997**, *30* (26), 8165–8171. https://doi.org/10.1021/ma9712662.

(44) Wallraff, G. M.; Miller, R. D.; Clecak, N. J.; Baier, M. Polysilanes for Microlithography. *Adv. Resist Technol. Process. VIII* **1991**, *1466* (June 1991), 211–217. https://doi.org/10.1117/12.46372.

(45) Acheson, G. U.S. Patent 492,767: Production of Artificial Crystalline Carbonaceous Material, 1893.

(46) Fuchs, F.; Soltamov, V. A.; Väth, S.; Baranov, P. G.; Mokhov, E. N.; Astakhov, G. V.; Dyakonov, V. Silicon Carbide Light-Emitting Diode as a Prospective Room Temperature

Source for Single Photons. *Sci. Rep.* **2013**, *3*, 3–6. https://doi.org/10.1038/srep01637.

(47) Strokan, N. B.; Ivanov, A. M.; Lebedev, A. A. SiC Nuclear-Radiation Detectors. **2004**.

(48) Hasegawa, Y.; Iimura, M.; Yajima, S. Synthesis of Continuous Silicon Carbide Fibre - Part 2 Conversion of Polycarbosilane Fibre into Silicon Carbide Fibres. *J. Mater. Sci.* **1980**, *15* (3), 720–728. https://doi.org/10.1007/BF00551739.

(49) Branch, T. O.; Uni-, T.; Yajima, S.; Hasegawa, Y.; Hayashi, J.; Iimura, M. Synthesis of Continuous Silicon Carbide Fibre with High Tensile Strength and High Young ' s Modulus. *J. Mater. Sci.* **1978**, *13* (12), 2569–2576.

(50) Mucha, N. Catalytic Main Group Element Bond Formation Reactions Toward the Preparation of Conjugated Materials. **2015**.

(51) Miller, R. D.; Thompson, D.; Sooriyakumaran, R.; Fickes, G. N. The Synthesis of Soluble, Substituted Silane High Polymers by Wurtz Coupling Techniques. *J. Polym. Sci. Part A Polym. Chem.* **1991**, *29* (6), 813–824. https://doi.org/10.1002/pola.1991.080290604.

(52) Jones, R. G.; Holder, S. J. *SYNTHESIS OF POLYSILANES BY THE WURTZ REDUCTIVE-COUPLING REACTION*; 2000; pp 353–373.

(53) Sakurai, H. MASKED DISILENES. **2000**, 375–376.

(54) Kashimura, S.; Ishifune, M.; Yamashita, N.; Bu, H. B.; Takebayashi, M.; Kitajima, S.; Yoshiwara, D.; Kataoka, Y.; Nishida, R.; Kawasaki, S. I.; Murase, H.; Shono, T. Electroreductive Synthesis of Polysilanes, Polygermanes, and Related Polymers with Magnesium Electrodes. *J. Org. Chem.* **1999**, *64* (18), 6615–6621. https://doi.org/10.1021/jo990180z.

(55) Melen, R. L. Dehydrocoupling Routes to Element-Element Bonds Catalysed by Main Group Compounds. *Chem. Soc. Rev.* **2016**, *45* (4), 775–788. https://doi.org/10.1039/c5cs00521c.

(56) Ríos, P.; Fouilloux, H.; Díez, J.; Vidossich, P.; Lledós, A.; Conejero, S. σ-Silane Platinum(II) Complexes as Intermediates in C−Si Bond-Coupling Processes. *Chem. - A Eur. J.* **2019**, *25* (48), 11346–11355. https://doi.org/10.1002/chem.201902226.

(57) Dioumaev, V. K.; Harrod, J. F. Catalytic Dehydrocoupling of Phenylsilane with "Cation-like" Zirconocene Derivatives: A New Approach to Longer Silicon Chains. *Organometallics* **1994**, *13* (5), 1548–1550. https://doi.org/10.1021/om00017a004.

(58) Grimmond, B. J.; Corey, J. Y. Catalytic Dehydropolymerization of PhSiH3 to Polyphenylsilane with Substituted Group IV Metallocenes. *Organometallics* **1999**, *18* (11), 2223–2229. https://doi.org/10.1021/om9809264.

(59) Smith, E. E.; Du, G.; Fanwick, P. E.; Abu-Omar, M. M. Dehydrocoupling of Organosilanes with a Dinuclear Nickel Hydride Catalyst and Isolation of a Nickel Silyl Complex. *Organometallics* **2010**, *29* (23), 6527–6533. https://doi.org/10.1021/om100887v.

(60) Press, E. M.; Marro, E. A.; Surampudi, S. K.; Siegler, M. A.; Tang, J. A.; Klausen, R. S. Synthesis of a Fragment of Crystalline Silicon: Poly(Cyclosilane). *Angew. Chemie - Int. Ed.* **2017**, *56* (2), 568–572. https://doi.org/10.1002/anie.201610208.

(61) Sohn, H.; Sailor, M. J.; Magde, D.; Trogler, W. C. Detection of Nitroaromatic Explosives Based on Photoluminescent Polymers Containing Metalloles. *J. Am. Chem. Soc.* **2003**, *125* (13), 3821–3830. https://doi.org/10.1021/ja021214e.

(62) Tanabe, M.; Iwase, S.; Osakada, K. Nickel(0)-Catalyzed Polycondensation of Silafluorene: Control over Molecular Weight and Polymer Growth Mechanism. *Organometallics* **2016**, *35* (15), 2557–2562. https://doi.org/10.1021/acs.organomet.6b00459.

(63) Deeken, S.; Proch, S.; Casini, E.; Braun, H. F.; Mechtler, C.; Marschner, C.; Motz, G.; Kempe, R. Group 10 Metal Aminopyridinato Complexes: Synthesis, Structure, and Application as Aryl-Cl Activation and Hydrosilane Polymerization Catalysts. *Inorg. Chem.* **2006**, *45* (4), 1871–1879. https://doi.org/10.1021/ic0518273.

(64) Dioumaev, V. K.; Rahimian, K.; Gauvin, F.; Harrod, J. F. Stereostructures of Linear and Cyclic Polyphenylsilanes Produced by Dehydrocoupling in the Presence of Group 4 Metallocene Catalysts. *Organometallics* **1999**, *18* (11), 2249–2255. https://doi.org/10.1021/om980816x.

(65) Chauhan, B. P. S.; Shimizu, T.; Tanaka, M. New Vistas in Dehydrocoupling Polymerization of Hydrosilanes Platinum Complex-Catalyzed Dehydrocoupling of Cyclic and Acyclic Secondary Silanes.Pdf. *Chem. Lett.* **1997**, 785–786.

(66) Tilley, T. D. The Coordination Polymerization of Silanes to Polysilanes by a "σ-Bond Metathesis" Mechanism. Implications for Linear Chain Growth. *Acc. Chem. Res.* **1993**, *26* (1), 22–29. https://doi.org/10.1021/ar00025a004.

(67) Leitao, E. M.; Jurca, T.; Manners, I. Catalysis in Service of Main Group Chemistry Offers a Versatile Approach to P-Block Molecules and Materials. *Nat. Chem.* **2013**, *5* (10), 817–829. https://doi.org/10.1038/nchem.1749.

(68) Harrod, J. F.; Mu, Y.; Samuel, E. Catalytic Dehydrocoupling: A General Method for the Formation of Element-Element Bonds. *Polyhedron* **1991**, *10* (11), 1239–1245. https://doi.org/10.1016/S0277-5387(00)86101-X.

(69) Azpeitia, S.; Fernández, B.; Garralda, M. A.; Huertos, M. A. Dehydrogenative Coupling of a Tertiary Silane Using Wilkinson's Catalyst. *Eur. J. Inorg. Chem.* **2016**, *2016* (18), 2891–2895. https://doi.org/10.1002/ejic.201600395.

(70) Rosenberg, L.; Kobus, D. N. Dehydrogenative Coupling of Primary Alkyl Silanes Using Wilkinson's Catalyst. *J. Organomet. Chem.* **2003**, *685* (1–2), 107–112. https://doi.org/10.1016/S0022-328X(03)00712-5.

(71) Chang, L. S.; Corey, J. Y. Dehydrogenative Coupling of Diarylsilanes. *Organometallics* **1989**, *8* (8), 1885–1893. https://doi.org/10.1021/om00110a010.

(72) Tanaka, M.; Kobayashi, T. -A; Hayashi, T.; Sakakura, T. Dehydrogenative Condensation of Monohydrosilanes Yielding Disilanes in the Presence of Platinum Complex Catalysts. *Appl. Organomet. Chem.* **1988**, *2* (1), 91–92. https://doi.org/10.1002/aoc.590020114.

(73) Chen, Y.; Zargarian, D. Phenylsilane Dehydrocoupling and Addition to Styrene Catalyzed by (R-Indenyl)Ni(Phosphine)(Methyl) Complexes. *Can. J. Chem.* **2009**, *87* (1 SPEC. ISS.), 280–287. https://doi.org/10.1139/V08-132.

(74) Affan, M. A.; Schatte, G.; Jessop, P. G. Synthesis, Characterization and Catalytic Studies of Two Ni(II) Complexes of Pentane-2,4-Dionate. *Inorganica Chim. Acta* **2018**, *471*, 777–781. https://doi.org/10.1016/j.ica.2017.11.057.

(75) Smith, E. E.; Du, G.; Fanwick, P. E.; Abu-omar, M. M. Dehydrocoupling of Organosilanes with a Dinuclear Nickel Hydride Catalyst and Isolation of a Nickel Silyl Complex. *Organometallics* **2010**, *29* (23), 6527–6533. https://doi.org/10.1021/om100887v.

(76) Mucha, N. T.; Waterman, R. Iridium Pincer Catalysts for Silane Dehydrocoupling: Ligand Effects on Selectivity and Activity. *Organometallics* **2015**, *34* (15), 3865–3872. https://doi.org/10.1021/acs.organomet.5b00486.

(77) Koizumi, T.; Osakada, K.; Yamamoto, T. Thermal Si - C Bond Cleavage of LRhH (SiAr 3)(μ -H)(μ -Cl) RhH (SiAr 3) L (Ar) C 6 H 5 , C 6 H 4 F- P ; L) P (i -Pr) 3) To Give LRhH (μ -SiAr 3)(μ -SiAr 2)(μ -Cl) RhHL Containing Symmetrically Bridging Triarylsilyl and

Diarylsilylene L. *Organometallics* **1998**, *17* (26), 5721–5727.

(78) Fontaine, F. G.; Kadkhodazadeh, T.; Zargarian, D. Nickel Indenyl Complexes as Precatalysts for Dehydropolymerization of Phenylsilane. *Chem. Commun.* **1998**, No. 12, 1253–1254. https://doi.org/10.1039/a802428f.

(79) Sawamura, M.; Hamashima, H.; Ito, Y. Catalytic Asymmetric Synthesis with Trans-Chelating Chiral Diphosphine Ligand TRAP Rhodium-Catalyzed Asymmetric Michael Addition of a-Cyano Carboxylates. *J. Am. Chem. Soc.* **1992**, *114* (21), 8295–8296.

(80) Pindwal, A.; Ellern, A.; Sadow, A. D. Homoleptic Divalent Dialkyl Lanthanide-Catalyzed Cross-Dehydrocoupling of Silanes and Amines. *Organometallics* **2016**, *35* (11), 1674–1683. https://doi.org/10.1021/acs.organomet.6b00138.

(81) Nako, A. E.; Chen, W.; White, A. J. P.; Crimmin, M. R. Yttrium-Catalyzed Amine-Silane Dehydrocoupling: Extended Reaction Scope with a Phosphorus-Based Ligand. *Organometallics* **2015**, *34* (17), 4369–4375. https://doi.org/10.1021/acs.organomet.5b00607.

(82) Erickson, K. A.; Cibuzar, M. P.; Mucha, N. T.; Waterman, R. Catalytic N-Si Coupling as a Vehicle for Silane Dehydrocoupling: Via α-Silylene Elimination. *Daltan Trans.* **2018**, *47* (7), 2138–2142. https://doi.org/10.1039/c7dt04507g.

(83) Hill, M. S.; Liptrot, D. J.; Macdougall, D. J.; Mahon, M. F.; Robinson, T. P. Hetero-Dehydrocoupling of Silanes and Amines by Heavier Alkaline Earth Catalysis. *Chem. Sci.* **2013**, *4* (11), 4212–4222. https://doi.org/10.1039/c3sc51797g.

(84) Forsyth, C. M.; Nolan, S. P.; Marks, T. J. Organolanthanide-Catalyzed Dehydrogenative Coupling of Silanes. Mechanistic Implications. *Organometallics* **1991**, *10*, 2543–2545.

(85) Hughes, C. E. Investigation of Si-Si Bond Formation by Rh (1) Catalysts. **2005**, No. 1.

(86) Jackson, S. M.; Chisholm, D. M.; McIndoe, J. S.; Rosenberg, L. Using NMR and ESI-MS to Probe the Mechanism of Silane Dehydrocoupling Catalyzed by Wilkinson's Catalyst. *Eur. J. Inorg. Chem.* **2011**, No. 3, 327–330. https://doi.org/10.1002/ejic.201001165.

(87) Goodman, J.; Grushin, V. V.; Larichev, R. B.; MacGregor, S. A.; Marshall, W. J.; Roe, D. C. Fluxionality of [(Ph3P)3M(X)] (M = Rh, Ir). the Red and Orange Forms of [(Ph3P)3Ir(Cl)]. Which Phosphine Dissociates Faster from Wilkinson's Catalyst? *J. Am. Chem. Soc.* **2010**, *132* (34), 12013–12026. https://doi.org/10.1021/ja1039693.

(88) Marro, E. A.; Press, E. M.; Siegler, M. A.; Klausen, R. S. Directional Building Blocks Determine Linear and Cyclic Silicon Architectures. *J. Am. Chem. Soc.* **2018**, *140* (18), 5976–5986. https://doi.org/10.1021/jacs.8b02541.

(89) Folster, C. P.; Klausen, R. S. Metallocene Influence on Poly(Cyclosilane) Structure and Properties. *Polym. Chem.* **2018**, *9* (15), 1938–1941. https://doi.org/10.1039/c8py00312b.

(90) Aitken, C.; Harrod, J. F.; Samuel, E. Polymerization of Primary Silanes to Linear Polysilanes Catalyzed by Titanocene Derivatives. *J. Organomet. Chem.* **1985**, *279* (1–2), 3–5. https://doi.org/10.1016/0022-328X(85)87029-7.

(91) Mu, Y.; Aitken, C.; Cote, B.; Harrod, J. F.; Samuel, E. Reactions of Silanes with Bis(Cyclopentadienyl)Dialkylzirconium Complexes. *Can. J. Chem.* **1991**, *69* (2), 264–276. https://doi.org/10.1139/v91-042.

(92) Woo, H. G.; Heyn, R. H.; Tilley, T. D. σ-Bond Metathesis Reactions for D0 Metal-Silicon Bonds That Produce Zirconocene and Hafnocene Hydrosilyl Complexes. *J. Am. Chem. Soc.* **1992**, *114* (14), 5698–5707. https://doi.org/10.1021/ja00040a032.

(93) Corey, J. Y.; Zhu, X. Condensation of Primary Silanes in the Presence of Cp , MCl ,/ " BuLi (M = Ti , Zr , Hf). *J. Organomet. Chem.* **1992**, *439*, 1–17.

(94) Corey, J. Y.; Rooney, S. M. Reactions of Symmetrical and Unsymmetrical Disilanes in the Presence of MCI2 / NBuLi (M = Ti , Zr , Hf }. *J. Organomet. Chem.* **1996**, *521*, 75–91.

(95) Woo, H. G.; Walzer, J. F.; Tilley, T. D. A σ-Bond Metathesis Mechanism for Dehydropolymerization of Silanes to Polysilanes by D0 Metal Catalysts. *J. Am. Chem. Soc.* **1992**, *114* (18), 7047–7055. https://doi.org/10.1021/ja00044a015.

(96) Campbell, W. H.; Hilty, T. K.; Yurga, L. Dimethylzirconocene-Catalyzed Polymerization of Alkylsilanes. *Organometallics* **1989**, *8* (11), 2615–2618. https://doi.org/10.1021/om00113a016.

(97) Corey, J. Y.; Zhu, X. H.; Bedard, T. C.; Lange, L. D. Catalytic Dehydrogenative Coupling of Secondary Silanes with Cp2MCI2/NBuLi. *Organometallics* **1991**, *10* (4), 924–930. https://doi.org/10.1021/om00050a024.

(98) Lunzer, F.; Marschner, C. Chemoselectivity in the Dehydrocoupling Synthesis of Higher Molecular Weight Polysilanes. *Materials (Basel).* **2010**, *3* (2), 1125–1137. https://doi.org/10.3390/ma3021125.

(99) Duckett, S.; Perutz, R. N. Mechanism of Homogeneous Hydrosilation of Alkenes by (.Eta.5-Cyclopentadienyl)Rhodium. *Organometallics* **1992**, *11* (1), 90–98.

(100) Dioumaev, V. K.; Harrod, J. F. Photo-Redox Mechanism for the Reaction of " Cation-like " Zirconocene Silyl Complexes with Silanes. *Organometallics* **2000**, *19* (10), 583–589.

(101) Neale, N. R.; Tilley, T. D. A New Mechanism for Metal-Catalyzed Stannane Dehydrocoupling Based on α-H-Elimination in a Hafnium Hydrostannyl Complex. *J. Am. Chem. Soc.* **2002**, *124* (15), 3802–3803. https://doi.org/10.1021/ja017495s.

(102) Kumar, V. Reinforcing Silicon-Silicon Bonds Using Bridges, Ph.D. Dissertation, University of Auckland, Auckland, June 2021.

(103) Rabanzo-Castillo, K. M.; Kumar, V. B.; Söhnel, T.; Leitao, E. M. Catalytic Synthesis of Oligosiloxanes Mediated by an Air Stable Catalyst, (C6F5)3B(OH2). *Front. Chem.* **2020**, *8* (June), 1–15. https://doi.org/10.3389/fchem.2020.00477.

(104) Takeda, K.; Shiraishi, K. Electronic Structure of Chain-like Polystannane. *Chem. Phys. Lett.* **1992**, *195* (2–3), 121–126. https://doi.org/10.1016/0009-2614(92)86123-Y.

(105) Miller, R. D.; Michl, J. Polysilane High Polymers. *Chem. Rev.* **1989**, *89* (6), 1359–1410. https://doi.org/10.1021/cr00096a006.

(106) Chaves, A.; Azadani, J. G.; Alsalman, H.; da Costa, D. R.; Frisenda, R.; Chaves, A. J.; Song, S. H.; Kim, Y. D.; He, D.; Zhou, J.; Castellanos-Gomez, A.; Peeters, F. M.; Liu, Z.; Hinkle, C. L.; Oh, S. H.; Ye, P. D.; Koester, S. J.; Lee, Y. H.; Avouris, P.; Wang, X.; Low, T. Bandgap Engineering of Two-Dimensional Semiconductor Materials. *npj 2D Mater. Appl.* **2020**, *4* (1). https://doi.org/10.1038/s41699-020-00162-4.

(107) Kumar, V. B.; Fleming, C. L.; Murali, S. S.; Hume, P. A.; Davis, N. J. L. K.; Söhnel, T.; Leitao, E. M. The Photophysical Properties of Naphthalene Bridged Disilanes. *RSC Adv.* **2021**, *11* (35), 21343–21350. https://doi.org/10.1039/d1ra02961d.

(108) Visco, M. D.; Wieting, J. M.; Mattson, A. E. Carbon-Silicon Bond Formation in the Synthesis of Benzylic Silanes. *Org. Lett.* **2016**, *18* (12), 2883–2885. https://doi.org/10.1021/acs.orglett.6b01223.

(109) Sladek, A. R Obert Schröck, Alexander Sladek, H Ubert Schmidbaur*. **1994**, *1040*, 1036–1040.

(110) Pool, J. A.; Bradley, C. A.; Chirik, P. J. A Convenient Method for the Synthesis of

Zirconocene Hydrido Chloride, Isobutyl Hydride, and Dihydride Complexes Using Tert-Butyl Lithium. *Organometallics* **2002**, *21* (6), 1271–1277. https://doi.org/10.1021/om011090z.

(111) Bourg, S.; Corriu, R. J. P.; Enders, M.; Moreau, J. J. E. New Stable Titanocene and Zirconocene Catalyst Precursors for Polysilane Synthesis via Dehydrocoupling of Hydrosilanes. *Organometallics* **1995**, *14* (1), 564–566. https://doi.org/10.1021/om00001a079.

(112) Tanabe, M.; Iwase, S.; Takahashi, A.; Osakada, K. Tetramer and Polymer of 2,7-Dialkoxy-9H-9-Silafluorene Composed of Si Backbone and π-Stacked Biphenylene Groups. *Chem. Lett.* **2016**, *45* (4), 394–396. https://doi.org/10.1246/cl.151173.

Chapter 7. Appendix

7.1 Benzyl Silane Synthesis

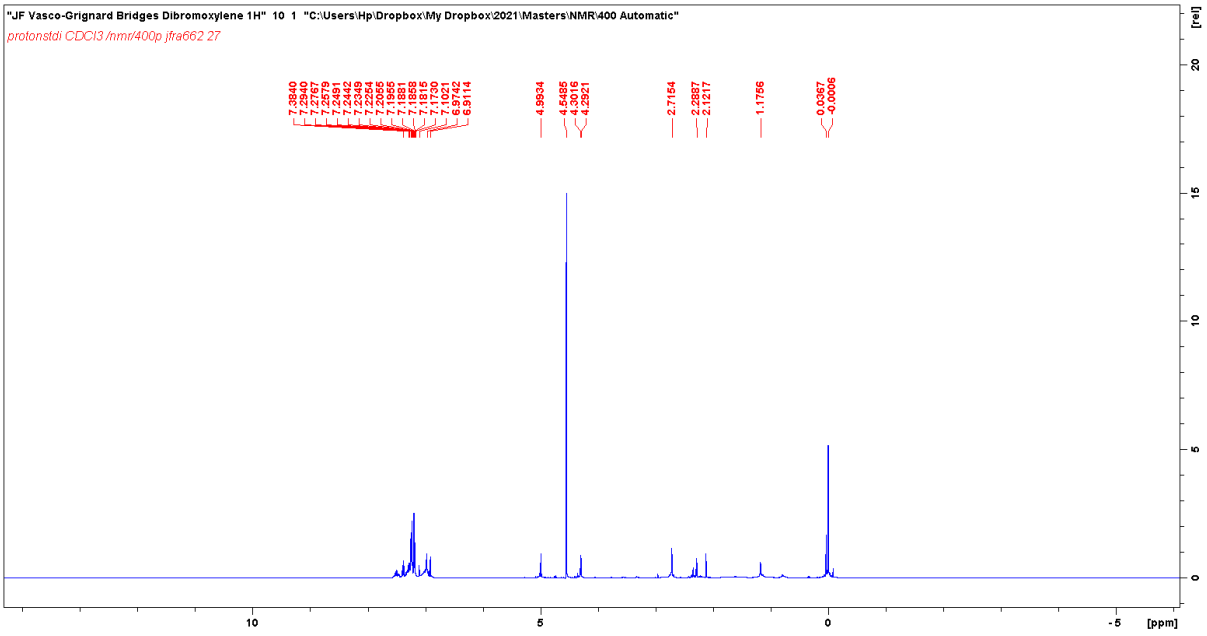

Figure 7.1 *^{1}H NMR spectrum of the Grignard reaction of α,α'-dibromo-o-xylene (**1a**) and chloro(phenyl)silane through the Visco adopted procedure.*

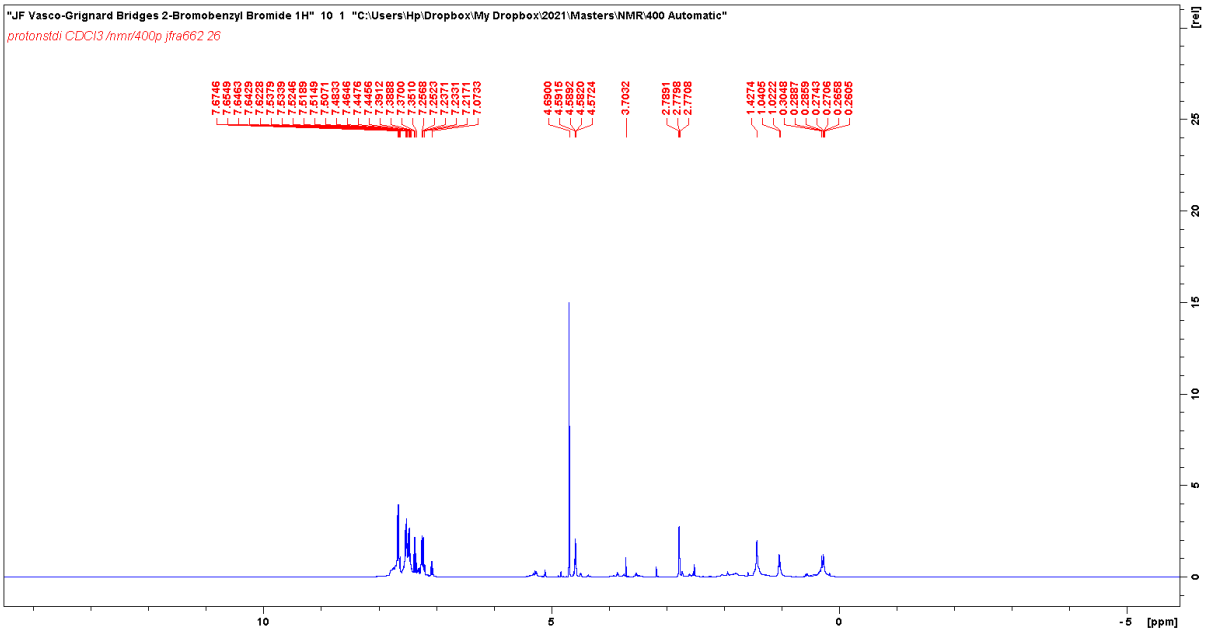

Figure 7.2 *^{1}H NMR spectrum of the Grignard reaction of 2-bromobenzyl bromide (**1b**) and chloro(phenyl)silane through the Visco adopted procedure.*

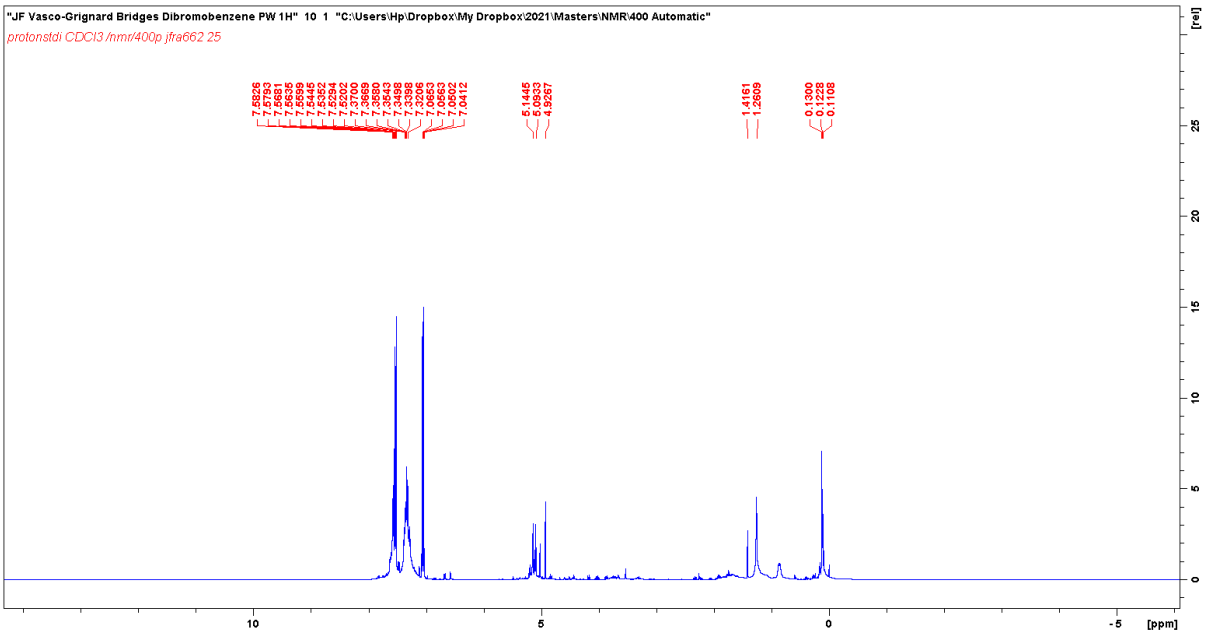

Figure 7.3 *^{1}H NMR spectrum of the Grignard reaction of 1,2-dibromobenzene (**1c**) and chloro(phenyl)silane through the Visco adopted procedure.*

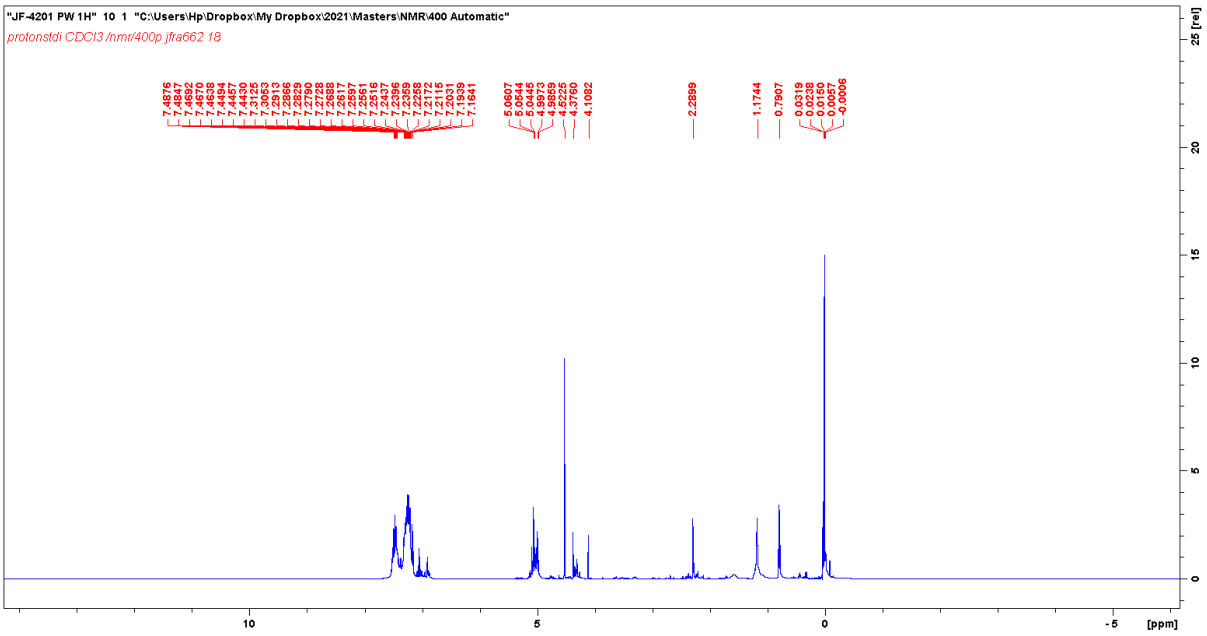

Figure 7.4 *^{1}H NMR spectrum of the Grignard reaction of α,α'-dibromo-o-xylene (**1a**) and chloro(phenyl)silane through the Schrock adopted procedure.*

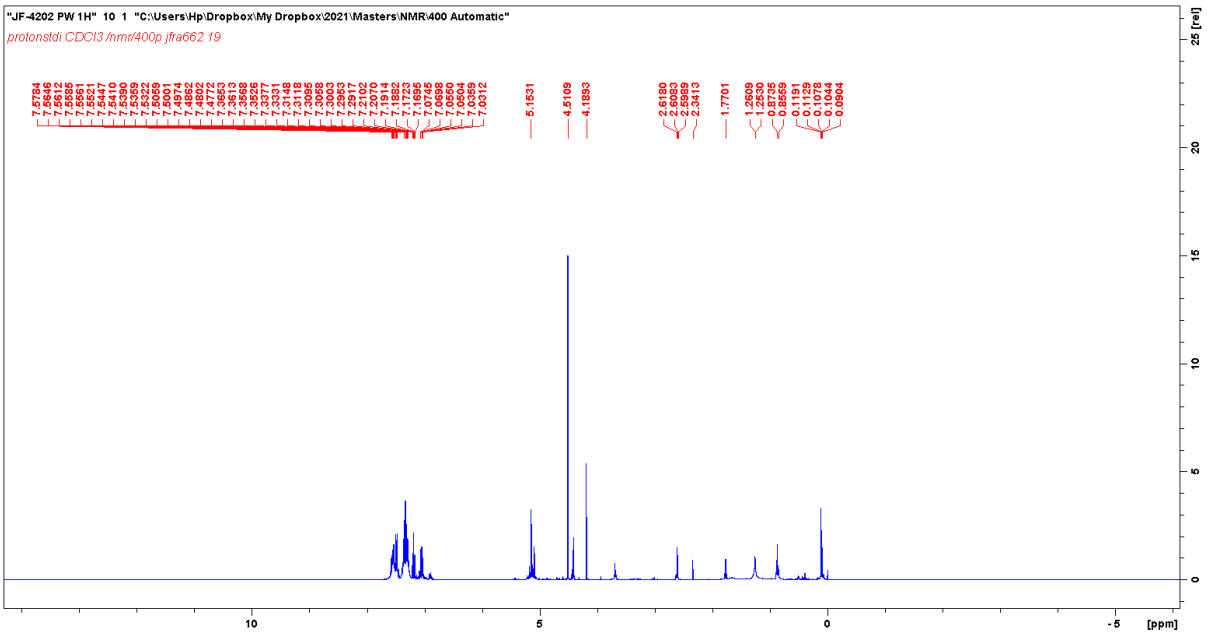

Figure 7.5 *^{1}H NMR spectrum of the Grignard reaction of 2-bromobenzyl bromide (**1b**) and chloro(phenyl)silane through the Schrock adopted procedure.*

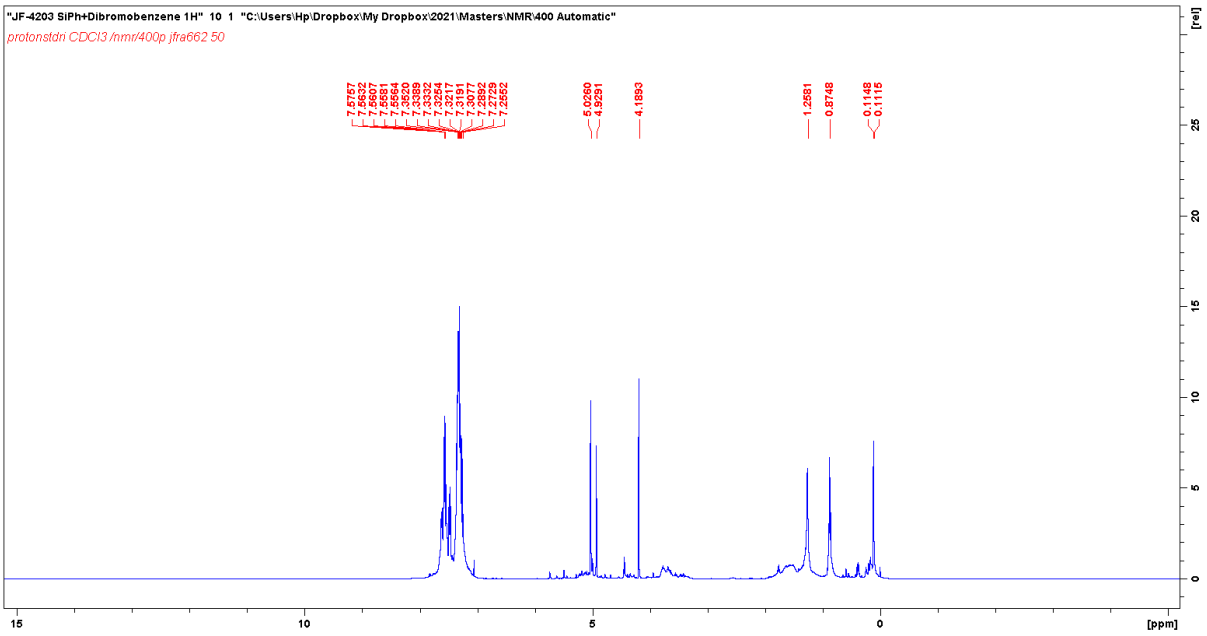

Figure 7.6 *^{1}H NMR spectrum of the Grignard reaction of 1,2-dibromobenzene (**1c**) and chloro(phenyl)silane through the Schrock adopted procedure.*

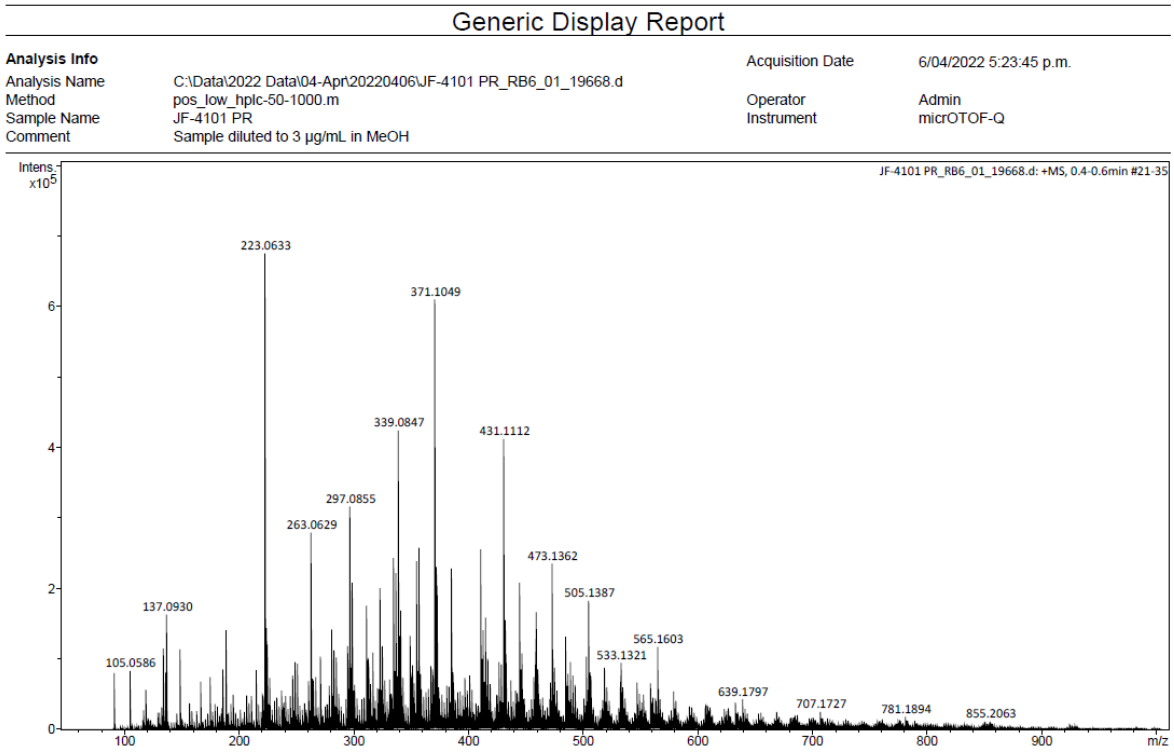

Figure 7.7 *ESI mass spectrum of the Grignard reaction of α,α'-dibromo-o-xylene (**1a**) and chloro(phenyl)silane through the Visco adopted procedure.*

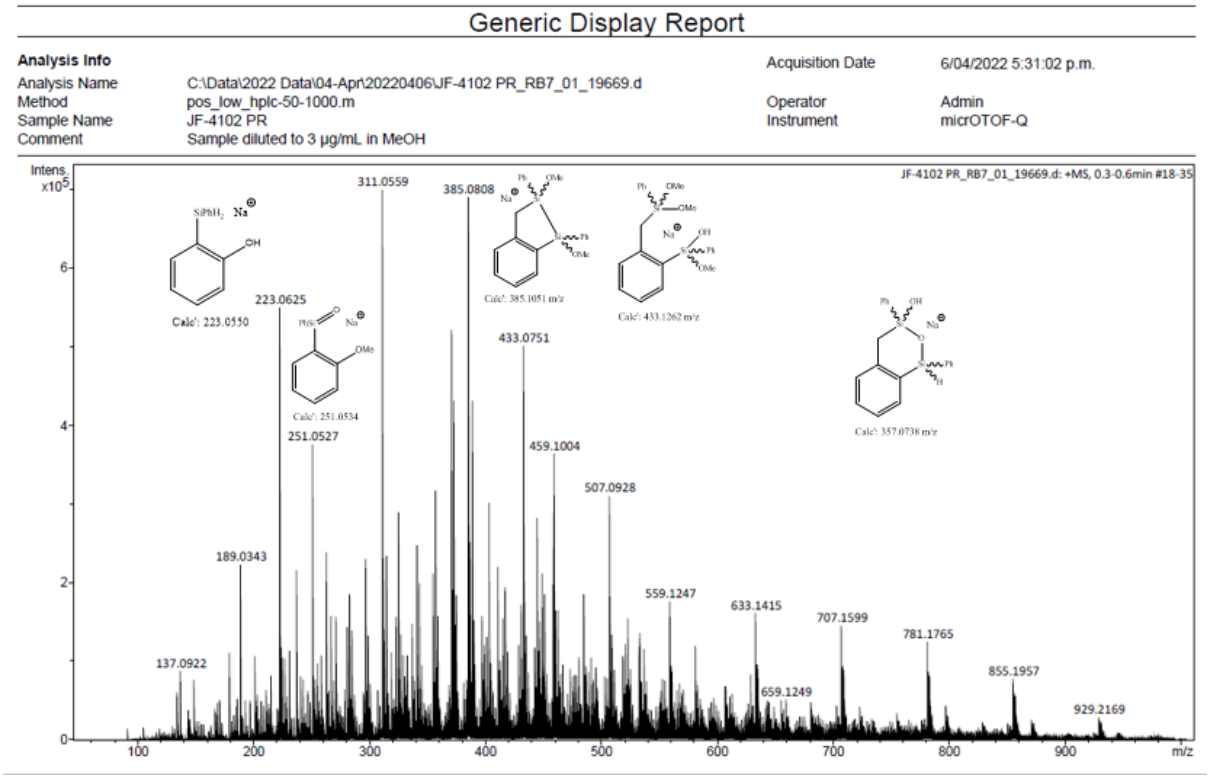

Figure 7.8 *ESI mass spectrum of the Grignard reaction of 2-bromobenzyl bromide (**1b**) and chloro(phenyl)silane through the Visco adopted procedure.*

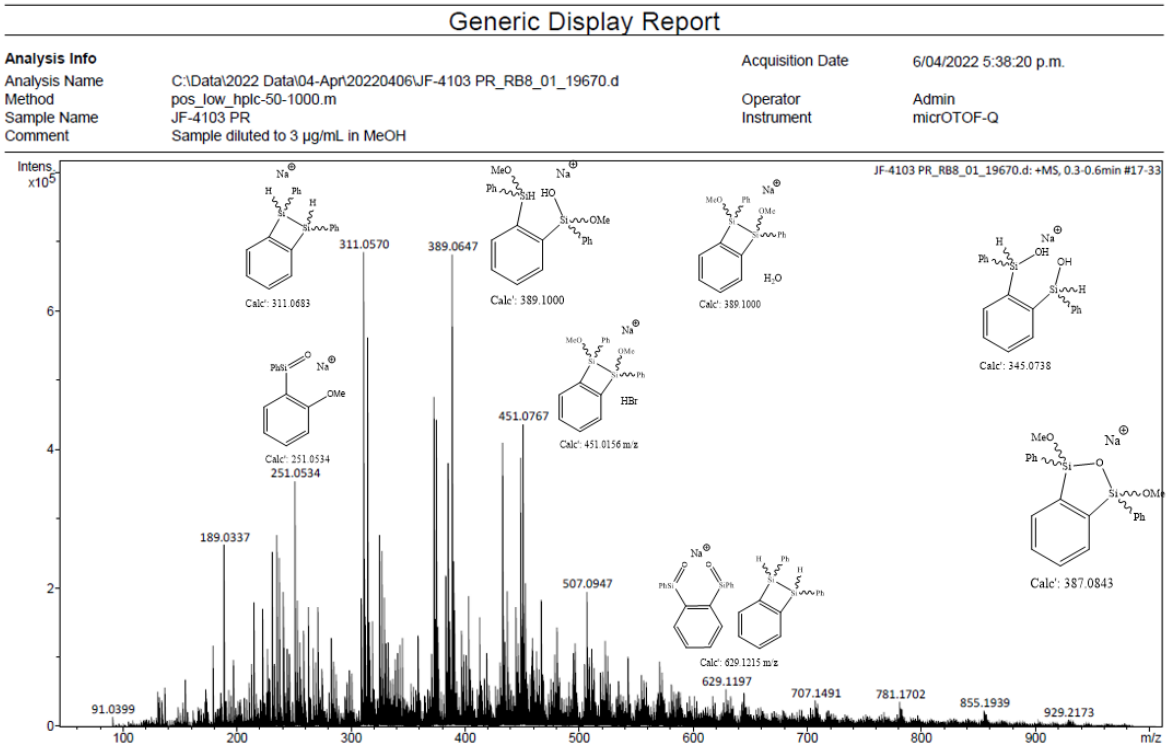

Figure 7.9 *ESI mass spectrum of the Grignard reaction of 1,2-dibromobenzene (**1c**) and chloro(phenyl)silane through the Visco adopted procedure.*

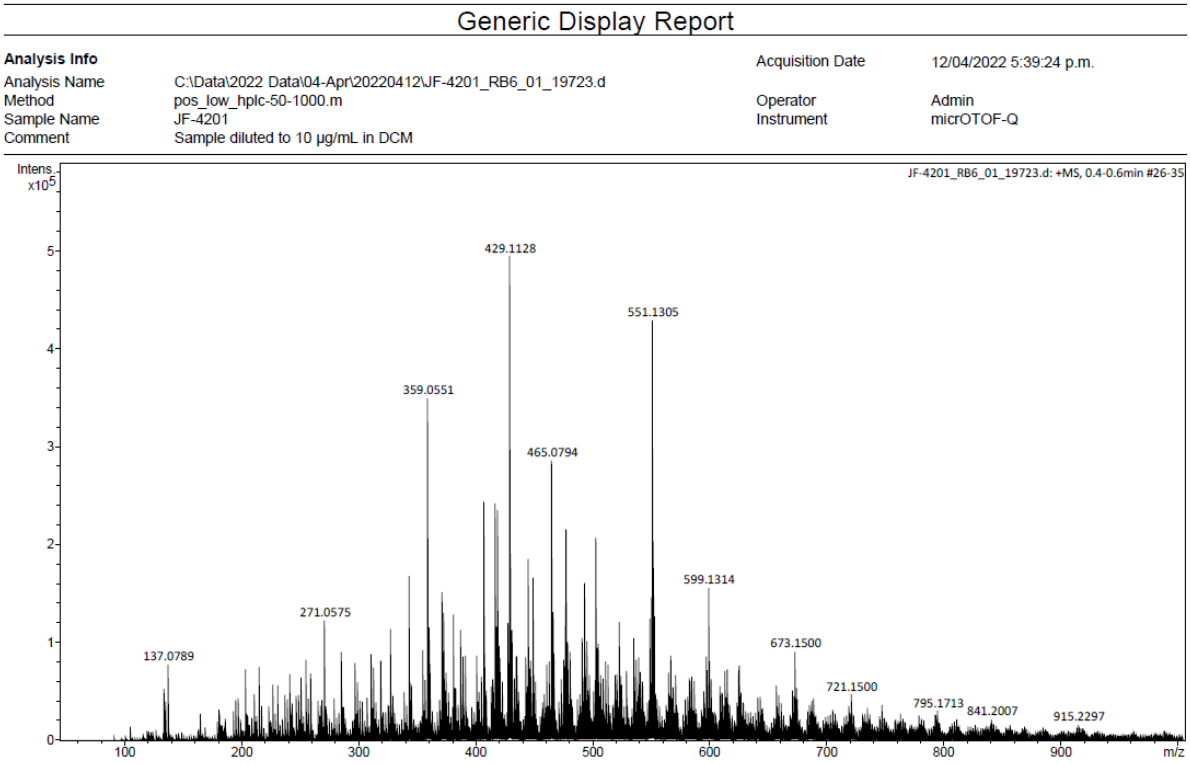

Figure 7.10 *ESI mass spectrum of the Grignard reaction of α,α'-dibromo-o-xylene (**1a**) and chloro(phenyl)silane through the Schrock adopted procedure.*

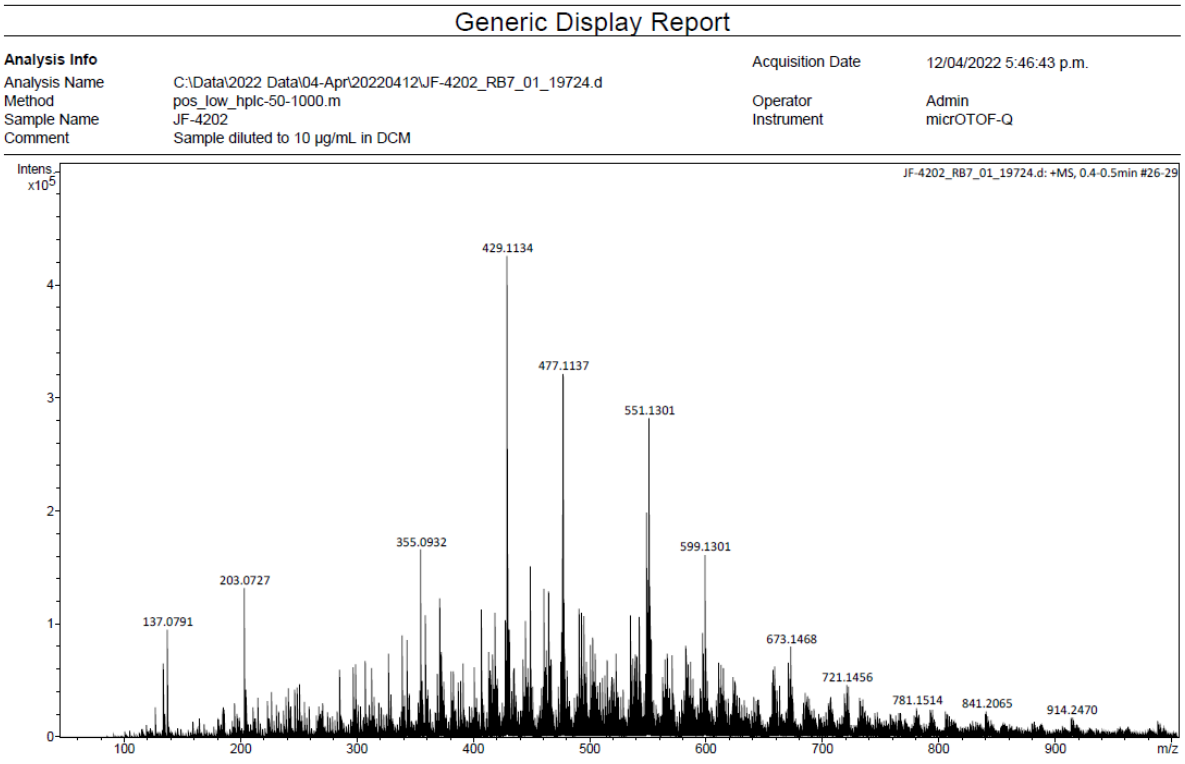

Figure 7.11 *ESI mass spectrum of the Grignard reaction of 2-bromobenzyl bromide (**1b**) and chloro(phenyl)silane through the Schrock adopted procedure.*

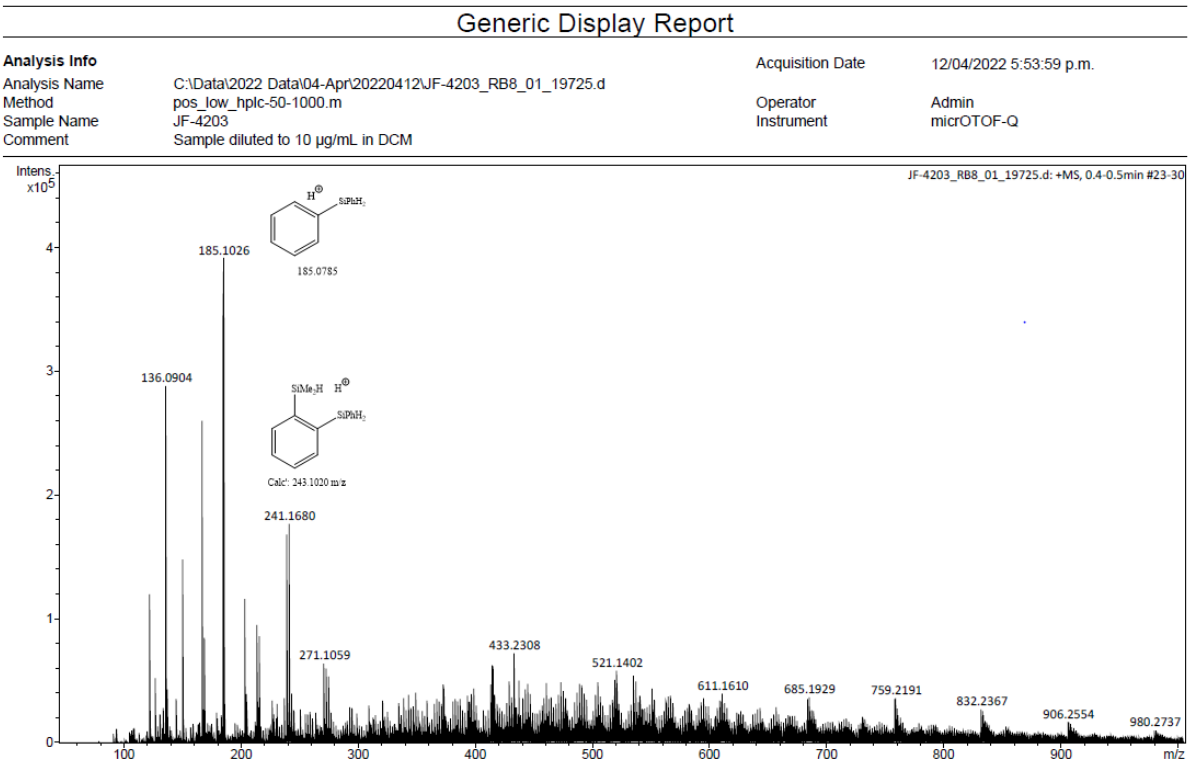

Figure 7.12 *ESI mass spectrum of the Grignard reaction of 1,2-dibromobenzene (**1c**) and chloro(phenyl)silane through the Schrock adopted procedure.*

7.2 Naphthalene-Bridged Dehydrocoupling Catalyst Investigation

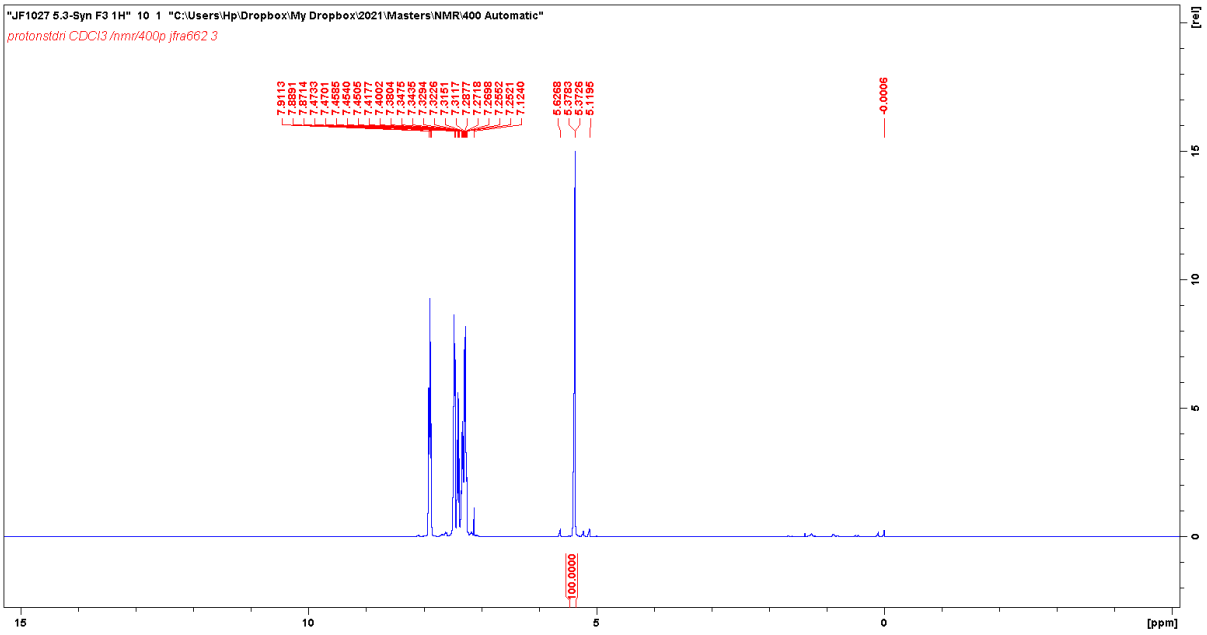

Figure 7.13 *^{1}H NMR spectrum of 1,8-bis(phenylsilyl)naphthalene (**4**)*

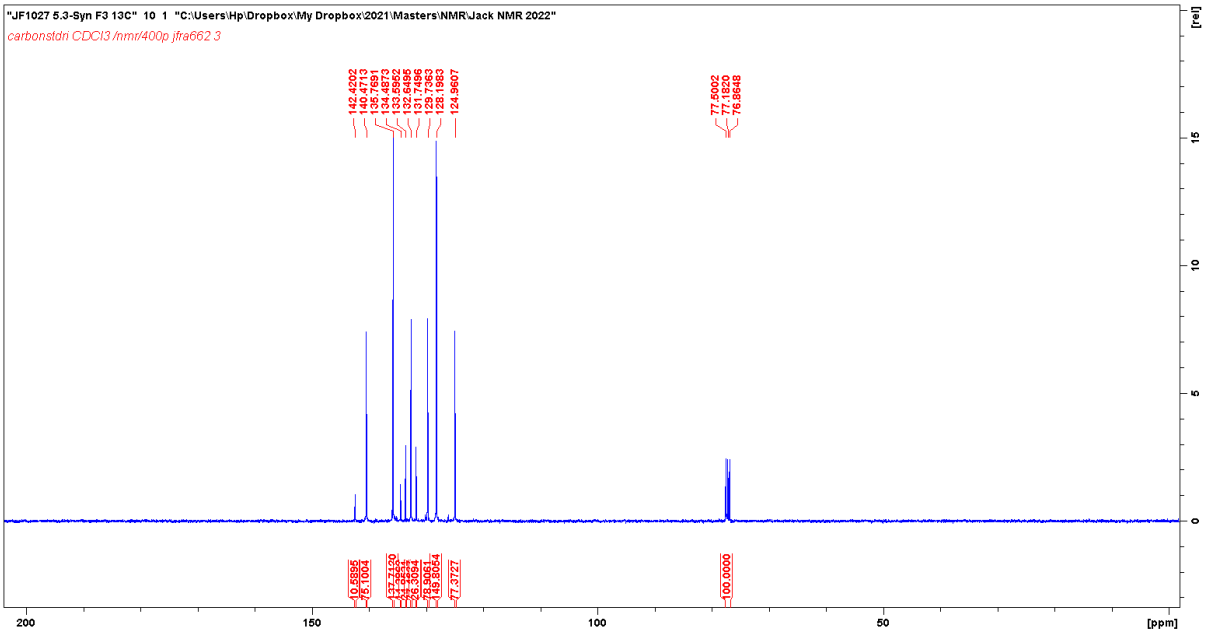

Figure 7.14 *^{13}C NMR spectrum of 1,8-bis(phenylsilyl)naphthalene (**4**)*

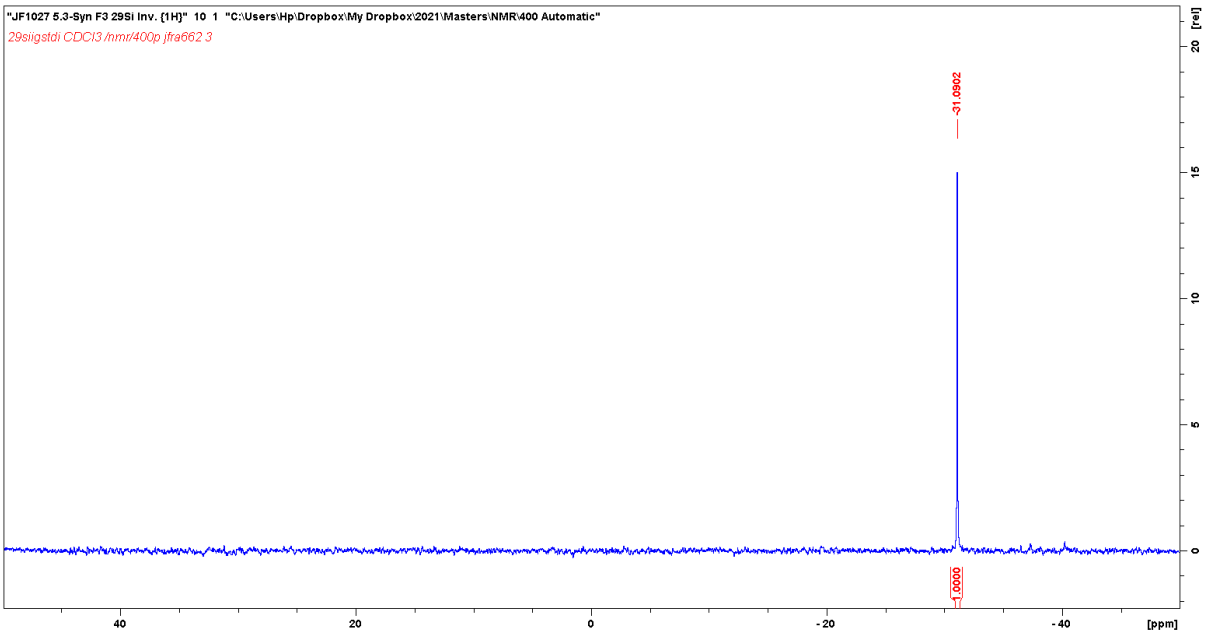

Figure 7.15 *$^{29}Si\{^{1}H\}$ NMR spectrum of 1,8-bis(phenylsilyl)naphthalene (**4**)*

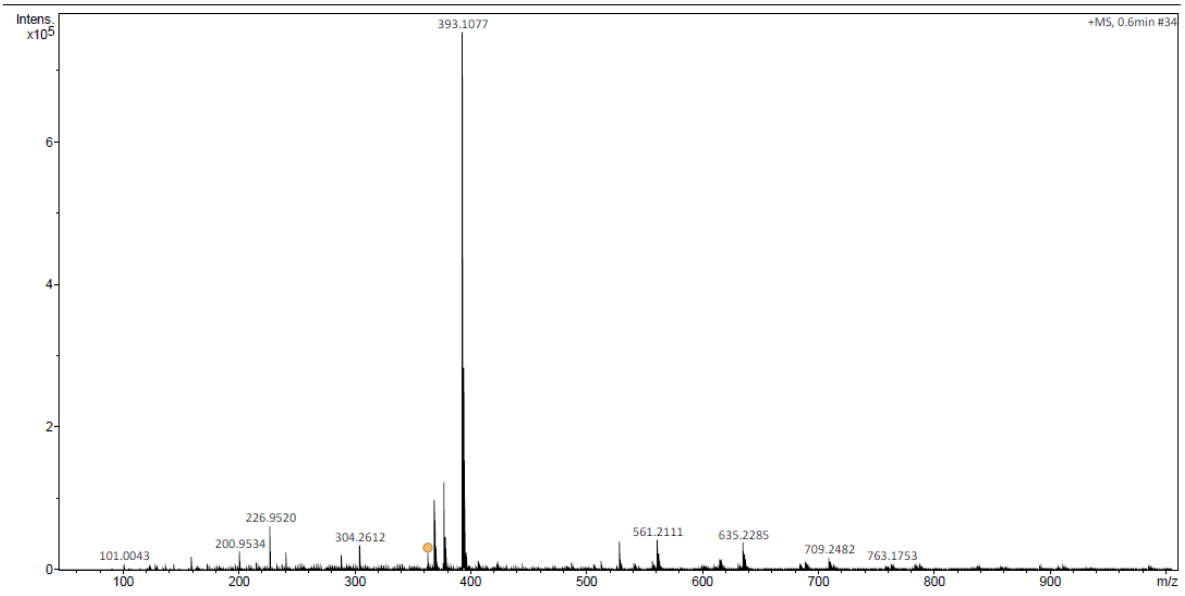

Figure 7.16 *ESI mass spectrum of 1,8-bis(phenylsilyl)naphthalene (**4**)*

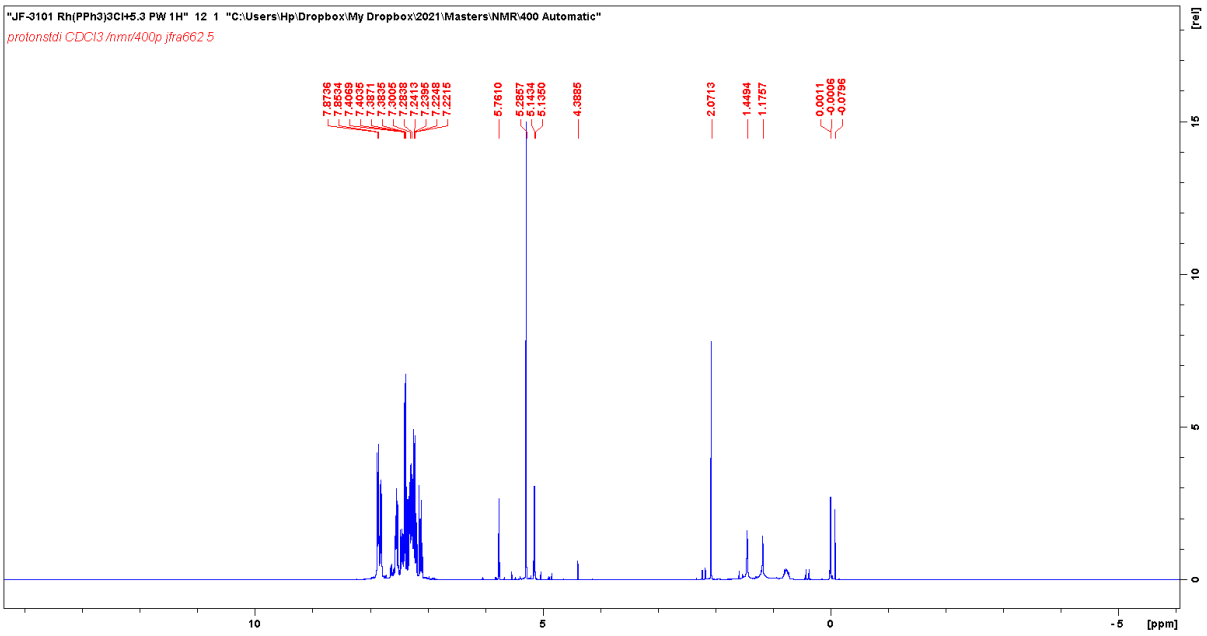

Figure 7.17 *^{1}H NMR spectrum of the dehydrocoupling reaction of 1,8-bis(phenylsilyl)naphthalene (**4**) and the $Rh(PPh_3)_3Cl$ catalyst.*

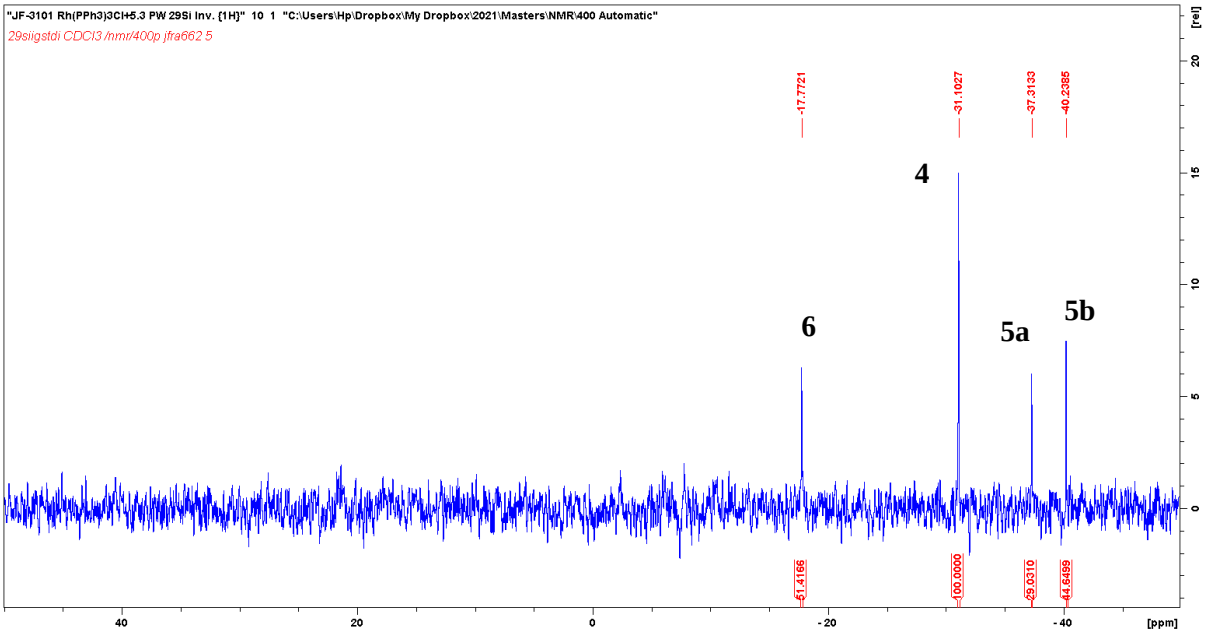

Figure 7.18 *$^{29}Si\{^{1}H\}$ NMR spectrum of the dehydrocoupling reaction of 1,8-bis(phenylsilyl)naphthalene (**4**) and the $Rh(PPh_3)_3Cl$ catalyst.*

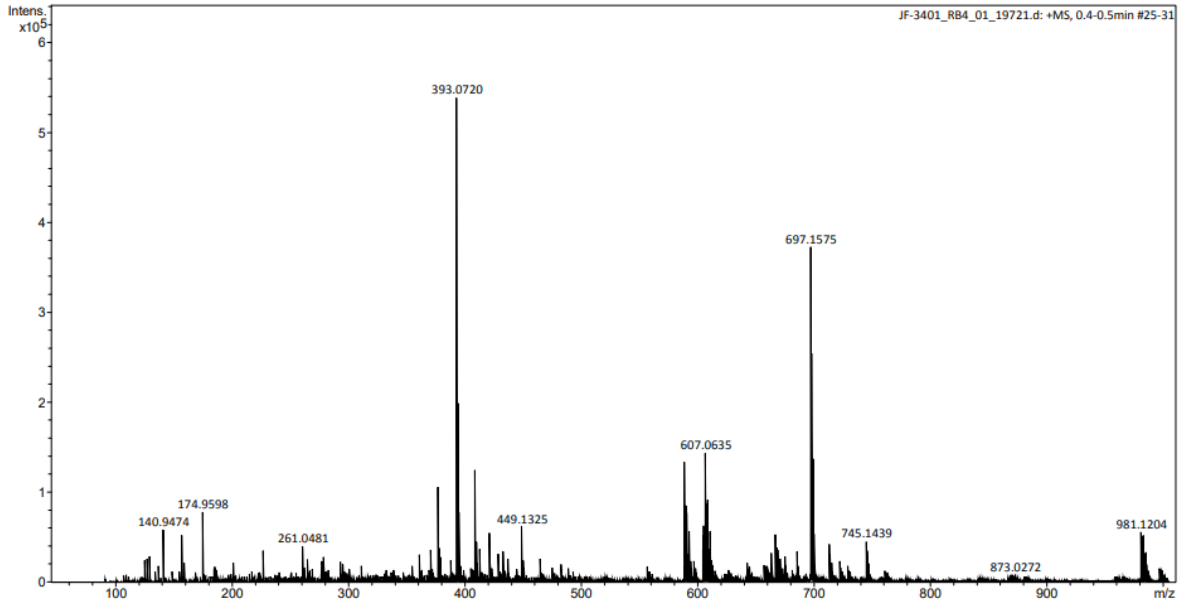

Figure 7.19 *ESI mass spectrum of the dehydrocoupling reaction between 1,8-bis(phenylsilyl)naphthalene (**4**) and the $Rh(PPh_3)_3Cl$ catalyst.*

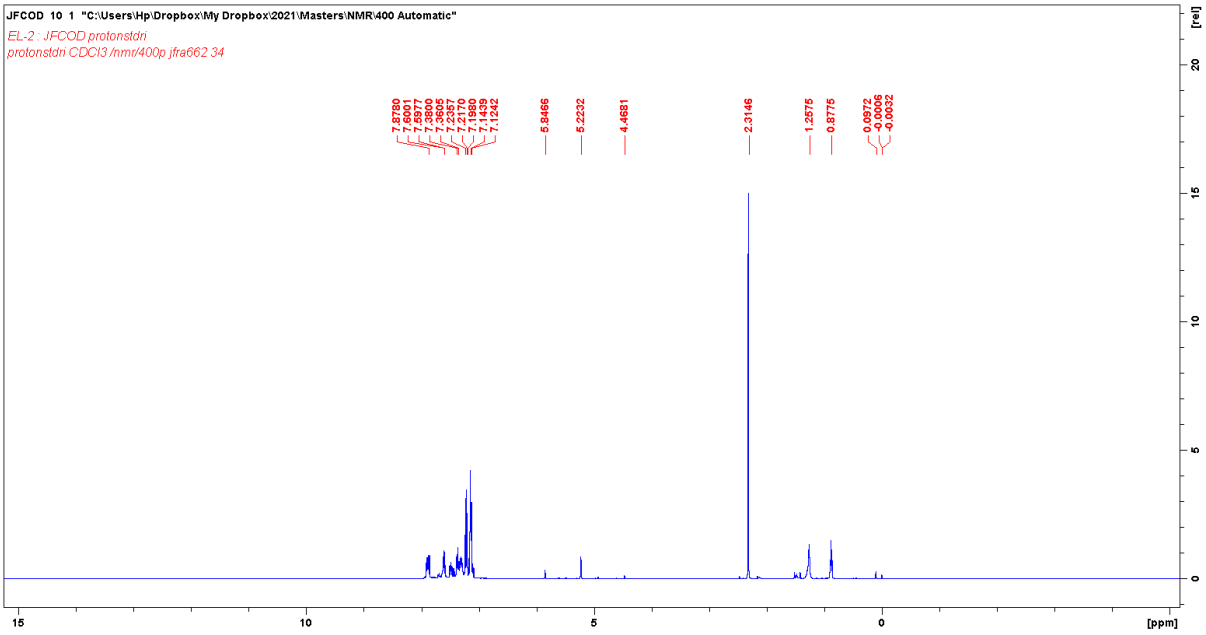

Figure 7.20 *^1H NMR spectrum of the dehydrocoupling reaction of 1,8-bis(phenylsilyl)naphthalene (**4**) and the $[Rh(cod)Cl]_2$ catalyst.*

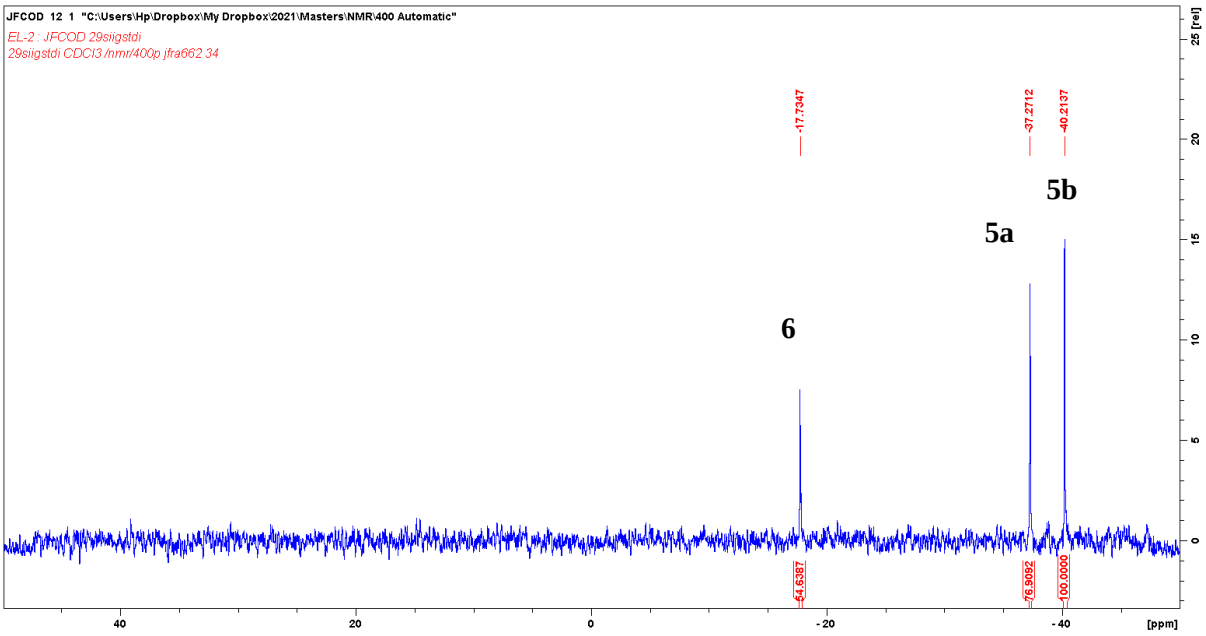

Figure 7.21 *$^{29}Si\{^{1}H\}$ NMR spectrum of the dehydrocoupling reaction of 1,8-bis(phenylsilyl)naphthalene (**4**) and the $[Rh(cod)Cl]_2$ catalyst.*

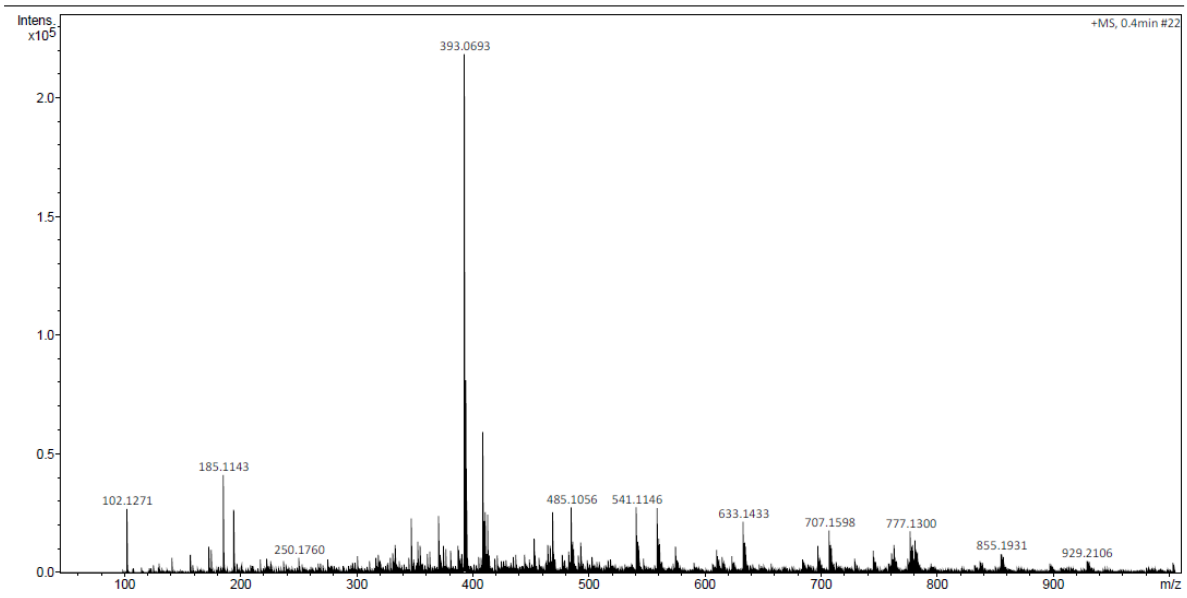

Figure 7.22 *ESI mass spectrum of the dehydrocoupling reaction between 1,8-bis(phenylsilyl)naphthalene (**4**) and the $[Rh(cod)Cl]_2$ catalyst (5 mol %).*

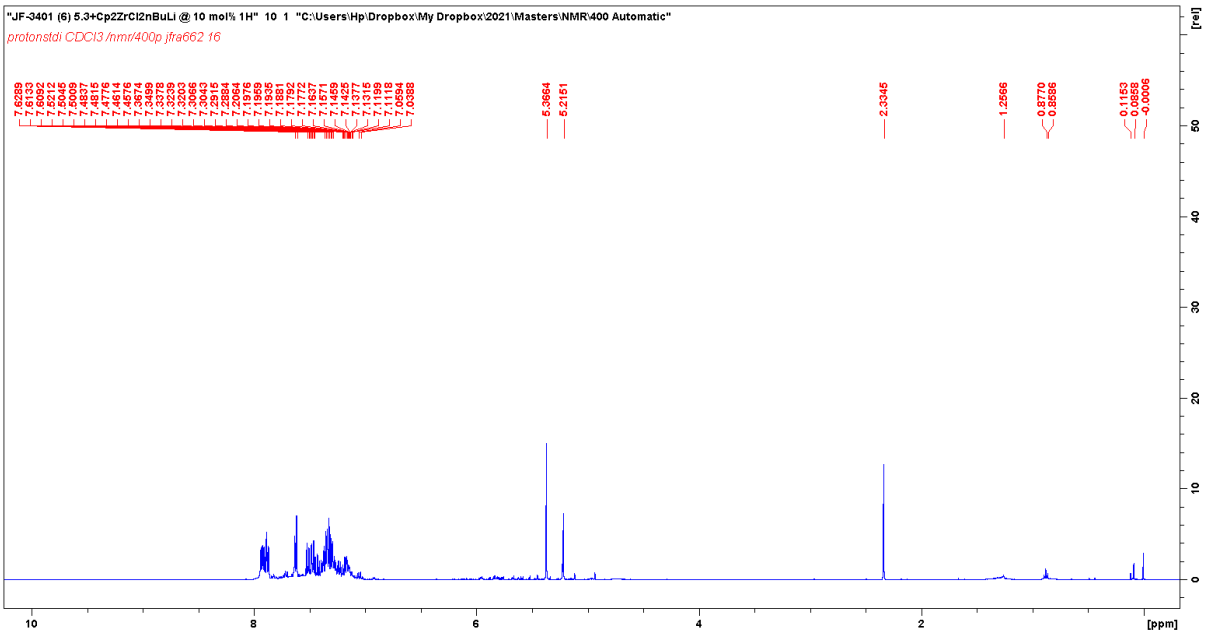

Figure 7.23 *^{1}H NMR spectrum of the dehydrocoupling reaction of 1,8-bis(phenylsilyl)naphthalene (**4**) and the Cp_2ZrCl_2/2nBuLi catalyst.*

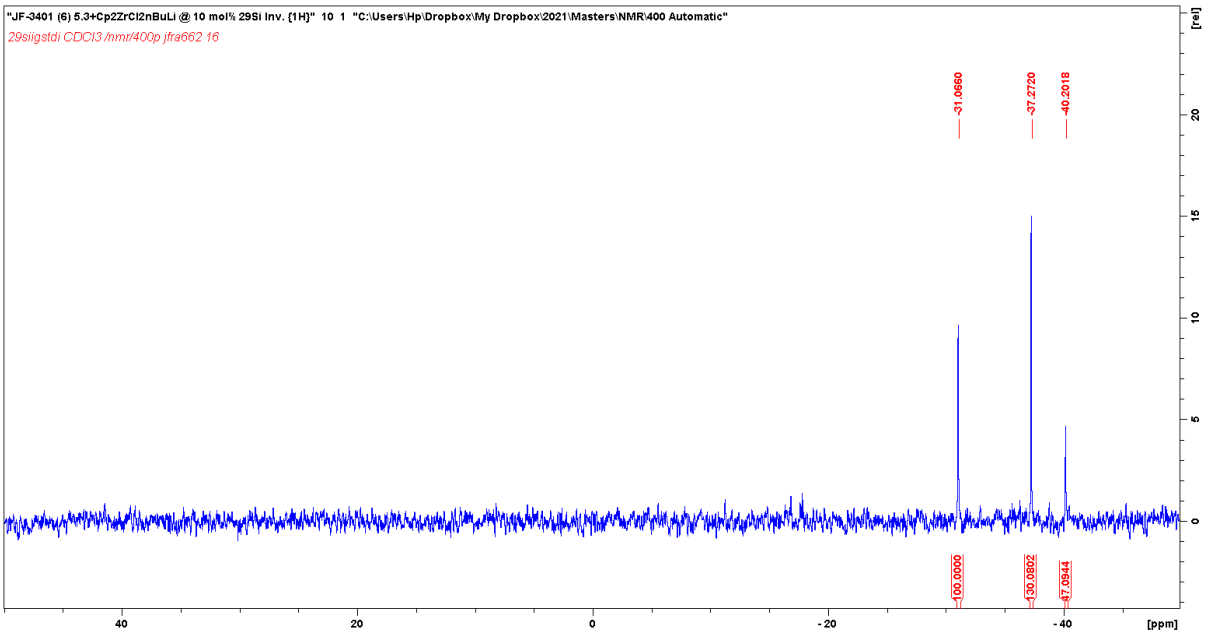

Figure 7.24 *$^{29}Si\{^{1}H\}$ NMR spectrum of the dehydrocoupling reaction of 1,8-bis(phenylsilyl)naphthalene (**4**) and the Cp_2ZrCl_2/2nBuLi catalyst.*

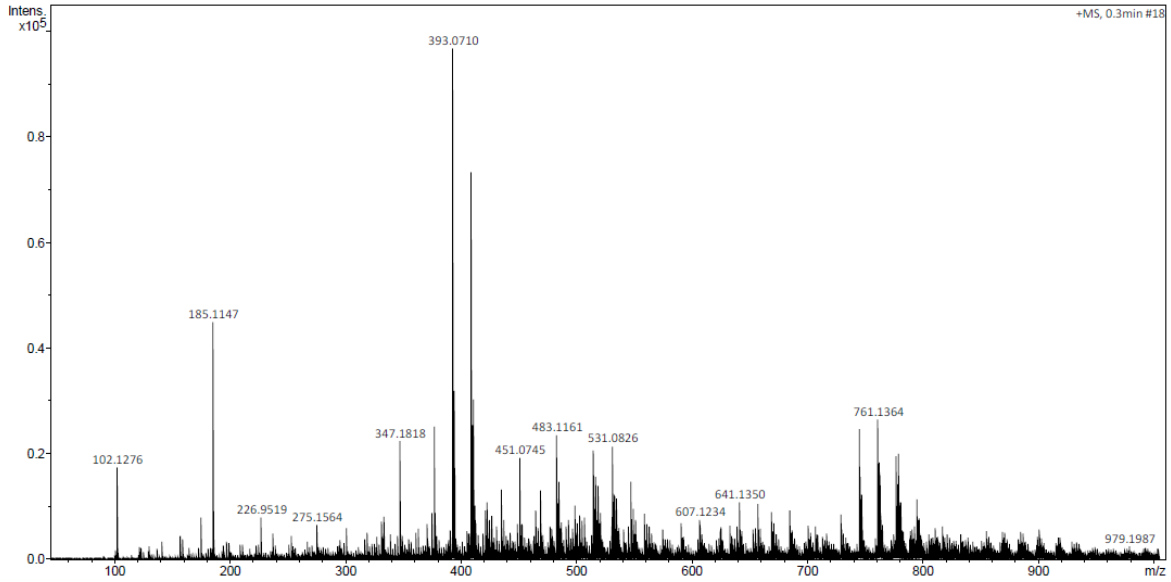

Figure 7.25 *ESI mass spectrum of the dehydrocoupling reaction between 1,8-bis(phenylsilyl)naphthalene (**4**) and the Cp_2ZrCl_2/2nBuLi catalyst.*

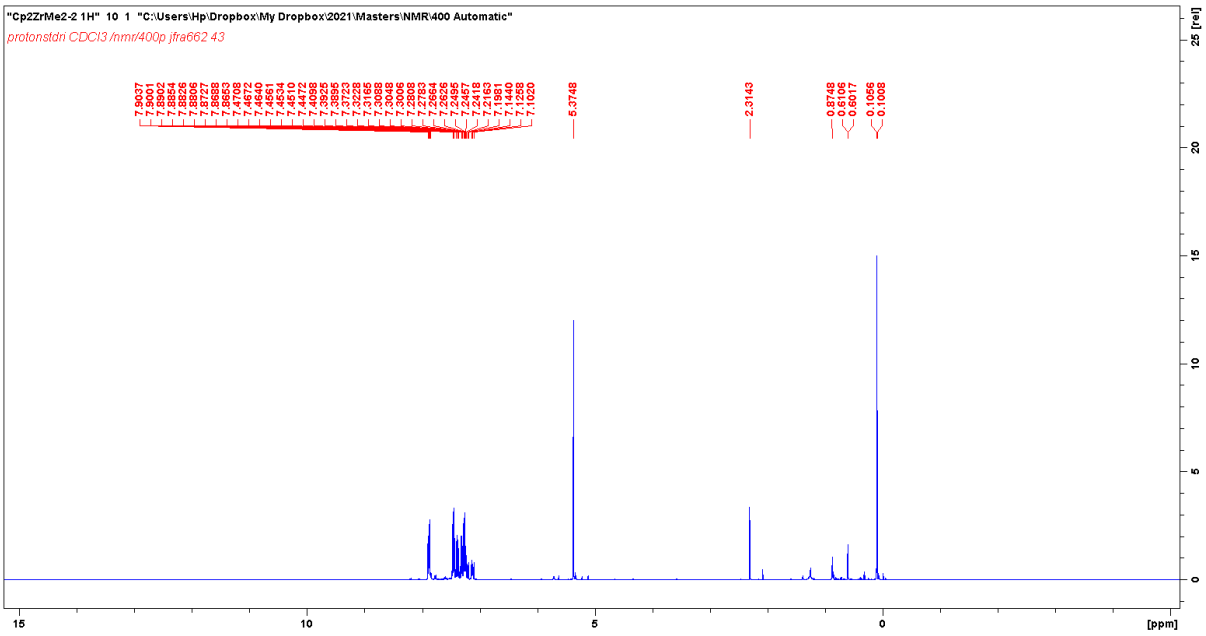

Figure 7.26 *^{1}H NMR spectrum of the dehydrocoupling reaction of 1,8-bis(phenylsilyl)naphthalene (**4**) and the Cp_2ZrCl_2/2MeLi catalyst.*

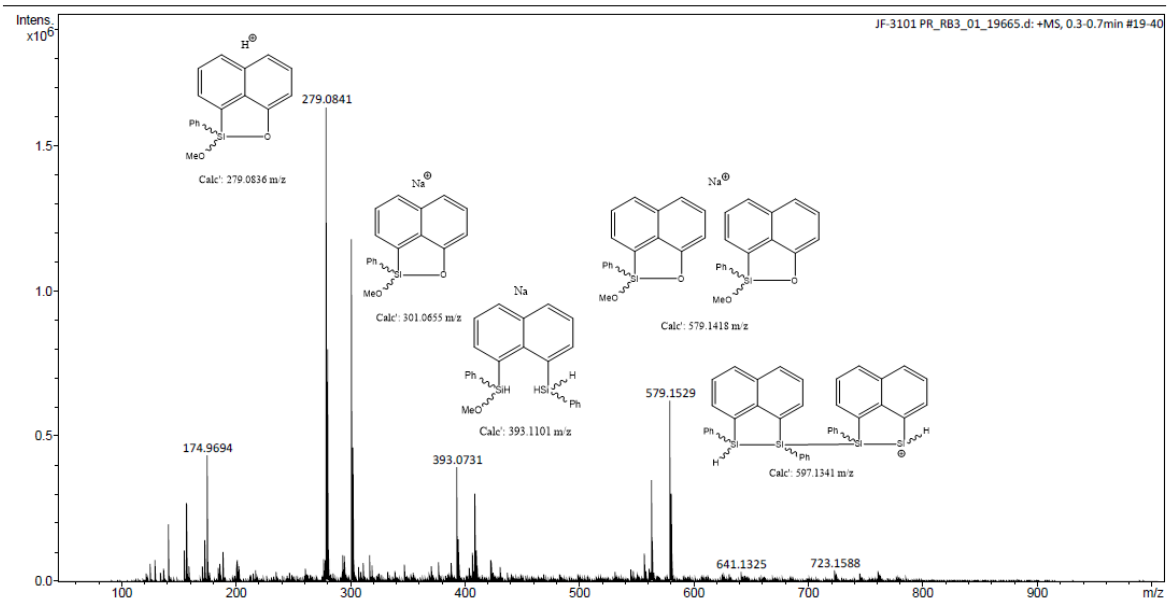

Figure 7.27 *ESI mass spectrum of the dehydrocoupling reaction between 1,8-bis(phenylsilyl)naphthalene (**4**) and the Cp_2ZrCl_2/2MeLi catalyst.*

7.3 Ferrocene-Bridged Dehydrocoupling Catalyst Investigation

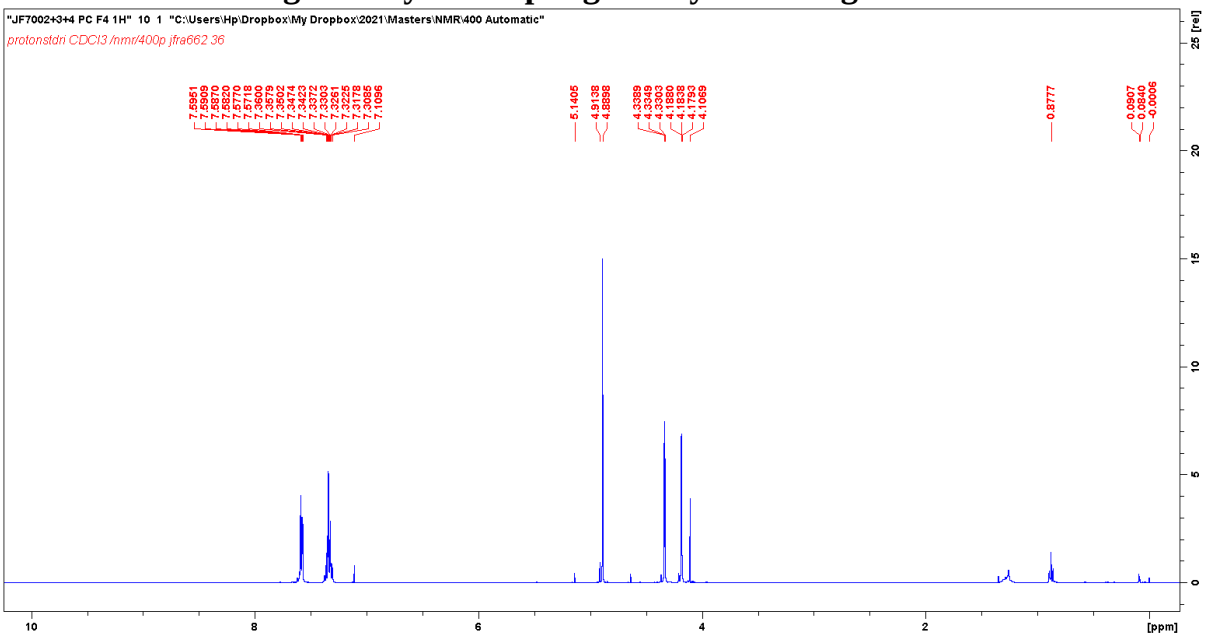

Figure 7.28 *^{1}H NMR spectrum of 1,1-bis(phenylsilyl)ferrocene (**7a**).*

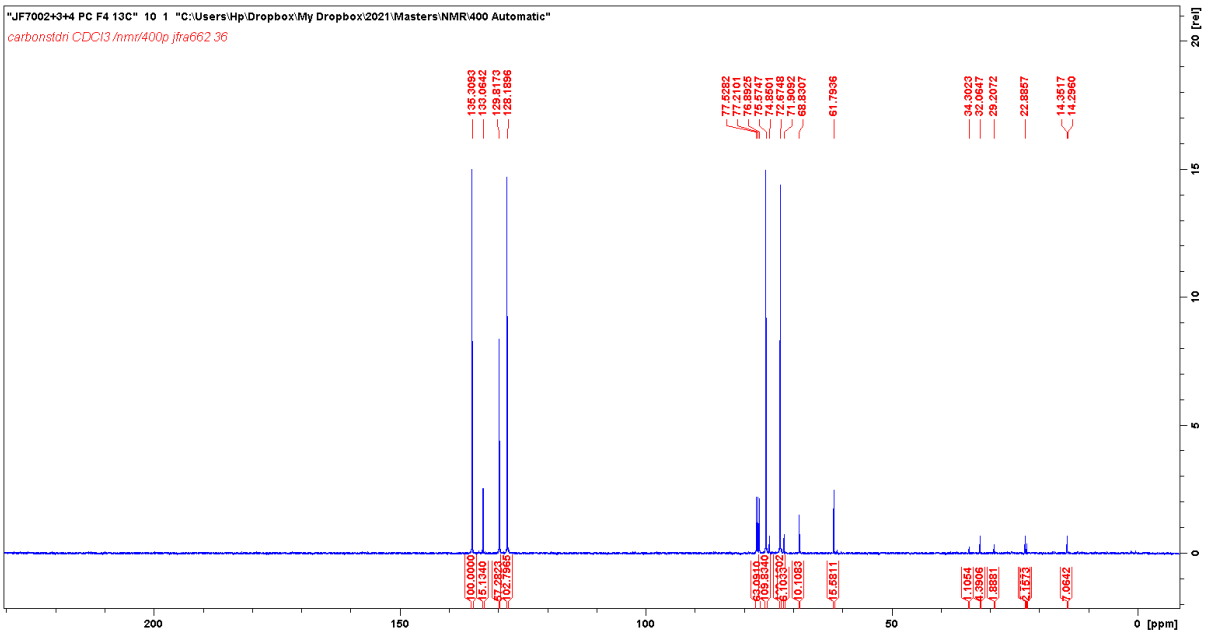

Figure 7.29 *^{13}C NMR spectrum of 1,1-bis(phenylsilyl)ferrocene (**7a**).*

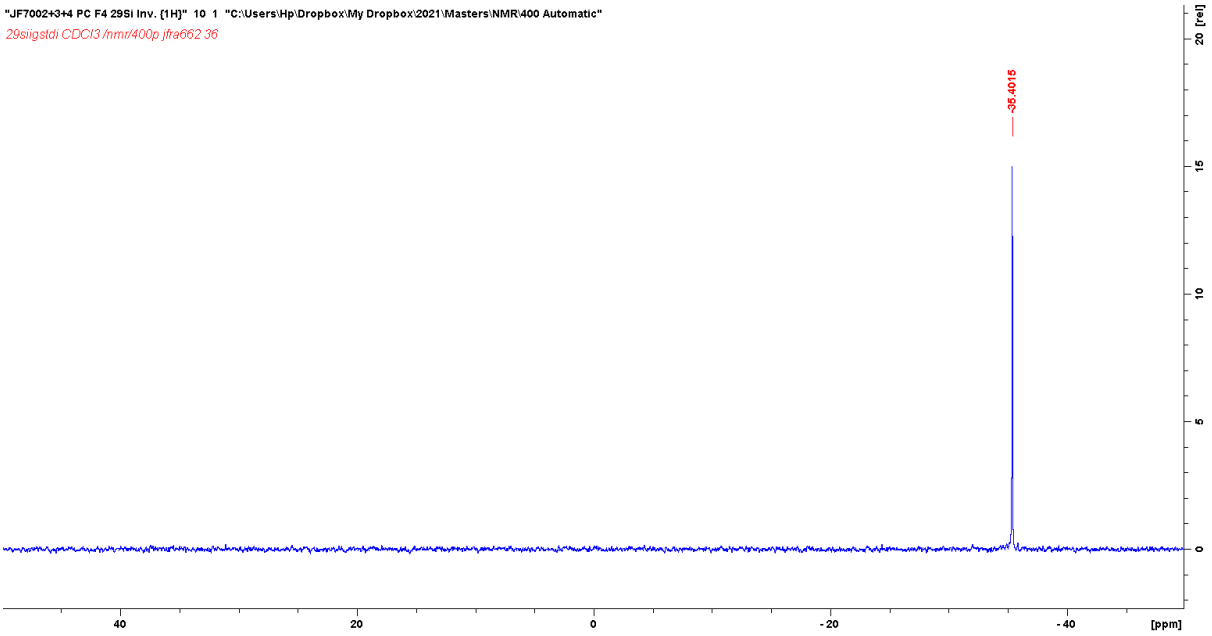

Figure 7.30 *^{29}Si{^{1}H} NMR spectrum of 1,1-bis(phenylsilyl)ferrocene (**7a**).*

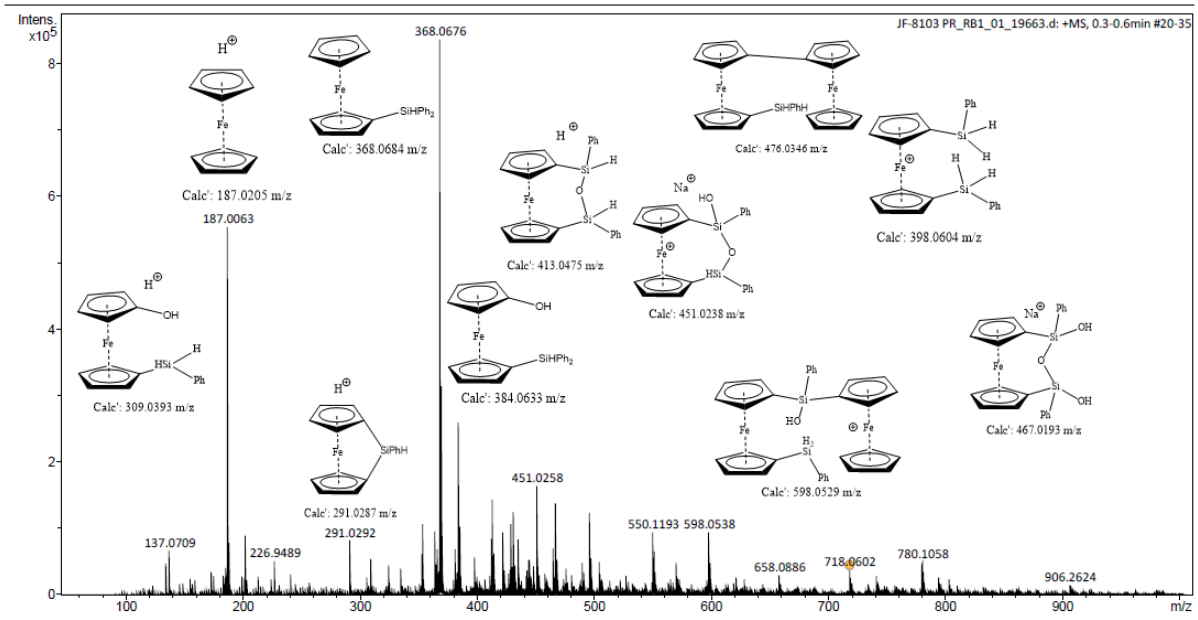

Figure 7.31 *ESI mass spectrum of dehydrocoupling reaction between 1,1-bis(phenylsilyl)ferrocene (**7a**) and the [Rh(cod)Cl]$_2$ catalyst.*

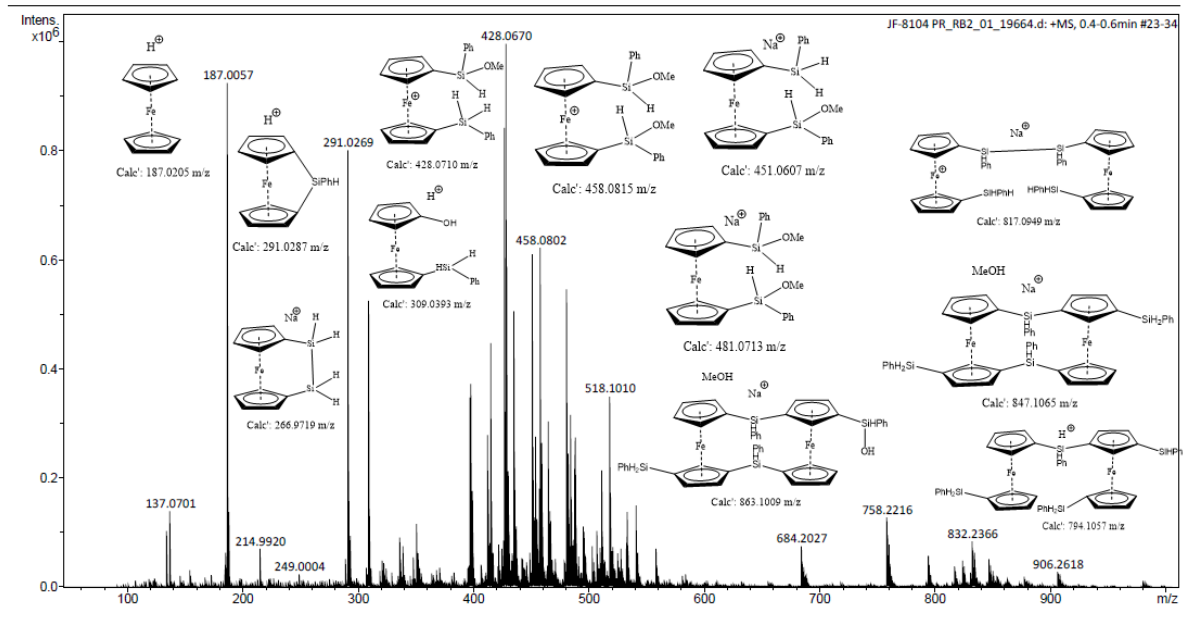

Figure 7.32 *ESI mass spectrum of dehydrocoupling reaction between 1,1-bis(phenylsilyl)ferrocene (**7a**) and the Cp$_2$ZrCl$_2$/2nBuLi catalyst.*

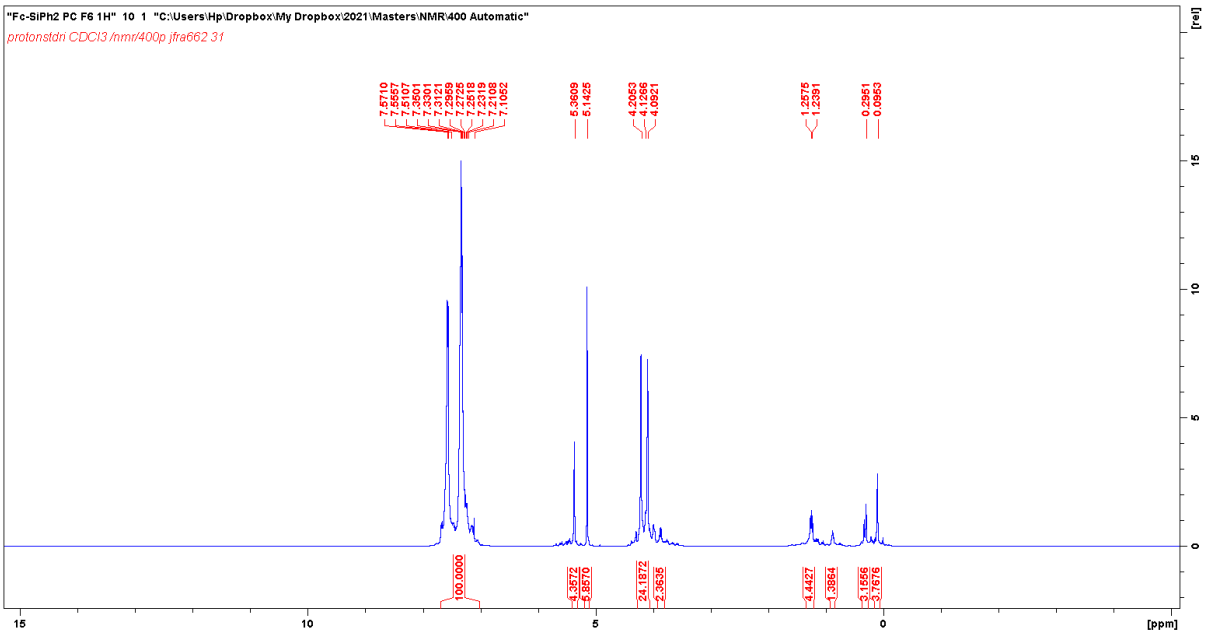

Figure 7.33 *^{1}H NMR spectrum of 1,1-bis(diphenylsilyl)ferrocene (**7b**).*

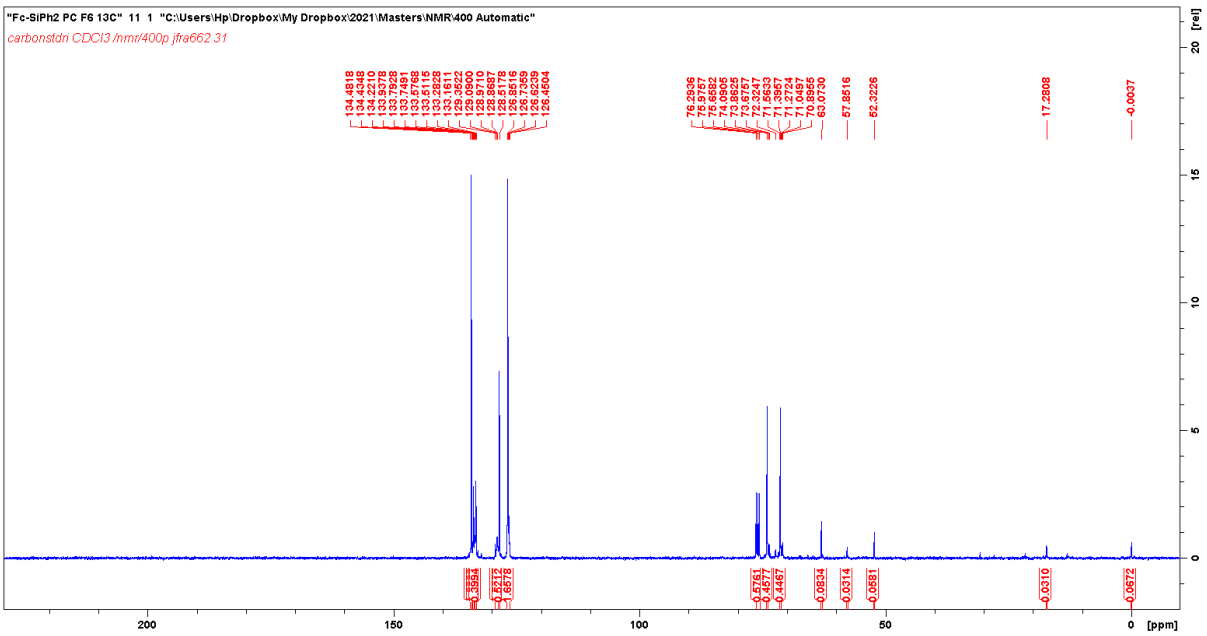

Figure 7.34 *^{13}C NMR spectrum of 1,1-bis(diphenylsilyl)ferrocene (**7b**).*

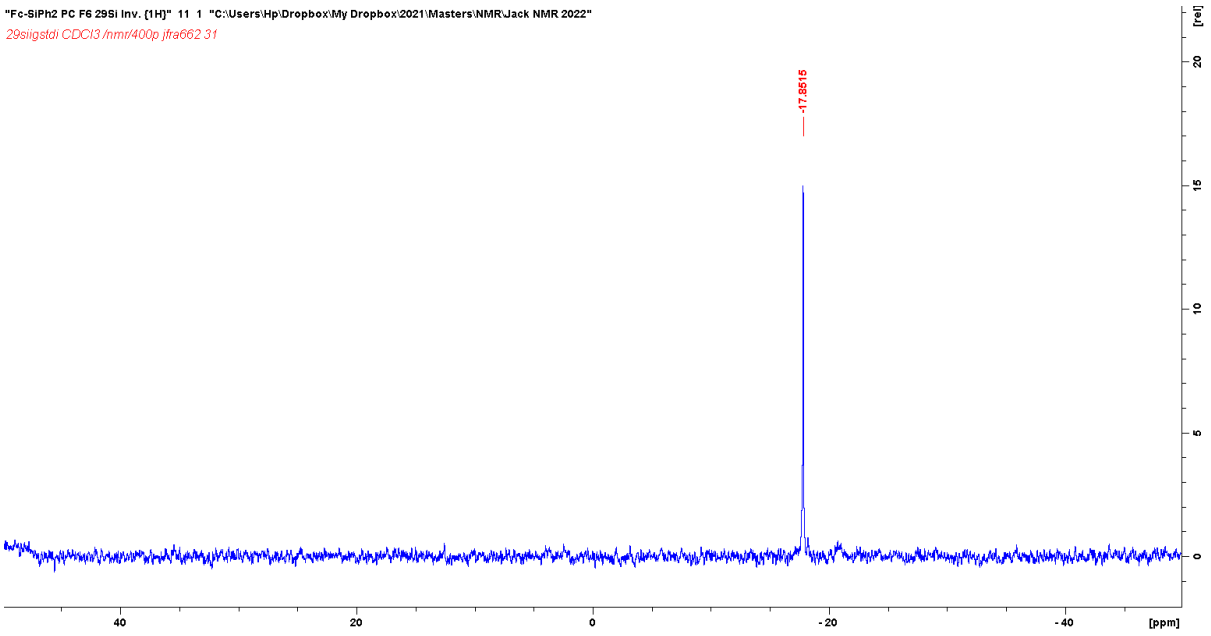

Figure 7.35 *$^{29}Si\{^{1}H\}$ NMR spectrum of 1,1-bis(diphenylsilyl)ferrocene (**7b**).*

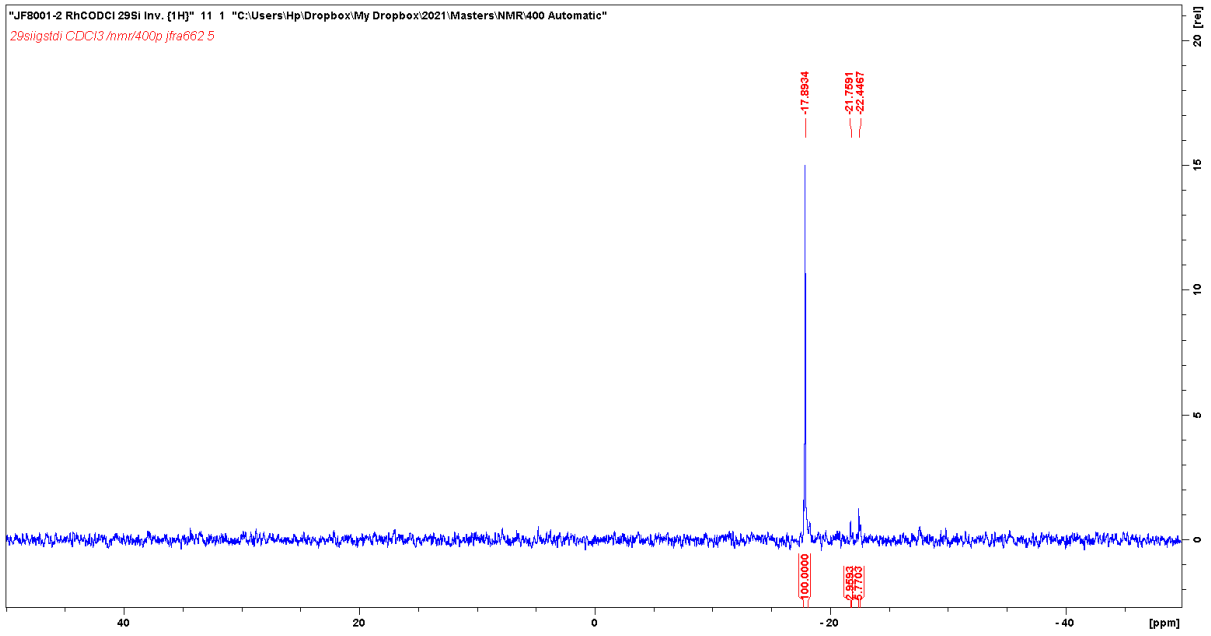

Figure 7.36 *$^{29}Si\{^{1}H\}$ NMR spectrum of the dehydrocoupling reaction between 1,1-bis(diphenylsilyl)ferrocene (**7b**) and the $[Rh(cod)Cl]_2$ catalyst.*

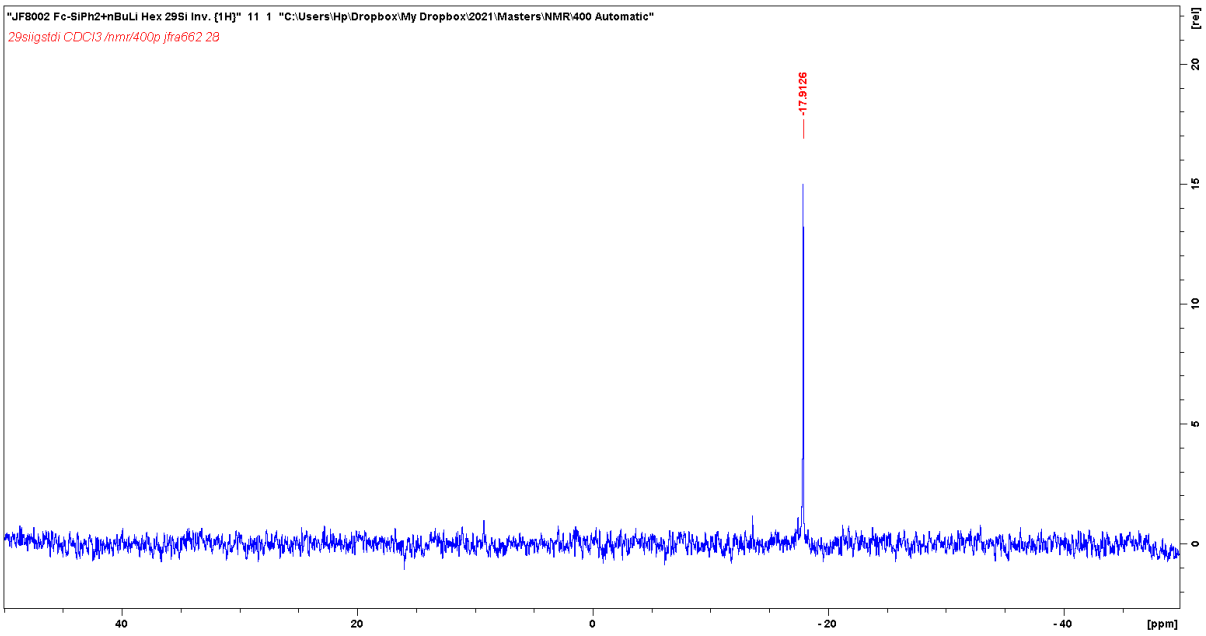

Figure 7.37 *$^{29}Si\{^{1}H\}$ NMR spectrum of the dehydrocoupling reaction between 1,1-bis(diphenylsilyl)ferrocene (**7b**) and the Cp_2ZrCl_2/2nBuLi catalyst.*

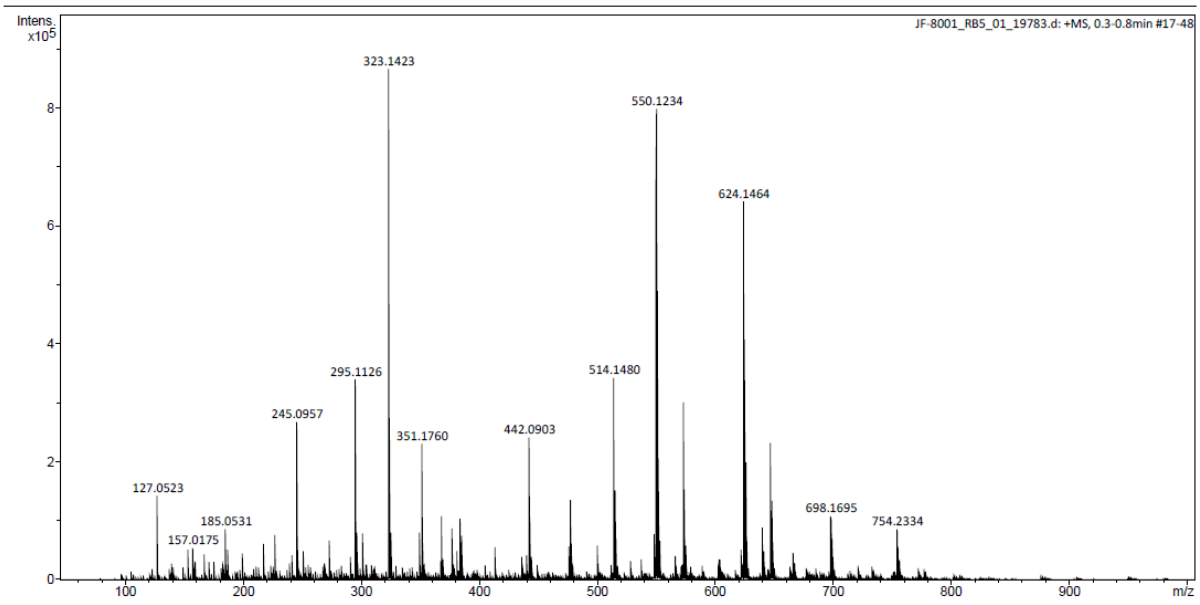

Figure 7.38 *ESI mass spectrum of the dehydrocoupling reaction between 1,1-bis(diphenylsilyl)ferrocene (**7b**) and the $[Rh(cod)Cl]_2$ catalyst.*

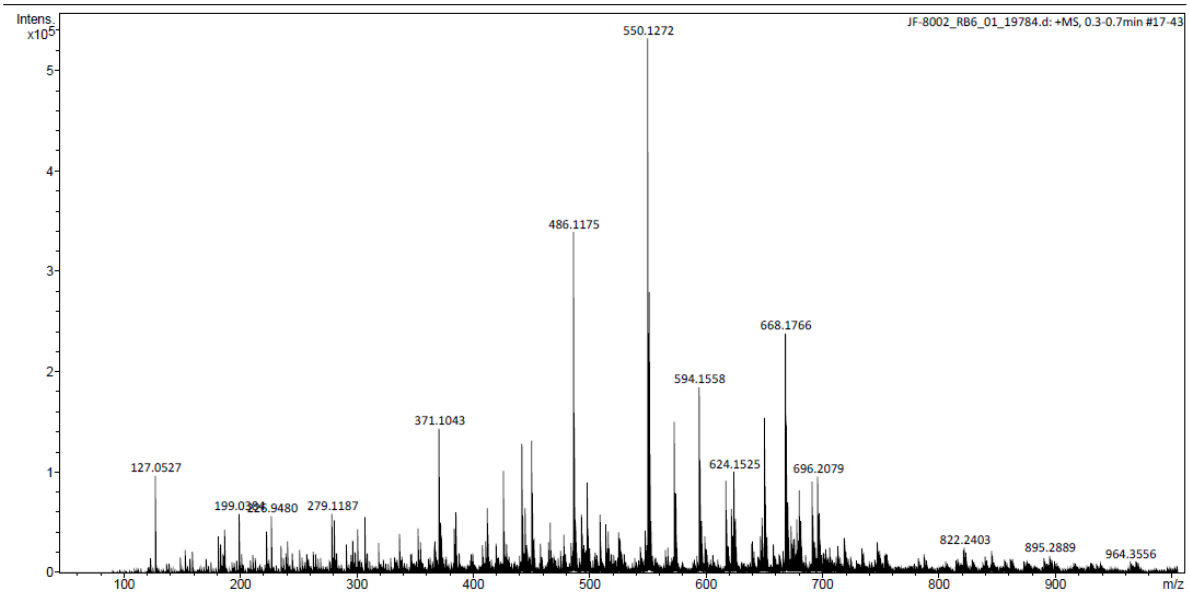

Figure 7.39 *ESI mass spectrum of the dehydrocoupling reaction between 1,1-bis(diphenylsilyl)ferrocene (**7b**) and the Cp_2ZrCl_2/2nBuLi catalyst.*